Studies of the pigment-type switching genes ATRN and MGRN1: evidence for a defect in endosomal/lysosomal protein trafficking as a cause of hyperpigmentation and spongiform neurodegeneration

by Will Pope Walker

STUDIES OF THE PIGMENT–TYPE SWITCHING GENES ATRN AND MGRN1: EVIDENCE FOR A DEFECT IN ENDOSOMAL/LYSOSOMAL PROTEIN TRAFFICKING AS A CAUSE OF HYPERPIGMENTATION AND SPONGIFORM NEURODEGENERATION

A Dissertation

Presented to the Faculty of the Graduate School

of Cornell University

In Partial Fulfillment of the Requirements for the Degree of

Doctor of Philosophy

by

Will Pope Walker

August 2010

STUDIES OF THE PIGMENT–TYPE SWITCHING GENES *ATRN* AND *MGRN1:* EVIDENCE FOR A DEFECT IN ENDOSOMAL/LYSOSOMAL PROTEIN TRAFFICKING AS A CAUSE OF HYPERPIGMENTATION AND SPONGIFORM NEURODEGENERATION.

Will Pope Walker, Ph.D.

Cornell University 2010

Mice with mutations in the genes *Attractin (Atrn)* and *Mahogunin ring finger-1 (Mgrn1)* have remarkably similar phenotypes: null mutations at either locus cause both a hyperpigmented coat-color phenotype and a progressive spongiform neurodegeneration. This noteworthy phenotypic overlap suggests that ATRN and MGRN1 gene products work together to accomplish a conserved cellular process that is important for both pigmentation and the prevention of neurodegeneration. In the pigment cell, the function of ATRN and MGRN1 is known to be important for the downregulation of signaling by the master regulator of pigment production, the melanocortin 1 receptor (MC1R). Using the convenient model system of the pigment cell, I have determined that ATRN physically interacts with both MGRN1 and MC1R, and that ATRN displays a constitutive endolysosomal trafficking behavior that is MGRN1-dependent. I propose a model wherein the interaction between ATRN and MGRN1 localizes the ATRN/MC1R complex to the site of protein sorting by the Endosomal Sorting Complex Required for Transport (ESCRT) protein TSG101, which is a known MGRN1 interactor and a target of MGRN1's E3 ubiquitin ligase activity. This coordinated behavior of ATRN and MGRN1 may direct the sorting of ATRN-associated MC1R into the intracisternal vesicles of multivesicular bodies (MVBs) by ESCRT proteins, providing a novel mechanism for attenuation of MC1R signaling.

If the pigment-type switching defects of *Atrn* and *Mgrn1* mutants are caused by a defect in ESCRT activity, a similar failure of ESCRT sorting could underlie the spongiform neurodegeneration seen in these mutants, and perhaps in human spongiform encephalopathies such as prion disease and HIV-associated dementia. As a proof-of-concept experiment to test this hypothesis, I knocked out the ESCRT protein TSG101 in neurons of adult mice to determine whether ESCRT dysfunction can cause spongiform neurodegeneration. Here I present preliminary results suggesting a profound neurodegenerative consequence of ECSRT dysfunction.

Keywords: attractin, mahogunin ring finger 1, melanocortin 1 receptor, ATRN, MGRN1, MC1R, pigment-type switching, spongiform neurodegeneration, spongiform change, spongiform encephalopathy, lysosomal targeting, lysosomal trafficking, multivesicular body sorting, TSG101, ESCRT, endogenous retrovirus, prion.

BIOGRAPHICAL SKETCH

Will Pope Walker is a native of Pensacola, FL. Home-educated through primary and secondary school, his first exposure to formal education was as a dual-enrollment student at Pensacola Junior College, where an introductory lab course in zoology deeply impressed him with the incredible diversity of ways there are of being alive. He transferred to the University of West Florida planning to study "critters" as a marine biology major, but became enchanted by the exquisite processes by which biological function emerges from genomic information and received his B.S. in molecular biology *summa cum laude* 1999. After spending a few years at a variety of jobs including lab technician, adjunct lecturer, anatomy lab instructor, and professional bushwhacker leading a survey crew through the snake-infested wetlands of his home county, he began graduate studies at Cornell University in 2004 and joined the lab of Teresa M. Gunn in 2005. While there he was fortunate to see a bit more of the world than some graduate students do, working on experiments both on campus in Ithaca and at the McLaughlin Research Institute for Biomedical Sciences in Great Falls, MT. Will is a skeptical but still rather easily excitable fellow who smiles when he talks about biology, unless the subject turns to the over-credulous use of ill-characterized antibodies.

For my grandparents.

ACKNOWLEDGEMENTS

A dissertation project becomes a curious thing, the outcome of a deeply individual obsession and struggle, and at the same time a monument to countless gestures of goodwill generously given. I have been greatly helped in this journey by many, many kind people. My greatest debt is to my advisor, Dr. Teresa M. Gunn, who has provided me with my lab home these last five years and has ceaselessly modeled the primary scientific virtues of curiosity, openness, enthusiasm, and indomitability. I think the transformation involved in becoming a scientist comes gradually; it's partly forged in intense moments of frustration or excitement, but it's mostly absorbed imperceptibly from immersion in the life of the lab. Teresa's wide interests and confident approach to science make her lab a truly exciting place to work, and for the many lessons I've absorbed in it I owe a debt that I can only pay forward.

One of the greatest unexpected revelations I encountered when I entered the scientific community was the collegial generosity prevailing among so many in the discipline. Many fellow scientists have given graciously of their time, consideration, and expertise to help me overcome experimental obstacles or learn new techniques, and have freely shared reagents, constructs, and mouse lines that cost them much labor to produce. I especially appreciate the generosity of Melissa Burmeister, who spent hours in a bare concrete room huddled over a stereotactic injection apparatus with me until I got a new technique into my hands. Elodie Le Pape, whom I have not yet met but for whom I hope to be able to do a good turn one day, demonstrated extraordinary generosity by sending me one of the only Eppendorf tubes of purified recombinant agouti protein in the whole world, saving me months of work at the cost of at least a few weeks of her own. The ready willingness of many other scientists at Cornell and around the world to help out with gifts of plasmids, cell lines, antibodies, and mice has

been instrumental in the completion of this project. I have learned to greatly value the attitude of these generous colleagues, for whom to offer help is second nature. Despite our individual scientific preoccupations, the general enterprise of scientific progress is something that we are all in together.

My committee members, Drs. Dave Lin, William Brown, and Eric Alani, I sincerely thank for investing their time, critical consideration, and scientific acumen in helping a young scientist fumble his way into the ancient and honorable company of scholars.

I thank all members of the Gunn Lab, past and present, for the countless small considerations and big favors accumulated over the years. Not all labs get along as well as Teresa's always seems to, so I feel lucky to have been surrounded all this time by so many good eggs. Christina, I'm sure I'd still be useless in the lab if I hadn't had the good fortune to share a lab bay with you. Thanks for your encouraging presence and your ready advice.

For more than two years in Teresa's lab I had the good fortune to work with a very dedicated and thoughtful undergraduate scholar, Caroline Wee. Caroline, thanks for hanging in there with me back when I had no idea how to design and delegate a workable project. "Helping" you with your honors thesis was a great lesson for me in the tactics of experimental strategy. I'm just glad the experience didn't chase you off to medical school!

My family has provided unconditional love and countless gestures of support during my time Upstate and out West. All I can do is love them back.

To my friends in Ithaca who have so often provided companionship for good times or a sympathetic ear during the frustrating periods, you know who you are. I'm glad our lives crossed paths. Let's stay friends for a long time.

I feel very blessed to have been welcomed by a special community. We scientists are fortunate that we are enabled by society to do what we do, to follow our curiosity and engage in that uniquely human calling, the difficult but rewarding journey of learning how to come to understand. I'm very blessed. When I think of the many kindnesses I've encountered on the way to this dissertation, sometimes I'm surprised to find tears come to my eyes.

TABLE OF CONTENTS

LIST OF FIGURES

LIST OF TABLES

LIST OF ABBREVIATIONS

Agouti Signaling Protein	ASP/ASIP
Adenylate Cyclase	AC
Amyloid Beta peptide	Aβ
Attractin	ATRN
Attractin-like protein 1	ATRNL1
Base pair	bp
Bovine Spongiform Encephalopathy	BSE
Central Nervous System	CNS
Chronic Wasting Disease	CWS
Coding Sequence	CDS
Creutzfeldt-Jakob Disease	CJD
Delta Opioid Receptor	DOR
Endogenous Retrovirus	ERV
Endoplasmic Reticulum	ER
Endosomal Complex Required for Sorting	ESCRT
Endosomal Recycling Complex	ERC
Epidermal Growth Factor	EGF
Epidermal Growth Factor Receptor	EGFR
Factor Induced Gene 4	FIG4
Fetal Bovine Serum	FBS
Formation of Aploid and Binucleates 1	FAB1
Frontotemporal Dementia	FTD
G protein alpha	Gα
G protein-coupled Receptor	GPCR
G protein-coupled Receptor Kinase	GRK

Gerstmann-Straussler-Scheinker disease	GSS
Glycophosphatidylinositol	GPI
Hematoxylin and Eosin	H&E
HEPES-Buffered Saline	HBS
Human Immunodeficiency Virus	HIV
Intracisternal A Particle	IAP
Lateral Plate Mesoderm	LPM
Left-Right Patterning	L-R Patterning
Lysosome-associated Membrane Protein	LAMP
Mahogunin Ring-finger 1	MGRN1
Mannose-6-Phosphate Receptor	M6PR
Melanocortin 1 Receptor	MC1R
Melanocortin 2 Receptor	MC2R
Melanocortin 4 Receptor	MC4R
Melanocortin Receptor Accessory Protein	MRAP
Molecular Weight	mw
1-methyl-4-phenylpyridinium	MPP+
Multiple EGF domains 8	MEGF8
Multivesicular Body	MVB
Open Reading Frame	ORF
Peptide N-glycosidase F	PNGase F
Phosphatidylinositol (3,5) biphosphate	$PI(3,5)P_2$
Polyacrylamide Gel Electrophoresis	PAGE
Prion Protein	PrP
Prion Protein (gene)	*Prnp*
Reactive Oxygen Species	ROS

Really Interesting New Gene	RING
Receptor Associated Membrane Protein	RAMP
RING finger protein 157	RNF157
Sodium Dodecyl Sulfate	SDS
Superoxide Dismutase 1	SOD1
12-O-tetradecanoylphorbol-13-acetate	TPA
Trans-Golgi network	TGN
Transmissible Spongiform Encephalopathy	TSE
Tris-buffered Saline	TBS
Tris-buffered Saline with Tween-20	TBS/T
Tumor Susceptibility Gene 101	TSG101
Vacuole partitioning 14	VAC14
Variant Creutzfeldt-Jakob Disease	vCJD
5-bromo-4-chloro-3-indolyl-β-D-galactopyranoside	X-gal

CHAPTER ONE

SPONGIFORM NEURODEGENERATION & THE PIGMENT-TYPE SWITCHING SYSTEM[1]

Introduction

Spongiform neurodegeneration is a histopathologically striking form of brain disease: under the light microscope, sections of affected brain tissue appear to be riddled with thousands of tiny holes. The appearance, enlargement, and spread of these vacuoles herald dementia and, eventually, death for the unfortunate victims of several different human diseases, but little is known about how these spongiform vacuoles form. To explore this problem, I have made use of a fascinating pair of mouse mutants, each of which develops spongiform neurodegeneration. Mice with null mutations in the genes *attractin* (*Atrn*) and *mahogunin ring finger-1* (*Mgrn1*) exhibit a remarkable degree of phenotypic overlap, sharing both a progressive spongiform neuroencephalopathy and a particular defect in the control of pigment production (Figure 1.1). This peculiar genetic situation indicates that the protein products ATRN and MGRN1 are likely to be cooperating partners in a conserved molecular pathway that functions in the brain to prevent spongiform neurodegeneration, and also in the pigment cell to regulate pigment-type switching. Therefore, I have used the pigment cell as a model system in which to explore this functional relationship of ATRN and MGRN1, with the expectation that the insights gained will translate into a new understanding of the mysterious and destructive phenomenon of spongiform neurodegeneration. To provide the necessary background for this study, this chapter reviews the problem of spongiform change, and then introduces the model system of pigment-type switching. After exploring the functions

[1] Portions of this chapter are modified with the permission of the publisher from Walker and Gunn, 2010a and Walker and Gunn, 2010b.

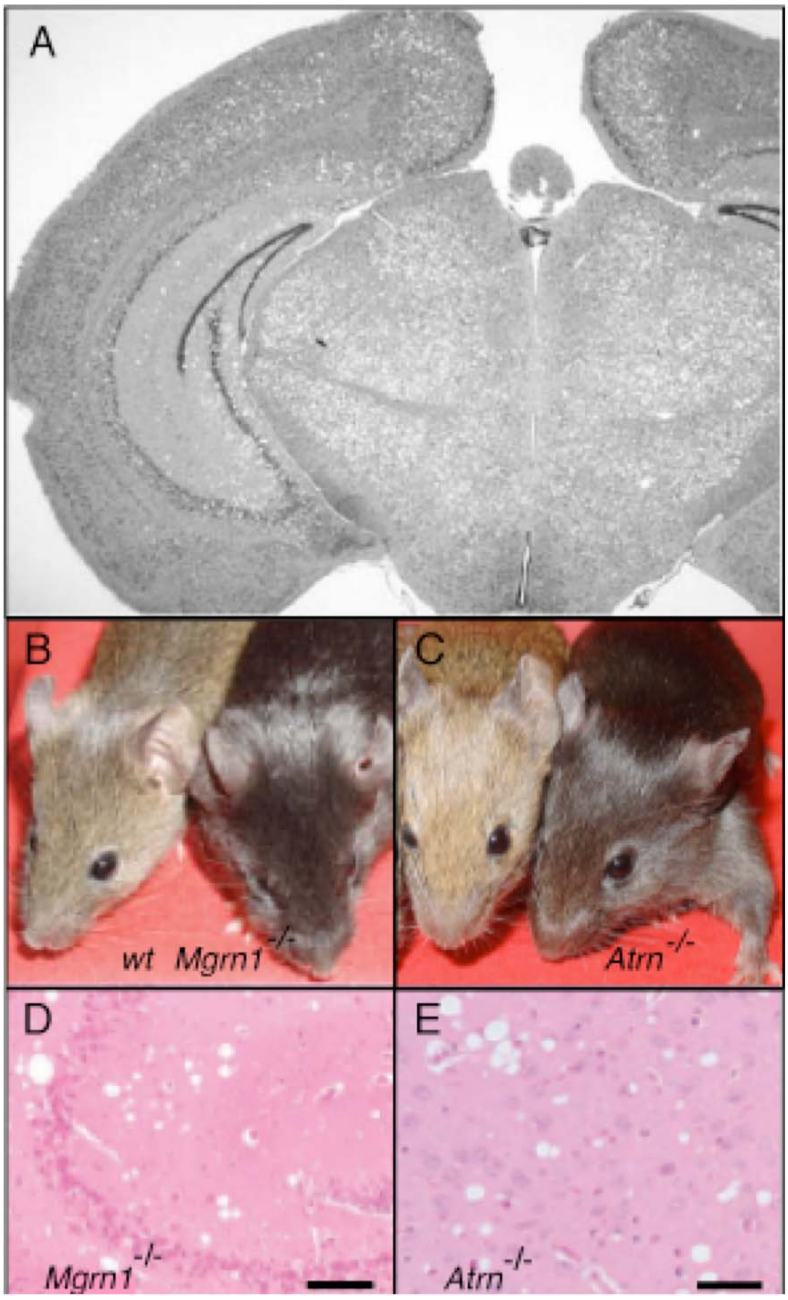

Figure 1.1. Spongiform neurodegeneration and hyperpigmentation in *Atrn* and *Mgrn1* mutant mice. A: Low-magnification view of widespread spongiform neurodegeneration in *Atrn*$^{mg/mg}$ brain. B: *Mgrn1*$^{-/-}$ mice (*right*) are hyperpigmented. C: *Atrn*$^{-/-}$ mice (*right*) are hyperpigmented phenotypes. D: Spongiform neurodegeneration in hippocampus of 13-month-old *Mgrn1*$^{-/-}$ mouse. E: Spongiform neurodegeneration in thalamus of 4-month-old *Atrn*$^{-/-}$ mouse. Scale bars in D&E represent 50 μm. Images are modified with permission from (A) Bronson *et al.*, 2001; (B) Jiao *et al.*, 2009b; (C) Walker *et al.*, 2007; (D) He *et al.*, 2003; and (E) Gunn *et al.*, 2001. (Note: the unlabeled mouse in C is an animal from a transgenic rescue experiment with a complex genotype; it displays an agouti coat coloration similar to a wild-type mouse.)

of ATRN and MGRN1 from the perspective of pigment-type switching in Chapters 2 through 4, this study will return to the subject of spongiform neurodegeneration in Chapter 5, in which insights from studies in the pigment model system will be applied to build and test a hypothesis regarding the underlying mechanism of spongiform change.

Characteristics of spongiform neurodegeneration in human disease

Spongiform neurodegeneration (also referred to as spongiform encephalopathy or spongiform change) is defined as the appearance of membrane-bound vacuoles within the neuropil; that is, within the dense meshwork of axonal and dendritic processes (and embedded cell bodies) of the cells of the nervous system (Masters and Richardson, 1978). These vacuoles typically become larger and more numerous as disease progresses, displacing normal cell contents and presumably disrupting normal cellular processes. Human spongiform neuroencephalopathies are uniformly fatal. Among these, the canonical examples of spongiform neuropathology are the various transmissible spongiform encephalopathies (TSEs), which are understood to result from the spread of an infectious conformational form of the prion protein; however, histopathologically similar spongiform change occurs in other diseases and it can be induced in several experimental mouse model systems by genetic means, as discussed below. From the perspective of public health, understanding the mechanism of this peculiar neuropathology is of considerable interest because of the devastating consequences of the various spongiform pathologies on their human (and animal) victims. As a scientific puzzle, spongiform change offers one paramount challenge: to understand the disease, one must explain how the abnormal vacuolar membranous compartments arise. This gives the investigation of spongiform change a tractably delimited focus, unlike many other neuropathologies for which the phenomenon to be

explained is, broadly, “cell death.” While a great deal has been learned about the characteristics of dying neurons in other pathologies, it is often difficult to know whether the common mechanisms so frequently uncovered (such as apoptotic and/or autophagic cell death, oxidative stress, and synaptic dysfunction) represent specific disease pathways or are merely common end-stage characteristics of distressed neurons. Obviously, if an ultimate goal of neurodegeneration research is to identify etiologically important points for intervention in specific disease pathways, then the earlier disease-specific events are especially important to understand. In the case of the spongiform encephalopathies, the defining disease-specific event is the formation of the spongiform vacuole itself; therefore, the major question to be asked is, what is the origin of the abnormal membrane that accumulates to become a vacuole? Some light can be shed on this question by considering the best-characterized examples of spongiform encephalopathies, the prion-related TSEs.

Spongiform degeneration in transmissible spongiform encephalopathies

Prion-related disorders provide classic examples of human spongiform encephalopathy. The first of these disorders to be described was Creutzfeldt-Jakob disease (CJD)(Creutzfeldt 1920; Jakob 1921), which occurs sporadically in the population at a frequency of about 1:1,000,000 persons, and also in a rare, dominantly inherited fashion in a few identified families (Masters *et al.*, 1978, Brown *et al.*, 1987, Will, 1993). Progressive spongiform neurodegeneration, astrogliosis and microglial activation with neuronal loss, and the extracellular accumulation of proteinacious amyloid plaques are the classical pathological hallmarks of CJD (Masters and Richardson, 1978). The clinical manifestation of the disease typically begins with a prodromal constellation of mood and sleep disturbances, leading within a year to dementia, loss of motor control, torpor, and finally death (Roos *et al.*, 1973). The

disorder arises from a remarkable property of the prion protein (PrP), which is the major component of the CJD amyloid plaques (McKinley, Bolton, and Prusiner, 1983). As is now understood, the underlying cause of the disease is the spread of an abnormal conformational state of PrP within the nervous system (reviewed in Prusiner *et al.,* 2004a). This disease-related conformational state (referred to as PrP^{D} or PrP^{Sc}) is capable of inducing the conversion of normally folded cellular PrP^{C} molecules into its own toxic conformational state. A single founder inoculum of PrP^{D} can therefore seed a chain reaction of prion conversion into the PrP^{D} form, which resists degradation, undergoes oligomerization, and accumulates in the brain. The initial conversion of PrP from PrP^{C} to the pathological conformation can occur spontaneously (as is likely to be the case in victims of sporadic CJD) or as a result of mutations in the prion *(Prnp)* gene sequence in familial CJD and in the related disorders Gerstmann-Straussler-Scheinker disease (GSS) (Hsiao *et al.*, 1989) and fatal familial insomnia (FFI) (Goldfarb *et al.*, 1992). Remarkably, the ability of PrP^{D} to initiate disease is not necessarily limited to the body of its original host; PrP^{D} can act as an infectious agent, spreading from one individual to another via ingestion or other exposure. The realization of this fact grew out of investigations of an obscure disease, kuru, which once afflicted the Fore people of the highlands of Papua New Guinea (Liberski and Brown, 2004). This spongiform encephalopathy (recognized to bear close histopathological resemblance to CJD) was transmitted through the population by the cannibalistic funerary rites of the Fore people, who became infected with PrP^{D} by consuming the brains of their dead (kuru-infected) kinsmen. While the kuru epidemic among the Fore has ceased along with their traditional funerary cannibalism, prion infection has become a matter of significant public health concern ever since the British bovine spongiform encephalopathy (BSE) outbreak of the 1990s. This epidemic of prion disease spread widely among the British cattle population as a result

of the industrial use of bovine slaughterhouse remnants in cattle feed (reviewed in Wells and Wilesmith, 2004). Subsequent ingestion of "mad cow disease-" infected meat products spread prion disease to human consumers, causing a variant form of CJD (vCJD). Infectious prion disease is also endemic in domestic sheep, where it is known as scrapie, and in several North American populations of deer and elk, in which it causes a syndrome known as chronic wasting disease (CWD) (reviewed by Prusiner *et al.*, 2004b).

Work by many labs has elucidated many aspects of the PrP conversion process, including structural features of cellular and disease-related PrP, the kinetics and characteristics of PrP^D conversion, the intracellular trafficking and post-translational modifications of PrP, and the contributions of various regions of the protein to PrP^D formation. However, how the spread of PrP^D leads to the characteristic syndrome of neurodegeneration of prion disease is still poorly understood. It is clear that spongiform neurodegeneration is essentially a "gain-of-function" phenotype of the PrP^D conformer itself, and not a result of the loss of PrP^C functionality, as *Prnp* knockout mice do not develop neurodegeneration (reviewed by Flechsig *et al.*, 2004). $Prnp^{-/-}$ mice lack any overt neurodegenerative phenotype (although subtle behavioral effects can be demonstrated), a fact which has significantly hindered progress toward identifying the physiological function(s) of PrP^C and thus determining the likely pathogenic mechanism of PrP^D. In the absence of strong genetic data to guide investigators, interaction studies have provided a default starting point for exploration of the functions of PrP^C, and the result has been a steady proliferation of studies reporting interactions between PrP and myriad putative interaction partners as dissimilar as (for example) tubulin, heat shock proteins, complement proteins, metalloproteases, RNA, and the Alzheimer-related peptide Aβ (Petrakis and Sklaviadis, 2006; Costa *et al.*, 2009; Osiecka *et al.*, 2009; Satoh *et al.*, 2009; Chen,

Yadov, and Surewicz 2010; Erlich *et al.*, 2010, Silva *et al.*, 2010). The diversity of identified interactors has fueled a similarly wide range of hypotheses about the physiological function of PrP, with various groups suggesting roles for PrP in metal binding, cell survival signaling, synaptic transmission, immune functions, defense against oxidative stress, and other pathways (for recent reviews see Hu *et al.*, 2008; Westergard, Christensen, and Harris, 2007; Hu, Rosenberg, and Stuve, 2007;Aguzzi, Baumann, and Bremer, 2008).

Whatever the physiological function of PrP^C, it has become clear that trafficking and membrane localization of the protein are important both for the conversion of PrP^C to PrP^D and for the subsequent induction of pathological changes by the abnormal conformer. Trafficking studies have demonstrated that nascent PrP travels through the secretory pathway, acquiring N-linked glycosylation modifications and a glycophosphatidylinositol (GPI) anchor as post-translational modifications on the way (Campana, Sarnataro, and Zurzolo, 2005). Once PrP arrives at the cell surface (to which it is held by the GPI anchor) it undergoes repeated rounds of endocytosis and recycling to the plasma membrane before traveling along the endosomal/lysosomal pathway for degradation (Reviewed by Harris *et al.*, 2004). Secretion of PrP to the cell surface is necessary for conversion to PrP^D, suggesting that conversion may take place on the plasma membrane or within endosomal compartments. Whereas normal trafficking of PrP is necessary for its conformational conversion, the topological localization of PrP to membrane appears to be important for disease progression as mutant PrP without its GPI anchor can convert to the PrP^D conformational state and propagate in mice but does not cause classical neuropathology (Campana *et al,* 2007). Conversely, a mutant PrP that adopts an abnormal transmembrane localization has been shown to underlie a particular form of GSS, perhaps as a result of its altered membrane association (Hegde *et al.*, 1998).

Histopathological and ultrastructural studies of prion-infected brains reveal a characteristic suite of membranous abnormalities within the affected cells (reviewed by DeArmond *et al.,* 2004; Liberski, 2004; Peden and Ironside, 2004). The vacuoles themselves are membrane-bound structures of approximately 5-25 μm in diameter, sometimes containing cellular debris and membrane fragments (Figure 1.2). Like other neurodegenerative diseases, prion diseases exhibit characteristic patterns of neuronal subpopulation vulnerability, with the distribution and severity of vacuolation in the brain dependent on both the "strain" of the initiating PrP^D prion (which is considered to reflect the protein's particular conformational form) and by the host PrP genotype. Some vacuoles are apparently bounded by the plasma membrane and are typically interpreted as swollen dendritic processes, which appear to be largely cleared of cytoplasmic contents. Other vacuoles are membrane-bound structures occurring within cytoplasm, and are of uncertain origin. Because these vacuoles can contain

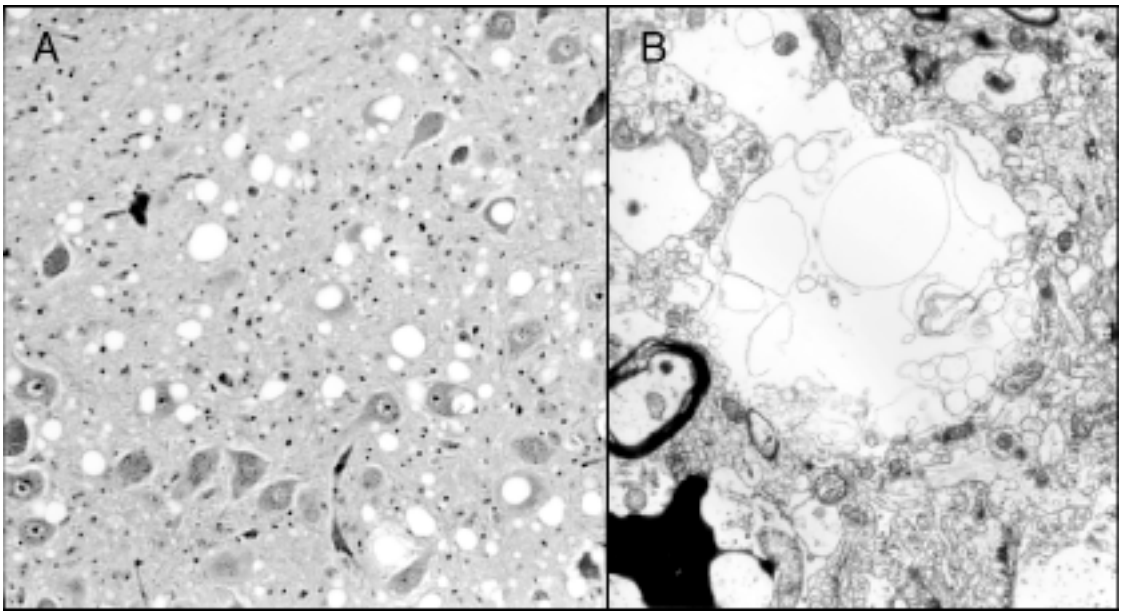

Figure 1.2. Histopathology of prion disease. A: Spongiform vacuoles from brain of a goat with scrapie. B: Ultrastructural appearance of spongiform vacuole of CJD. Images used with permission from Liberski, 2004.

large inclusions (such as damaged mitochondria) and may appear to have a double-layered peripheral membrane, some have suggested that autophagosomes may contribute to the formation of spongiform vacuoles. In addition to vacuoles, other membranous abnormalities are typically observed in prion diseases. Abnormally long invaginations of the plasma membrane, resembling extended caveolar cisternae and labeled with caveolin protein, have been reported by several groups and may reflect an abnormality in caveolar endocytosis. Another feature reported to accompany many different types of prion disease is the appearance of minute "tubulovesicular bodies" in the prion disease-affected brain tissue (Liberski *et al.*, 2008) and in prion-infected cultured cells (Manuelidis *et al.*, 2007). These enigmatic spherical or ovoid structures are 25-35 nm in size, and are not labeled by anti-PrP antibodies.

Retrovirus-induced spongiform neurodegeneration

Infection with certain retroviruses causes spongiform neurodegeneration. In humans, spongiform change appearing very similar to that seen in prion disease occurs in patients with HIV-associated dementia (Artigas *et al.*, 1989), but PrP^D is not detectable in the brains of these patients (Goldwater and Paton, 1989). In mice, spongiform change histopathologically indistinguishable from prion encephalopathy is caused by several members of the murine leukemia virus (MuLV) family (*e.g.*, see Brooks *et al.*, 1979; Gravel, Kay, and Jolicoeur, 1993; Takase-Yoden and Watanabe, 1997; Choe *et al.*, 1998; reviewed by Gomez-Lucia, 2005), again without detectable involvement of PrP^D (Jolicoeur, Masse, and Kay, 1996).

Spongiform degeneration in PI(3,5)P2 mutants

Phosphatidylinositol (3,5) diphosphate ($PI[3,5]P_2$) is a low-abundance signaling lipid that is important for a variety of endosomal trafficking processes in yeast and

metazoa. According to the current understanding of this molecule, $PI(3,5)P_2$ is produced on the surface of endosomal compartments, where it mediates interactions between membrane proteins and trafficking effectors (Dove *et al.*, 2009). In yeast, a trio of interacting proteins named Fab1p, Fig4p, and Vac14p are required to produce $PI(3,5)P_2$ and deletion of any of them results in a distended vacuole phenotype (Odorizzi, Babst, and Emr, 1998; Bonangelino *et al.*, 2002; Duex *et al.*, 2006). (The yeast vacuole is a large membrane-bound organelle which has no exact counterpart in mammals but which shares features of mammalian late endosomes and lysosomes.) In mammals, Fab1 has been shown to occupy the surface of early and/or late endosomes (Ikonomov, Sbrissa, and Shisheva, 2001; Rutherford *et al.*, 2006) and colocalize with Vac14, suggesting that the entire complex is active on endosomes in a similar manner to that in yeast. Spontaneous mutations in *Fig4* or *Vac14* (the *pale tremor* and *infantile gliosis* mutants, respectively) cause spongiform neurodegeneration in mice (Chow *et al.*, 2007; Jin *et al.*, 2008), implicating disruption of a $PI(3,5)P_2$-dependent endosomal trafficking process in the formation of spongiform vacuoles. Cytoplasmic vacuoles marked with the late endosome and lysosome marker, LAMP2, arise in cultured cells from *Vac14* and *Fig4* mutant mice, suggesting that late endosomal or lysosomal compartments contribute to the spongiform vacuoles in these mutants (Chow *et al.*, 2007; Zhang *et al.*, 2007). More than one endosomal trafficking pathway is disrupted by impairment of $PI(3,5)P_2$ production as cells isolated from *Vac14* null mutant mice show defects in the endosome-to-Golgi retrograde trafficking of M6PR, as well as an apparent impairment of endo-lysosomal trafficking of cathepsin D (Zhang *et al.*, 2007). Further evidence of a defect in the endo-lysosomal axis comes from the dilute pigmentation phenotype shared by the *pale tremor* and *infantile gliosis* mutants, the former of which has been shown to show a “clumped melanosome” abnormality suggestive of a lysosomal/melanosomal biogenesis defect

(Chow *et al.*, 2007). Other trafficking deficiencies may be downstream of these defects in endo-lysosomal maturation or processing. Both *Fig4* and *Vac14* null mutants show impaired autophagy (Ferguson, Lenk, and Meisler, 2009), which is a lysosome-dependent process. In humans, *FIG4* mutations cause spongiform pathology in a form of Charcot-Marie-Tooth disease. In cells cultured from these patients, organelle trafficking is disrupted as a consequence of physical obstruction by vacuoles (Zhang *et al.*, 2008).

$PI(3,5)P_2$ mutants illustrate that defects in endosomal membrane trafficking can be associated with spongiform neurodegeneration. Identifying the precise source of the abnormal membrane that accumulates to form the spongiform vacuole, however, is not necessarily easy. The multiple trafficking defects seen in these mutants underscore the extreme degree of interconnection of intracellular trafficking pathways as well as the potential difficulty of pinning down a singular "identity" of an abnormal membrane such as that seen in spongiform neurodegeneration. In contrast to vacuolar defects such as lysosomal storage disorders that are caused by a defect at the end of a trafficking pathway, spongiform neurodegeneration causes apparently "empty" vacuoles that cannot be identified as any particular cellular compartment on the basis of their lumenal contents. The observation that a "compartment specific marker" such as LAMP2 labels the vacuoles in *Fig4* and *Vac14* mutants can be interpreted in multiple ways. One interpretation would take the presence of the marker at face value and conclude that the LAMP2-labeled vacuoles represent abnormally swollen late endosomes or lysosomes. Assuming this interpretation is correct, swelling could be the result of a general block at some point in endo/lysosomal maturation, meaning that the affected compartments could continue to receive, but not to process, new cargo, resulting in hypertrophy of their limiting membranes. Alternatively, specific populations of cargo molecules may be accumulating in otherwise normal late

endosomes or lysosomes, not as the result of a general block in endolysosomal maturation or processing but because they specifically require PIP(3,5)P_2 either to progress toward the lysosome or to be reclaimed by a recycling or retrograde trafficking pathway. If one or the other of these mechanisms is correct and spongiform vacuoles are in fact abnormal late endosomes or lysosomes, these structures could act as sinks for any number of trafficking factors, the sequestration of which could have an effect on diverse trafficking pathways. It is important to note, however, that transmembrane proteins such as LAMP2 are themselves dependent on membrane protein trafficking pathways for their normal localization. The LAMP2 labeling the vacuoles of *Fig4* and *Vac14* mutant cells could therefore signify not an endolysosomal identity of the abnormal compartment, but rather an aberration in the trafficking of LAMP2 itself. If this is the case, one would look for an "identity" of the abnormal membrane by considering the biosynthetic pathway of LAMP2 and determining the point at which its normal progression is halted, or the compartment to which it is rerouted. Finally, it may be that, from the point of view of the cellular trafficking machinery, abnormal membrane and its cargo may be, in a biologically meaningful sense, without an identity. PI(3,5)P_2 is thought to be one of the signals that, in combination with membrane cargo proteins and trafficking regulators, provide the combination of inputs to allow "coincidence detectors" to recognize compartment identity (Dove *et al.*, 2009). One may imagine the system-wide loss of such a signal could result in the general accumulation of all manner of membranes (and associated cargo) that cannot generate the signals to fall within the purview of any particular processing system. These caveats aside, the discovery of spongiform encephalopathy in PI(3,5)P_2 regulatory mutants is an exciting advance and it focuses attention on the late endosome/lysosome axis as an area of interest in explaining spongiform neurodegeneration.

Spongiform neurodegeneration in ATRN mutant rodents

Mouse and rat mutants bearing mutations in *Atrn* are well-characterized models of spongiform encephalopathy. Spongiform change morphologically indistinguishable from that found in prion disease was first described in the *zitter* mutant rat by Rehm and colleagues (1982) and subsequently characterized at the ultrastructural level in a series of papers by Kondo and colleagues (Kondo *et al.*, 1991; Kondo et al., 1992; Kondo et al., 1995; Kondo, Sato, and Nagara, 1991). As *zitter* mapped to rat chromosome 3(which bears a region of homology to the prion locus in mice), it was suspected that *zitter* might be a mutation in *Prnp.* However, no abnormalities were found in the coding sequence of *zitter* rat *Prnp* and there was no accumulation of aberrant PrP^{D} (Gomi *et al.*, 1994), suggesting that the causative mutation of *zitter* was a separate point of entry into a spongiform degenerative pathway. A similar encephalopathy was identified in the *mahogany* mutant mouse gene (He *et al.*, 2001, Gunn *et al*, 2001, Bronson *et al.*, 2001), which was known to be caused by a mutation in the *attractin* (*Atrn*) gene (see chapters 2 and 3 for discussion of this protein). At about the same time it was confirmed that the *zitter* phenotype was also due to a null mutation at the *Atrn* locus (Kuramoto *et al*, 2001), as was the spongiform phenotype of the *myelin vacuolation* (*mv*) rat (Kuwamura *et al.*, 2002).

Clinically, *Atrn* null animals present with tremor and, in mice, hyperactivity (Kuramoto *et al.*, 2001; Gunn *et al*, 2001). Light microscopy reveals a classical spongiform encephalopathic appearance, with vacuoles becoming more numerous and larger with age. By two months of age, vacuolation is noticeable in *Atrn null* homozygotes and the pathology spreads to affect most regions of the brain with extensive vacuolation by 9 months (Bronson *et al.*, 2001). Some apoptotic neuron death has been reported to occur in the brainstem (Ookohchi *et al.*, 1997), although it is not clear that extensive neural death occurs in *Atrn* mutant brains. Ultrastructurally,

vacuoles occur within axons, dendrites, and soma of neurons, as well as within the cytoplasm of some astrocytes and oligodendrocytes (Kondo *et al.,* 1995; Bronson *et al.,* 2001; He *et al.,* 2003). Oligodendrocytes evidently experience severe defects in membrane biosynthesis or trafficking, as these cells accumulate abnormal "whirled" membrane stacks within the cytoplasm in association with the nucleus, lysosomes, and other membrane-bound organelles (Kondo *et al.,* 1991). Possibly as a consequence of this oligodendroglial dysfunction, myelination is slow and aberrant in *zitter* rats (Kondo *et al.,* 1992) with abnormal and split myelin sheaths becoming widespread as myelination of the CNS progresses. Some apparent "spongiform vacuoles" are therefore actually lacunae that open between concentric layers of the myelin sheath (Kuwamura *et al.,* 2002). Apparently as a result of difficulties in myelin production and /or maintenance, hypomyelination of the CNS is observable from an early age in *Atrn* mutant mice and rats (Kondo *et al.,* 1992; Kuramoto *et al.,* 2001).

Studies of the pathological consequences of *Atrn* deficiency have mostly focused on evaluating oxidative stress as a potential disease mechanism. In cultured cells, ATRN has a protective effect against reactive oxygen species (ROS) such as peroxide (Muto and Sato, 2003) and against the neurotoxin MPP+, which causes the increased production of ROS by impairing mitochondrial function (Paz *et al.,* 2006). In addition, the antioxidant enzyme superoxide dismutase 1 (SOD1) is over-expressed in *zitter* brains, suggesting a response to elevated ROS (Gomi, Ueno, and Yamanouchi, 1994). $Atrn^{mg\text{-}3J/mg\text{-}3J}$ null mutant mouse brain extracts show elevated levels of protein carbonyls, which is also consistent with an increase in oxidative stress (Sun, Johnson, and Gunn, 2007). A likely consequence of this oxidative stress has been noted in the substantia nigra, in which dopaminergic neurons have been specifically noted to degenerate (Nakadate *et al.,* 2006). Loss of dopaminergic neurons was reduced by treatment with the antioxidant vitamin E (Ueda *et al.,* 2005). It seems likely that the

oxidative stress observed in *Atrn* mutant cells and tissues is related to the impaired function of mitochondrial complex 4 observed in *Atrn*$^{mg\text{-}3J/mg\text{-}3J}$ brain extracts (Sun, Johnson, and Gunn 2007). While it is clear that *Atrn* mutant cells suffer from oxidative stress, it is not known whether the oxidative stress contributes to spongiform neuropathology, is a cause of it, or occurs independently through a separate molecular pathway. As oxidative stress is a common feature of many non-spongiform neurodegenerative diseases, the elevated ROS activity seen in *Atrn* mutants may simply be a general response of stressed neurons rather than a major underlying factor leading to vacuolation.

Spongiform change in Mgrn1 mutant mice

Mice homozygous for a null mutation at the *mahogunin ring-finger 1 (Mgrn1)* locus develop a spongiform encephalopathy that appears almost identical to that seen in *Atrn* mutants, although the progression of vacuolation is somewhat delayed compared to the *Atrn* phenotype (He *et al.*, 2003). Vacuolation spreads throughout the brain of affected animals and *Mgrn1* mutant brain tissue shows similar changes to *Atrn* mutants in mitochondrial function and ROS damage (Sun, Johnson, and Gunn 2007). The similar encephalopathic phenotype of these two mutants is especially remarkable as *Atrn* and *Mgrn1* mutant mice were originally identified because of another shared phenotype: hyperpigmentation. As reflected in the names given the first *Atrn* and *Mgrn1* mutants identified (*mahogany* and *mahoganoid*, respectively), deficiency at either locus results in a darkened coat due to a reduction of yellow pigment production (see discussion of pigment-type switching below). By the time these mutants were recognized to develop spongiform change, genetic analysis of the two loci had already revealed a similar epigenetic placement of *mahogany* and *mahoganoid* in what is known as the pigment-type switching pathway (Miller *et al.*, 1997; for a recent review

of pigment-type switching see Walker and Gunn, 2010a). The identification of a second area of phenotypic overlap between *Atrn* and *Mgrn1* suggested strongly that *Atrn* and *Mgrn1* cooperate in a molecular pathway that operates both in the brain, where it is critically important for the prevention of spongiform neurodegeneration, and in the pigment cell, where it mediates pigment-type switching. This situation suggests that determining the mechanism by which *Atrn* and *Mgrn1* cooperate to control pigment-type switching in the pigment cell will simultaneously reveal the mechanism by which spongiform encephalopathy occurs in the brain. This is an extraordinary opportunity to study a neurodegeneration mechanism in a very tractable model system, as pigmentation biology benefits from over a century of investigation dating back to the dawn of modern genetics (Bennett and Lamoureaux, 2003). Therefore, this discussion now turns to what is known about *Atrn* and *Mgrn1* in the pigment-type switching system.

Pigment-type switching

Mice and other mammals produce melanin in two primary forms: a dark-brown or black form referred to as eumelanin, and a yellowish/reddish form known as pheomelanin. In the dorsal hair follicles of many mammals, including mice, the pigment-producing cells (melanocytes) switch production from eumelanin to pheomelanin at an early point in the hair growth cycle, depositing a subapical yellow band on an otherwise darkly pigmented hair (Silvers, 1979). This pigment-type switching event gives rise to the subtle “brushed” appearance of the agouti phenotype of wild-type mice (Figure 1.3A). In the ventral hair follicles of many species of mammals, the same pigment type-switching pathway is activated to produce the primarily pheomelanic belly fur exhibited by many mammals, contributing to a

cryptic, counter-shaded appearance valuable for camouflage (Millar *et al.*, 1995; Vrieling *et al.*, 1994).

The melanocortin-1 receptor and its ligands

The master regulator of pigment-type switching is the melanocortin 1 receptor (MC1R), a G-protein-coupled receptor (GPCR) expressed in melanocytes. In its active state, the MC1R signals through the stimulatory G-protein α subunit ($G\alpha_s$) to activate adenylyl cyclase, raising levels of the second messenger cyclic adenosine monophosphate (cAMP) (Figure 1.4), thereby activating a series of transcriptional events that support the production of eumelanin (discussed below). When MC1R is in its inactive state, cAMP levels are low and pheomelanin is produced. The phenotypes of *Mc1r* mutants illustrate the role of this receptor in pigment-type switching: mice carrying the continuously active *sombre* allele ($Mc1r^{E\text{-}so}$) or the hyperactive *tobacco darkening* allele ($Mc1r^{E\text{-}tob}$) have black coats (Figure 1.3B), while mice homozygous for an inactive truncation mutation (*extension*, $Mc1r^{e}$) are yellow (Figure 1.3C) (Robbins *et al.*, 1993). Similarly, loss-of-function *Mc1r* variants are associated with red hair in humans (Box *et al* 1997; Valverde *et al.*, 1995). The switch between the eumelanogenic and pheomelanogenic signaling states of the murine MC1R is normally mediated by the opposing effects of a pair of ligands: α-melanocyte signaling hormone (α-MSH) and agouti signaling protein (ASP) (Figure 1.4). Much of the fascination of the pigment-type switching system lies in the complex way these ligands modulate MC1R function.

The primary agonist of the MC1R, α-MSH, is produced in the skin by keratinocytes and melanocytes (Chakraborty *et al.*, 1996; Slominski *et al.*, 2000). It increases MC1R signaling through cAMP and protein kinase A (Cone *et al.*, 1993; Garcia-Borrón *et al.*, 2005) to activate genes required for pigment production (*e.g.*,

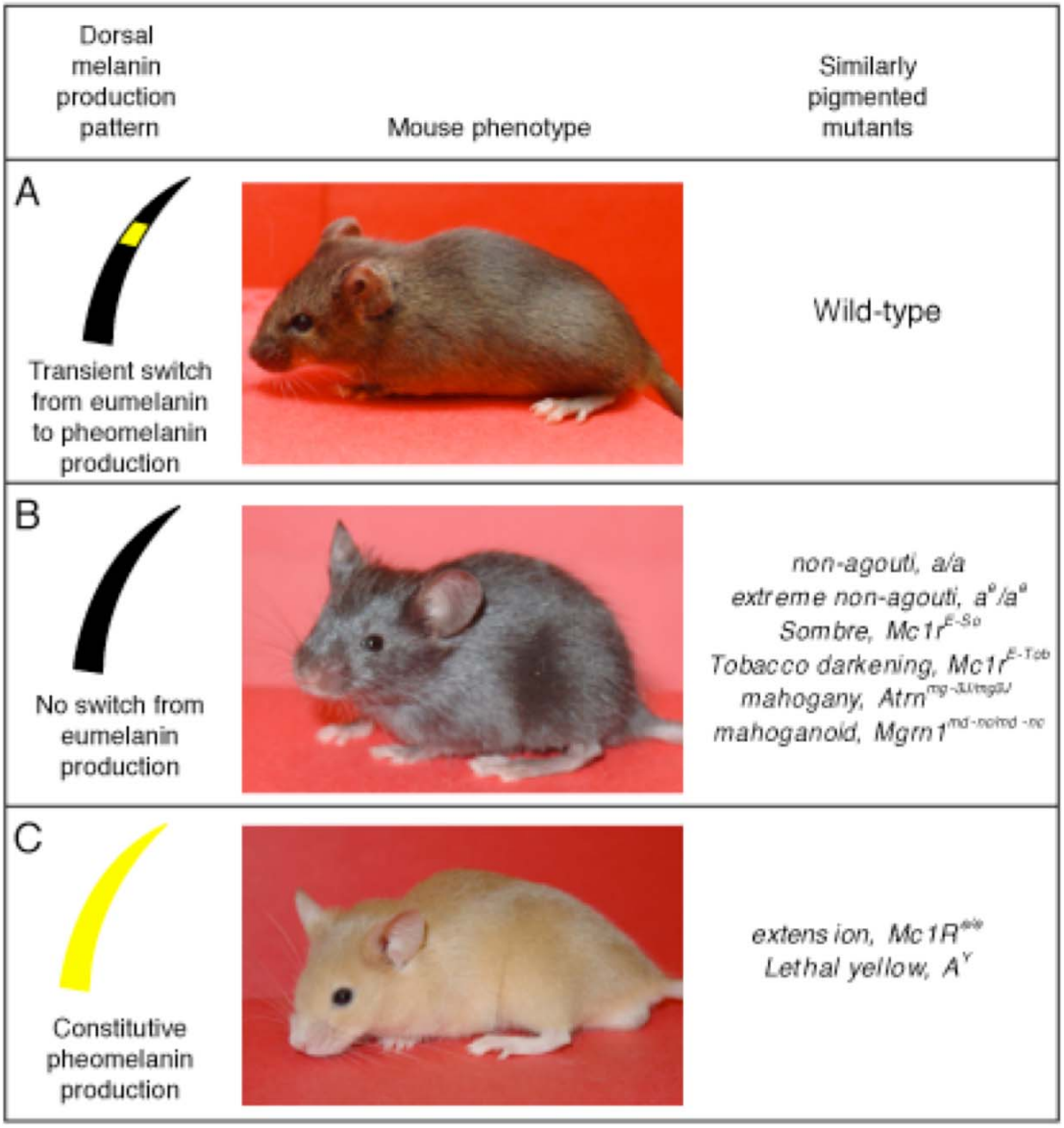

Figure 1.3. Coat color phenotypes of mouse pigment-type switching mutants. The wild type (agouti) pattern is caused by production of a subapical band of yellowish-red pheomelanin on an otherwise black (eumelanic) hair (A). Loss of eumelanin synthesis causes dark fur (B), while constitutive pheomelanin synthesis results in yellow fur (C).

Figure 1.4. A model of the pigment-type switching pathway. (A.) α-melanocyte stimulating hormone (α-MSH) enhances signaling through the melanocortin 1 receptor (MC1R), leading to GDP/GTP exchange by the stimulatory G protein subunit α ($G\alpha_s$) and liberation of GTP-bound $G\alpha_s$ from the G protein heterotrimer. Active, GTP-bound $G\alpha_s$ stimulates adenylyl cyclase (AC) to promote eumelanogenesis. (B.) The MC1R inverse agonist agouti signaling protein (ASP) binds to MC1R and the accessory receptor, attractin (ATRN) to inhibit Gαs activation and reduce signaling through AC, leading to pheomelanogenesis. Mahogunin ring finger 1 (MGRN1) interacts with MC1R and is required for ASP signaling.(C:.) Canine β-defensin 103 (β-D) can bind MC1R to inhibit ASP binding, promoting eumelanogenesis.

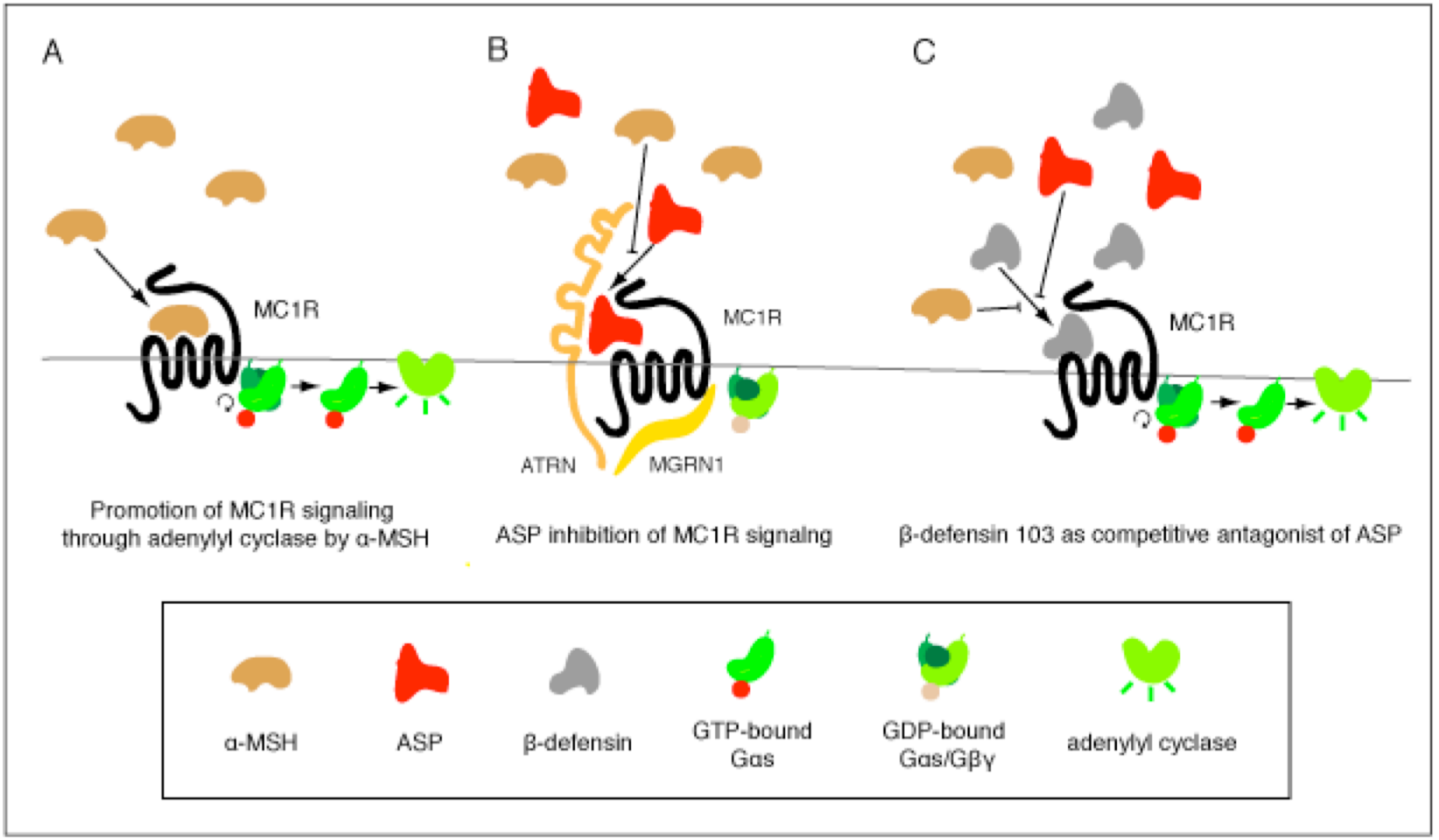
A
B
C
MC1R
MC1R
MC1R
ATRN
MGRN1
Promotion of MC1R signaling through adenylyl cyclase by α-MSH
ASP inhibition of MC1R signalng
β-defensin 103 as competitive antagonist of ASP
α-MSH
ASP
β-defensin
GTP-bound Gαs
GDP-bound Gαs/Gβγ
adenylyl cyclase

Tyr, *Tyrp1*, *Dct*) and melanosome biogenesis (*Pmel117*) and transport (*Rab27)*, largely through an effect on the master melanogenic transcription factor, MITF (Aberdam *et al*., 1998; Bertoletto *et al.*, 1998; Le Pape *et al.*, 2009; Levy, Khaled, and Fisher, 2006). This effect of α-MSH is reinforced by a positive feedback effect whereby α-MSH stimulus causes increased rates of translation of MC1R from a variant transcript (Rouzaud et al., 2003). The end result is that melanocytes treated with α-MSH become more dendritic and produce more eumelanin (Le Pape *et al*., 2008; Sakai *et al*., 1997). In humans, α-MSH is a critical promoter of MC1R function in pigmentation: rare mutations that result in loss of the α-MSH propeptide, proopiomelanocortin (POMC), cause red hair (Krude *et al.*, 1998). In mice, MC1R exhibits a significant level of constitutive activity, although administration of α-MSH does increase MC1R signaling (Cone *et al.*, 1993; Jackson *et al*., 2007; Sanchez-Mas *et al*., 2004). This constitutive activity of mouse MC1R appears to be sufficient to support eumelanin production, as indicated by the fact that the hairs of mice lacking POMC are only subtly yellower than those of wild-type mice (Slominski *et al*., 2005; Yaswen *et al*., 1999). Pigment-type switching thus appears to require a reduction of MC1R signaling below baseline levels, which normally occurs when the MC1R binds its second major ligand, ASP.

In mice, ASP is secreted by cells of the dermal papilla (a structure at the base of the hair follicle) during days 2-7 of the first hair growth cycle, partly as a response to BMP signaling (Bultman *et al*., 1992; Millar *et al*., 1995; Sharov *et al*., 2005). ASP competitively binds MC1R to inhibit the pro-eumelanogenic effects of α-MSH and promote the production of pheomelanin (Figure 1.4) (Blanchard *et al*., 1995; Lu *et al*., 1994), but its effect is not limited to antagonizing αMSH function (Hunt *et al*., 1995, Ollmann *et al*., 1998; Sakai *et al*., 1997). Pharmacologically, ASP is an inverse agonist of MC1R (Siegrist *et al*., 1997), binding the receptor not only to competitively

inhibit signaling by α-MSH but also to reduce the intrinsic signaling of MC1R to below constitutive levels. It is not clear whether the mechanistic basis of this inverse agonism is simply the stabilization of the receptor's inactive conformation or a more complex effect of alterations in MC1R trafficking, turnover, or post-translational modification. In addition to its effects on the activity of the MC1R proteins it binds, ASP also causes a reduction in the rate of new MC1R biosynthesis (Rouzaud *et al*., 2003), further depressing MC1R signaling. A recent microarray study demonstrated that ASP blocks the transcriptional effects of α-MSH and activates genes involved in morphogenesis and cell adhesion to cause a melanoblast-like appearance of the treated cells, suggesting that ASP promotes a functional de-differentiation of melanocytes (Le Pape *et al*., 2009). Interestingly, while genetic analyses confirm that all of ASP's effects on pigmentation are MC1R-dependent, some effects of ASP on melanocyte morphology *in vitro* have been reported to be cAMP independent (Hida *et al.*, 2009). In the absence of any known alternative ASP receptor, this suggests that some of the effects of ASP could involve a non-canonical pathway of MC1R signaling.

Genetic analysis of ASP function has benefited from the availability of a variety of interesting mouse mutant alleles. The fur of homozygotes for a null mutation (*a^e, extreme non-agouti;* Hollander and Gowen, 1956*)* is completely black (Figure 1.3B), reflecting constitutive signaling through the MC1R. The pigmentary role of *Mc1r* is epistatic to that of *agouti* as mice with loss-of function mutations for both *Mc1r* and *agouti* exhibit the yellow *$Mc1r^e$* coat color phenotype. Conversely, mice heterozygous for the *lethal yellow (A^y)* allele of *agouti* express ASP ubiquitously and are yellow, similar to *Mc1r* loss-of-function *extension* mutants (Figure 1.3C), reflecting continuous inverse agonism of the MC1R (Miller *et al.,* 1993). The *A* allele causes the classic agouti banding pattern on hairs across the entire pelage. The *A^{w-}* allele produces dorsal agouti-banded hairs and yellow belly hairs, the latter due to use

of an additional, ventral-specific promoter that drives constitutive expression of *ASP* in the ventrum (Millar *et al.*, 1995; Vrieling *et al*., 1994). This counter-shaded coloration pattern is widely found throughout the Mammalia, suggesting that A^w is the ancestral wild-type allele. Lastly, the *viable yellow agouti* allele, A^{vy}, provides an interesting model of epigenetic inheritance. The coat color of A^{vy} mice can range from agouti to completely yellow, reflecting variation in methylation of an intracisternal A particle (IAP) sequence inserted near the *agouti* locus (Duhl *et al*., 1994; Morgan *et al.*, 1999). This mutant has become a valuable model for studying epigenetic inheritance as *agouti* expression in a litter of pups tends to track maternal phenotype and can be influenced by maternal diet (Cropley *et al*., 2006). In addition to this well-characterized range of mutant *agouti* alleles in mice, variant *agouti* alleles cause distinct pigmentation phenotypes in other animals (Klungland and Vage, 2003). While the agouti-banding pattern is not seen in the hair of humans or other hominids, variations in *ASIP* have been associated with both hair and skin pigmentation traits in human populations (Bonilla *et al.*, 2005; Kanetsky *et al* 2002; Sulem *et al.*, 2008; Voisey *et al*., 2006)

Recently, Barsh and colleagues discovered a third ligand of the MC1R by mapping the "*K*" locus that determines dominant black coat color in dogs (Kerns *et al.*, 2004; Candille *et al*., 2007). Surprisingly, it turned out to be the gene that encodes β-defensin 103, a member of an ancient family of small anti-bacterial peptides best known for their role in the innate immune system. While no murine β-defensin alleles are known to cause pigmentation phenotypes, transgenic mice expressing either the black (K^B) or the yellow (k^y) canine allele had predominantly black coats with small patches of agouti-banded hairs. Biochemical investigations showed that β-defensin, like ASP, can bind MC1R to compete against α-MSH binding, without activating the cAMP pathway (Figure 1.4). This suggests that β-defensin's mode of action in the

pigment cell may involve exclusion of ASP from the binding site or interference with the activity of the ASP co-receptor, attractin (described below).

Accessory proteins for pigment type switching: ATRN and MGRN1

Mahogany (mg) and *mahoganoid (md)* were identified in the 1960s as separate loci required for transduction of the ASP signal (Lane, 1960; Lane and Green, 1960; Phillips, 1963). Genetic studies demonstrated that loss-of-function mutations at either of these loci resulted in dark fur in homozygotes, even in the presence of the ubiquitously overexpressed A^y allele of *agouti*. The phenotypic expression of either mutation depends upon *Mc1r*, however, in that $Mc1r^{e/e}$ mice are yellow regardless of their *mahogany* or *mahoganoid* genotype (Miller *et al.*, 1997). The similar phenotype and identical epistatic placement of these genes in agouti-melanocortin receptor signaling strongly suggested that their products work together to achieve a particular step in the pigment type-switching pathway.

The *mahogany* locus was identified by positional cloning (Gunn *et al.*, 1999; Nagle *et al*., 1999) as the mouse ortholog of the human *attractin (ATRN)* gene, which was named for its role in mediating clustering of immune cells (Duke-Cohan *et al.*, 1998). Murine *Atrn* encodes a type I (single-pass) transmembrane protein with a predicted molecular weight of ~160 kDa. Its large extracellular/lumenal domain contains EGF-like repeats and plexin/semaphorin/integrin motifs characteristic of extracellular receptors involved in cell migration, adhesion, or other developmental processes, as well as a CUB domain, a C-type lectin domain, and a predicted kelch propeller (discussed in chapter 3; see Figure 3.1). The intracellular/cytoplasmic tail of ATRN is short compared to the rest of the protein (128 amino acid residues out of 1428) and contains no named domains. Expression of full-length wild-type mouse *Atrn* under the control of melanocyte- or keratinocyte-specific promoters demonstrated

that ATRN is required in melanocytes to rescue the pigment-type switching phenotype of *Atrn* null mutant mice (He *et al.*, 2001). This, along with its transmembrane topology, suggested that ATRN might serve as an accessory receptor for ASP (Figure 2.2), and He *et al.* (2001) used surface plasmon resonance to detect an interaction between ATRN and the N-terminal region of ASP. This interaction had an estimated Kd of ~0.7 μM (He et al., 2001), which is in the range of values reported for other low-affinity or accessory receptors. Because MC1R binds to the C-terminal portion of ASP (Ollmann and Barsh, 1999; Willard *et al.*, 1995), these results suggest that ATRN and MC1R may simultaneously bind opposite ends of ASP to form a MC1R-ASP-ATRN ternary complex. While a physical association between ATRN and MC1R has not been reported to date, their paralogs (attractin-like 1 and the MC4R), have been shown to interact with each other (Haqq *et al*., 2003) and both ASP and its paralog, agouti-related protein (AGRP), can bind MC4R (Chai *et al*., 2005). These observations suggest that ATRN and MC1R are likely to be interacting partners, and support the consensus view that ATRN is an accessory receptor for ASP.

ATRN's role as an accessory receptor appears to go beyond the mere additive stabilization of the MC1R-ASP interaction as it is otherwise difficult to explain how the loss of ATRN's relatively weak ASP-binding ability could completely abolish pigment-type switching, even in mice overexpressing ASP. One possibility is that ATRN binds the N-terminus of ASP in a way that greatly increases the affinity of the bound ASP for MC1R. It is interesting to note that the N-terminus of AGRP inhibits the interaction of AGRP with the MC4R and is actually cleaved off by proprotein convertase 1 to release the pharmacologically active C-terminal peptide (Creemers *et al.*, 2006). ASP is not known to undergo any similar cleavage event, suggesting that if the N-terminal end of ASP has a similar autoinhibitory effect on MC1R binding, sequestration of this end of the molecule by ATRN could be a way of relieving the

inhibition. Another possibility is that ATRN, when bound to ASP and MC1R in a ternary complex, couples MC1R to a downstream event such as lysosomal trafficking of the ternary complex, recruitment of additional inhibitory factors, or activation of a non-canonical signaling pathway. This would make the effect on MC1R of binding both ASP and ATRN qualitatively different from the effect of binding ASP alone, explaining the absolute requirement for ATRN in pigment-type switching. It is noteworthy in this respect that *Atrn* null mutant melanocytes have a normal cAMP response to ASP treatment but exhibit an impairment of the cAMP-independent ASP-induced morphological changes reported by Hida *et al.* (2009). These morphological changes also require the N-terminal portion of ASP, which binds ATRN. Taken together, these observations suggest that ATRN does more than simply stabilize an "inactive" conformation of MC1R. Likewise, ASP seems to do more than simply "switch MC1R off," as shown by the fact that ASP-overexpressing mice are darker (rather than lighter as one might expect) in the absence of functional MC1R (Jackson *et al.*, 2007; Ollmann *et al*., 1998). The explanation of this counterintuitive situation seems likely to involve ATRN.

The second major accessory locus required for pigment-type switching, *mahoganoid*, encodes a novel RING-domain-containing protein (He *et al*., 2003; Phan *et al*., 2002). Now referred to as *Mahogunin ring finger 1* (*Mgrn1*), its gene product belongs to the large class of E3 ubiquitin ligase proteins, which serve as specificity factors in catalyzing the transfer of the multifunctional ubiquitin tag onto target proteins, as either single units or polyubiquitin chains (reviewed by Deshaies and Joazeiro, 2009). The consequences of ubiquitination are diverse and include targeting proteins for proteasomal degradation or trafficking through the endo-lysosomal protein degradation pathway. Ubiquitination can also alter the conformation or accessibility of sequences in target molecules to mediate changes in active state, subcellular

localization, and/or participation in protein complex formation (for recent reviews see Acconcia *et al.*, 2009; Ardley and Robinson, 2005; Chen and Sun, 2009; Li and Ye, 2008; Nandi *et al.*, 2006; Wickliffe *et al.*, 2009). This diversity of effects makes E3 ligases important players in development, cell division, cell signaling, and disease pathways.

Given the many roles of E3 ubiquitin ligases, exactly how *Mgrn1* mediates pigment-type switching has remained a fertile field for speculation. A long-standing hypothesis is that MGRN1 may ubiquitinate MC1R to direct its lysosomal degradation. This hypothesis is compatible with observations that ASP treatment reduces MC1R protein levels in cultured melanocytes and in rat skin (Rouzaud *et al.*, 2003; Yang *et al.*, 2004). A strong link between MGRN1 and the endo-lysosomal trafficking pathway has emerged from identification of the tumor susceptibility gene 101 product (TSG101) as a target of MGRN1-mediated ubiquitination (Jiao *et al.*, 2009a; Kim *et al*., 2007). TSG101 is a member of the Endosomal Complex Required for Trafficking I (ESCRT-I) group of proteins, which act at the surface of incipient multivesicular bodies (MVBs) to sort monoubiquitinated transmembrane proteins into the lumenal vesicles of the MVB (reviewed by Saksena *et al*., 2007, and discussed in greater detail in Chapter 5). The contents of the lumenal vesicles are subsequently transported to the lysosome for degradation. MGRN1-dependent ubiquitination of TSG101 appears to be important for its function: upon depletion of MGRN1 in HeLa cells, TSG101-mediated lysosomal trafficking of the epidermal growth factor receptor was impaired (Kim *et al.*, 2007). In the mouse brain, *Mgrn1* deficiency led to the accumulation of insoluble, multiubiquitinated TSG101 (Jiao *et al.*, 2009a).

Whether MGRN1 acts through TSG101 in the melanocyte to promote pigment-type switching remains an open question. Because TSG101 knockout mice are inviable as homozygotes (Wagner *et al*., 2003), the consequences of loss of

TSG101 function on pigment production are not known. If pigment-type switching does require a MGRN1-dependent function of TSG101, this would suggest that ASP-mediated inverse agonism of MC1R requires lysosomal trafficking, most likely of the MC1R itself. It is interesting to note that MGRN1 could hypothetically promote lysosomal trafficking of MC1R either by monoubiquitinating MC1R, or at the level of regulating TSG101/ESCRT activity. These hypotheses are not mutually incompatible. A scenario incorporating both roles for MGRN1 is an intriguing object for contemplation as it would represent a novel role for a single ubiquitin ligase as an integrator of the "supply" (target availability) and "demand" (ESCRT complex activation) sides of the lysosomal protein degradation pathway. Determining whether lysosomal trafficking of the MC1R contributes to pigment type-switching, and if so, how MGRN1 acts to enable this trafficking event, stand as important questions.

While hypotheses linking the role of MGRN1 in pigment type-switching to lysosomal trafficking are appealing, they have been challenged by a line of evidence suggesting that MGRN1 may directly disrupt MC1R signaling by uncoupling the receptor from its G proteins. Perez-Oliva *et al*. (2009) recently reported that, in HEK293T cells, transient expression of MGRN1 significantly decreased signaling by MC1R without altering its cell surface expression or changing its rate of turnover. Further experimentation established that MGRN1 binds the MC1R and that this decreases the interaction of MC1R with the Gαs, thereby uncoupling the receptor from its downstream effector, adenylyl cyclase (Figure 1.4). Overexpression of Gαs counteracted the effect of MGRN1 on MC1R signaling, suggesting that MGRN1 and Gαs may compete for a binding site on MC1R, although these data are also compatible with MGRN1 stabilizing the MC1R in an inactive conformation or targeting MC1R to an intracellular location less conducive to Gαs interaction As Perez-Oliva *et al*. (2009) showed that MGRN1 interacted with, but did not appear to

ubiquitinate, the MC1R, what role (if any) the E3 ligase ability of MGRN1 plays in this proposed regulatory mechanism is a mystery. Interestingly, Perez-Oliva *et al.* reported that when they immunoprecipitated MC1R from cells transfected with MGRN1, immunoblotting the precipitated proteins with an anti-ubiquitin antibody revealed the presence of a high molecular weight, ubiquitinated protein of unknown identity. The identity of this mystery molecule, which seems likely to be both an interaction partner of the MC1R and a ubiquitination target of MGRN1, is an obvious point of interest. It is even possible that the mystery molecule could turn out to be attractin, which is approximately the same molecular weight as the observed band. Should attractin turn out to be a ubiquitination target of MGRN1, the close phenotypic overlap and similar epistatic mapping of *Atrn* and *Mgrn1* would probably be explained: the reason would likely be that *Mgrn1* mutants display all the phenotypes of *Atrn* mutants because ATRN has to be ubiquitinated by MGRN1 to function. However, even this hypothetical result would leave open many questions regarding the significance of the ubiquitination event to the Gαs uncoupling mechanism, as well as raising questions about whether MGRN1-dependent ubiquitination of ATRN could point to a role for ATRN in the endosomal/lysosomal trafficking-related mechanisms discussed previously.

As the discussion above indicates, when one considers ATRN or MGRN1 individually, several plausible hypotheses may be proposed to explain their effects on signaling through the MC1R. As a starting point for investigation, the challenge is to synthesize these hypotheses with the relevant genetic, biochemical, and bioinformatics data, to develop a working hypothesis that places ATRN and MGRN1 together as partners in MC1R regulation. To that end, this study turns now to bioinformatic and genetic analyses of ATRN and its homologs.

CHAPTER TWO

BIOINFORMATIC AND GENETIC STUDIES OF ATTRACTIN HOMOLOGS[1]

Chapter Overview

Bioinformatic analysis of a gene of interest is a useful first step towards understanding its function. In this chapter, I show that murine ATRN is one member of an ancient family of similar receptor-like proteins and infer a likely conserved physical and functional interaction between MGRN1 and members of this family. I also show that a second member of the ATRN-like protein family (attractin-like 1 or ATRNL1) is capable of rescuing the phenotypes of Atrn mutant mice when transgenically overexpressed. The integration of this genetic information with what is known about the interactions of ATRNL1 and the melanocortin 2 receptor (MC2R) suggests a physical interaction between the cytoplasmic tails of ATRN and MC1R. Taken together, these bioinformatic and genetic studies provide guidance and motivation for the experiments described in Chapter Three and Chapter Four.

Introduction to the ATRN protein

Bioinformatic tools are valuable resources for the elucidation of gene function. While computational methods are far from perfect predictors of protein function, motif and domain prediction software programs are useful for identifying potentially important functional sequences in a protein of interest. By coupling these predictions with analysis of sequence conservation patterns across species, it is possible to identify higher-likelihood putative functional motifs on the basis of their evolutionary conservation. As the number of available animal genome sequences grows, and as genome-wide phenotypic information becomes available for model organisms, it is

[1] Portions of this chapter are modified with the permission of the publisher from Walker *et al.*, 2007.

becoming increasingly possible to gain biological insight on the potential functions of a gene of interest by thoughtful integration of available genetic and molecular evolutionary information. For *Atrn*, as for any other gene of interest in the post-genomic age, to find an answer to the question "how does this gene work?" it is helpful to turn first to an examination of its predicted protein structure.

As mentioned briefly in the previous chapter, the extracellular/lumenal region of mammalian ATRN contains several recognizable domains and motifs (Figure 2.1). One of the two large domains is a CUB domain, a compact globular domain named for its presence in the Cls/Clr proteins of the complement system, Uegf of sea urchin, and Bone morphogenetic protein 1/pro-collagen C proteinase (mTolloid) (Bork and Beckmann, 1993; Romero *et al.,* 1997). CUB domains occur in a diverse set of animal proteins with no obvious functional relationship, such as spermadhesins, the vitamin B12 receptor, and SCUBE3 (Moestrup *et al.,* 1998; Wu *et al,* 2004; Yang *et al.,* 2007). The importance of the CUB domain for the function of ATRN is not known. The second large domain in ATRN is a C-type lectin domain. This calcium-dependent carbohydrate binding domain typically mediates interactions with polysaccharide groups of N-glycosylated proteins, which may be significant for ATRN's function given that ATRN, MC1R, and ASP are all glycosylated (Duke-Cohan *et al.,* 1998; Willard *et al,* 1995; Sanchez *et al.,* 2002). ATRN also contains multiple EGF-like repeats, Plexin/Semaphorin/Integrin (PSI) repeats, and kelch repeats. EGF-like repeats occur in a several growth factor receptors and laminins, while PSI repeats are components of a variety of proteins involved in cell adhesion, axon guidance, and extracellular matrix interactions. The kelch repeats of ATRN are predicted to form a "kelch propeller," a structure that has been observed to mediate protein-protein interactions. The relatively short intracellular/cytoplasmic domain of ATRN contains no named domains, but does contain motifs of potential functional importance, such as

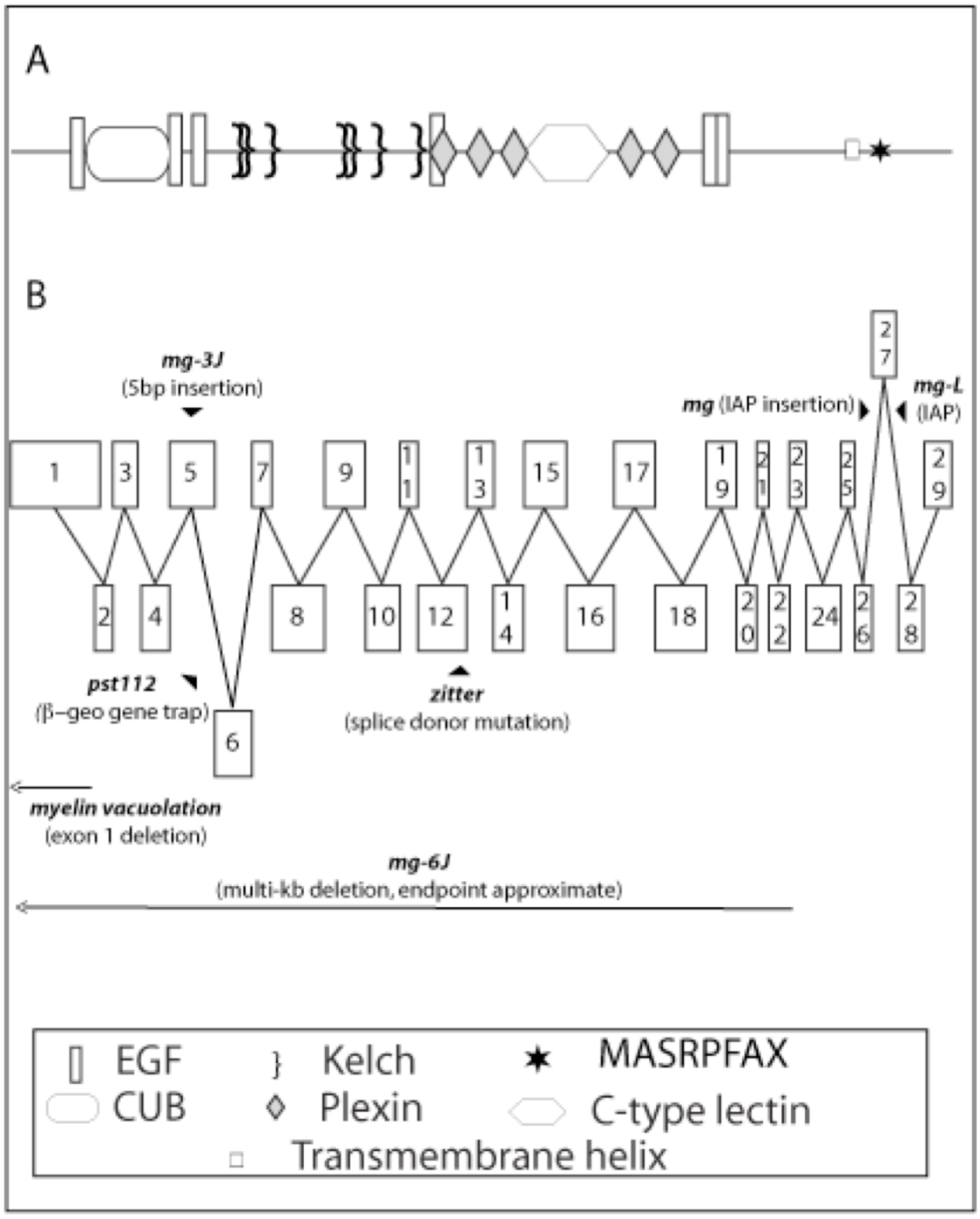

Figure 2.1. Protein and exon structure of murine ATRN/*Atrn*. A. Predicted domains and motifs of murine ATRN, shown to scale. B. Exon structure of *Atrn* transcript, with exons (numbered boxes) represented to scale underneath corresponding ATRN protein regions. Affected regions of known mutant alleles are indicated.

the highly conserved MASRPFAXVXV sequence that is found in ATRN homologs as evolutionarily divergent as mice, nematodes, and sea anemones, as discussed in a subsequent section.

Attractin mutant alleles in mouse and rat

There are several well-characterized mouse and rat *Atrn* alleles (Figure 2.1, Table 2.1). In mouse, two spontaneous alleles are null or near-null mutations: *Atrn*$^{mg\text{-}3J}$ and *Atrn*$^{mg\text{-}6J}$. The *Atrn*$^{mg\text{-}6J}$ mutation was described by Bronson *et al.* (2001) as exhibiting dark coat color, tremor, hypomyelination, and spongiform neurodegeneration by 2 months of age. This allele arose from a genomic deletion removing most of the codons that contribute to the extracellular/lumenal portion of the protein (and resulting in no detectable *Atrn* transcript), hence this is expected to be a null allele. The *Atrn* $^{mg\text{-}3J}$ homozygote is completely black on a C3H/HeJ genetic background, has a tremor, and rapidly develops spongiform neurodegeneration, with vacuoles evident in many brain regions by 1 month of age (Gunn *et al.,* 2001). Hypomyelination also occurs in this mutant (Kuramoto *et al.,* 2001). Expression of the *Atrn*$^{mg\text{-}3J}$ transcript is greatly reduced due to a 5 bp deletion at codon 937, which produces an early stop two codons downstream that presumably triggers nonsense-mediated decay of the mutant transcript (Nagle *et al.,* 1999; Gunn *et al.,* 1999). By western blot, *Atrn*$^{mg\text{-}3J}$ homozygotes produce no detectable ATRN protein (Gunn *et al.,* 2001). The original *mahogany* (*Atrn*^{mg}) mutation shows somewhat less severe phenotypes than these two null alleles (Gunn *et al.,* 2001). *Atrn*^{mg} homozygotes lack an obvious tremor, and develop spongiform change at a slower rate than do *Atrn*^{mg3J} homozygotes, although vacuoles are readily observable by four months of age. Pheomelanogenesis is much reduced but not completely impaired, as C3H/HeJ *Atrn*^{mg} mice produce some sub-apically striped hairs along their flanks and in the ventral fur.

Table 2.1. Phenotypes of rodent *Atrn* alleles.

Allele (species)	**Molecular lesion**	**Effect on gene products**	**Vacuolation**	**Tremor**	**Coat color**	**Comments**
$Atrn^{mg-6J}$ (mouse)	Large deletion of most of the extracellular/ lumenal domain.	Probable null allele.	Severe.	Yes.	Black.	Probably a null allele.
$Atrn^{mg-3J}$ (mouse)	5bp deletion at codon 937/1428.	Greatly reduced transcript, no detectable protein.	Severe.	Yes.	Black.	Probably a null allele.
$Atrn^{mg}$ (mouse)	IAP insertion in intron 26.	Abnormal transcripts, truncated protein presumed to lack much of cytoplasmic tail.	Moderately severe.	No.	Black dorsum with some yellow pigment laterally.	Mutation displays importance of cytoplasmic tail for ATRN function.
$Atrn^{mg-L}$ (mouse)	IAP insertion in intron 27.	Splicing defect. Reduced expression of transcript and possible production of mutant protein with abnormal C-terminus.	Mild.	No.	Dark agouti with narrow black stripe on dorsum.	A mild hypomorph.
$Atrn^{Gt(PST112)Byg}$ (mouse)	β-geo gene trap allele.	ATRN-β-geo fusion includes only first 5 exons of Atrn sequence.	Severe.	Yes.	Black.	Probably a null allele.
$Atrn^{zi}$ (rat)	Splice donor site mutation in exon 12.	Major reduction in transcript abundance.	Severe.	Yes.	Dark agouti.	A strong allele but probably not a complete null.
$Atrn^{mv}$ (rat)	3.6 kb deletion affecting all of first exon.	No detectable transcript.	Severe.	Yes.	Dark agouti.	Probably a null allele.

The causative molecular lesion is a ~5kb intracisternal A particle (IAP) insertion in the 26th intron of the *Atrn* locus. By Western blot, ATRN protein from *Atrn*^{mg} homozygotes is abundant but appears smaller than wild-type ATRN by approximately 20 kD, suggesting that the IAP insertion prevents normal splicing into the 27th exon, with concomitant loss of most of the 17kD cytoplasmic domain including the very highly conserved MASRPFAS sequence. The trace ATRN functionality evident in these mutants may be due to very low levels of normally spliced *Atrn* transcript, or may represent slight residual function of truncated ATRN. Either scenario implicates the cytoplasmic tail as an important mediator of ATRN's function in pigment-type switching and CNS function.

The least severe phenotypes of any known *Atrn* mutation are seen in the *mahogany* "Leicester" allele, *Atrn*$^{mg\text{-}L}$ (Gunn *et al.*, 2001). This hypomorph has a moderate pigment-type switching defect on the C3H/HeJ genetic background, resulting in a narrow dorsal region of completely black fur with increasing amounts of yellow pigment seen in lateral and ventral areas. *Atrn*$^{mg\text{-}L}$ mice develop spongiform vacuoles at a greatly reduced rate compared to *Atrn*^{mg} or *Atrn*$^{mg\text{-}3J}$ animals, with a histological appearance indistinguishable from wild-type animals at 4 months of age and only mild vacuolation occurring by 8 months (by which time both *Atrn*^{mg} and *Atrn*$^{mg\text{-}3J}$ homozygotes have developed severe widespread vacuolation). Like *Atrn*^{mg}, this mutation is the result of an IAP insertion, in this case into the 27th intron of *Atrn*. This appears to disrupt normal splicing to some extent, as abnormally large transcripts that evidently terminate within the IAP sequence are evident on Northern blots of brain RNA from *Atrn*$^{mg\text{-}L}$ mice. However, normally sized *Atrn* transcript is still produced in reduced quantity, and slightly reduced levels of a wild-type-sized ATRN protein are observable by Western blot. The mild phenotypical expression of this mutant is probably explained by the presence of wild-type ATRN at a reduced level,

although it is tempting to speculate that the severity of the mutation's effect on the functionality of any mutant ATRN produced may also be lessened by the location of the IAP insertion relative to conserved regions of the cytoplasmic tail. The IAP insertion in the *Atrn*$^{mg\text{-}L}$ allele is several codons downstream of the highly conserved MASRPFAS sequence, suggesting that any protein translated from the aberrantly spliced transcripts would contain MASRPFAS and might retain related function.

In addition to these spontaneous mutations in *Atrn*, a gene-trap allele has been generated that joins the first five exons of *Atrn* with a β-geo cassette (Leighton *et al.*, 2001). As expected for an *Atrn* null allele, mice homozygous for the gene-trap allele *Atrn*$^{Gt(PST112)Byg}$ are black and develop severe spongiform change and hypomyelination (Walker *et al.*, 2007).

In rat, two *Atrn* mutations have been identified. The *zitter (zi)* mutation was noticed first for the tremor, hypomyelination, and spongiform degeneration it caused in homozygotes, as it arose on the albino Sprague-Dawley background which masked its pigment-type switching defects (Rehm *et al.*, 1982; Yamada *et al.*, 1989). However, after *Atrn* mutant mice were shown to develop spongiform encephalopathy, the similarity of spongiform change in the rat mutants was noted and *zitter* was found to be a splice site donor mutation in exon 12 of rat *Atrn* (Kuramoto *et al.*, 2001). On a non-albino genetic background, *Atrn*^{zi} homozygotes have a dark agouti phenotype, consistent with the presence of reduced amounts of normal-sized *Atrn* transcript by Northern blot. The second rat *Atrn* mutation, *myelin vacuolation* (*mv*), was more recently identified on an albino genetic background, like *zitter* as a spontaneously arising tremorous mutant, and was discovered to be the result a 3.6 kb deletion which includes the first exon of *Atrn* (Kuwamura *et al.*, 2002). This mutation causes spongiform encephalopathy in both grey and white matter and pronounced hypomyelination and dysmyelination, similar to *zitter* mutants. Interestingly, although

Atrn^{mv} is almost certainly a null allele, when placed on a non-albino background it causes only a partial loss of pigment-type switching similar to that seen in *zitter* rats. *Atrn*^{mv} homozygotes are darker than *Atrn*$^{+/+}$ animals but not as dark as *nonagouti* rats, indicating that ASP can function with reduced efficiency in the rat pigment-type switching system in the absence of ATRN.

The attractin gene family

Attractin is one of a family of three mouse proteins with a similar domain organization (Figure 2.2). A second member of this family, attractin-like 1 (ATRNL1), is clearly a paralog of ATRN, with an almost identical arrangement of named domains and motifs and 58% amino acid identity to ATRN. The third family member, Multiple EGF-like domains 8 (MEGF8), is a larger protein that lacks the C-type lectin domain and has a tandem duplication of much of its extracellular/lumenal region. In addition to their similar domain organization, ATRN, ATRNL1, and MEGF8 share a conserved cytoplasmic motif (MASRPFAXVXV) of unknown function.

Our knowledge of the functions of ATRNL1 and MEGF8 is limited. Haqq *et al.* (2003) demonstrated that ATRNL1 and MC4R interact through their respective cytoplasmic tails, suggesting that, like ATRN, ATRNL1 may have a role in melanocortin receptor signaling. The effect of loss of ATRNL1 seems to be subtle, however, as *Atrnl1* knockout mice show no overt phenotypic abnormalities (Walker *et al.*, 2007). Interestingly, *Atrn/Atrnl1* double mutants develop a progressive cardiomyopathy (Walker *et al.*, 2007), indicating that the presence of functional ATRN may compensate for loss of ATRNL1 and mask *Atrnl1* mutant phenotypes. Unlike *Atrnl1* mutants, *Megf8* mutants exhibit obvious phenotypes. These mice have aberrant establishment of the left-right body axis, resulting in heterotaxy and cardiac

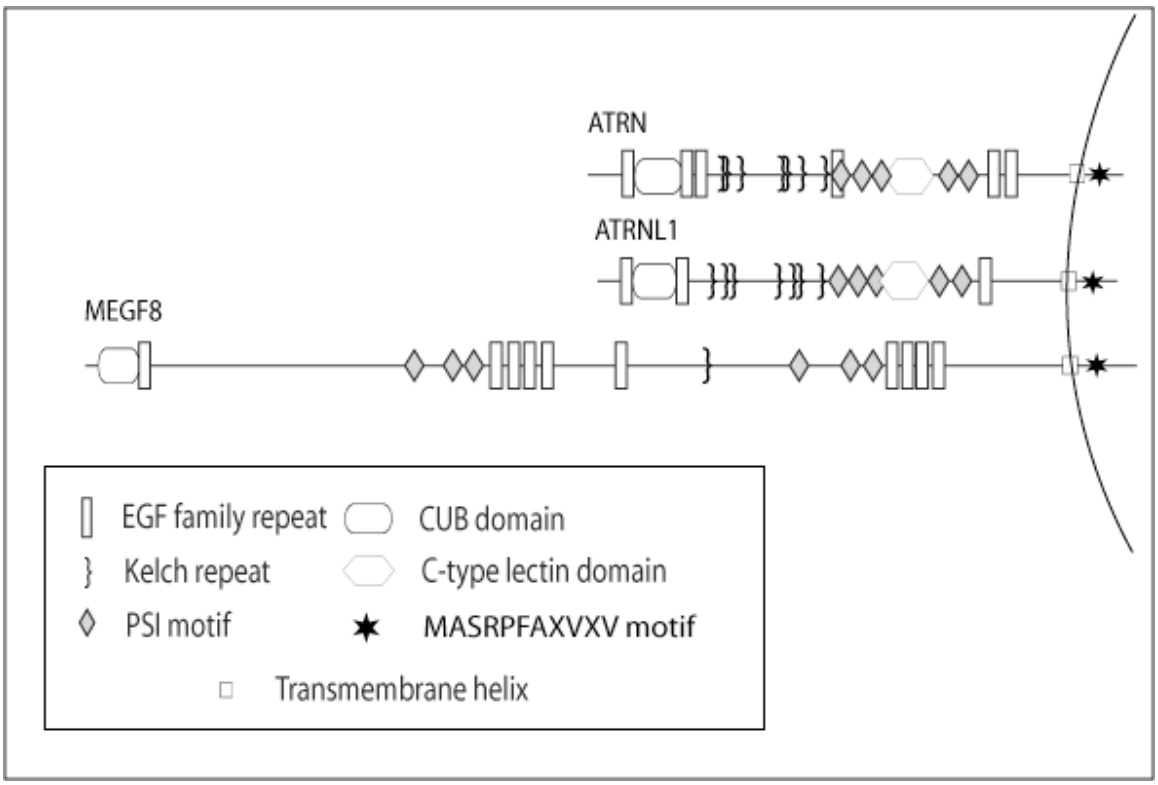

Figure 2.2. The murine ATRN family of proteins. EGF: Epidermal Growth Factor. PSI: Plexin/Semaphorin/Integrin motif.

defects (Aune *et al.,* 2008; Zhang *et al.,* 2009). The histopathological and molecular characteristics of these left-right patterning defects are remarkably similar to those reported for *Mgrn1* mutant mice (Cota *et al.,* 2006), suggesting that MEGF8, like ATRN, may depend on MGRN1 for proper function.

To gain insight into the structure/function relationships that underlie the phenotypes of *Atrn* mutants, I reconstructed the evolutionary history of the *Atrn* gene family by identifying and comparing members of the family (and their associated mutant phenotypes) across metazoan phyla. This analysis suggests that the members of the *Atrn* family of genes diverged from an ancient MEGF8-like gene in a prometazoan common ancestor and have subsequently been co-opted into different functional roles. To test the functional importance of motifs differing between ATRN and its most similar homolog, ATRNL1, I introduced transgenically overexpressed

Atrnl1 into an *Atrn* null mutant background and examined the phenotypes of the resulting mice.

Materials and Methods

Bioinformatics

Refseq protein sequences for vertebrate ATRN, ATRNL1, and MEGF8 proteins were downloaded from Ensembl release 57 (See Table 2.2 for Genbank and Ensembl reference ID numbers of sequences used in this study). A within-vertebrates sequence conservation analysis was performed using ClustalW (Larkin *et al.*, 2007), and named domains and motifs were identified using the SMART protein architecture research tool (Schultz *et al.*, 1998, Letunic, Doerks, and Bork, 2008). Invertebrate ATRN family genes were identified by BLAST against the amino acid sequence of mouse ATRN, and analyzed for conservation of domain organization using SMART. The cytoplasmic tails of ATRN family members were analyzed for putative linear motifs using the Eukaryotic Linear Motif online tool (Puntervoll *et al.*, 2003; Gould *et al.*, 2010), and analyzed with the COILS utility for identification of high-likelihood coiled-coil forming regions (Lupas, Van Dyke, and Stock, 1991).

Atrnl1 transgenic mice

The *Atrnl1* transgenic mice used for this study were generated by Ke-Yu Deng of the Cornell Transgenic Mouse Core Facility, using a DNA construct made by Dr. Chelin Jamie Hu, as described by Walker *et al.* (2007). Transgenic founders were identified by PCR using primers in exons 4 and 5 (GCTGGTCCAGGGATAAAATG and GCTGGCACAGTCAGCATATC) to amplify a 1,093-bp band from the endogenous locus and a 226-bp band from the transgene. Three founders were bred to C3H/HeJ-*Atrn*$^{mg\text{-}3J}$ and 129S1/SvImJ-*Atrn*$^{Gt(PST112)Byg}$ (*Atrn*^{PST112}) mice and transgenic

Table 2.2. Protein sequences used in this study.

Species	Homolog	Accession number
*Anopheles gambiae (*mosquito*)*	ATRN/ATRNL1	ENSANGP00000003873
*Aedes aegypti (*mosquito*)*	ATRN/ATRNL1	AAEL007331-PA
*Branchiostoma floridae (*lancelet*)*	ATRN/ATRNL1	XP_002601127.1
*Branchiostoma floridae (*lancelet*)*	MEGF8	XP_002613359.1
*Canis familiaris (*dog*)*	ATRN	ENSCAFP00000009513
*Canis familiaris (*dog*)*	ATRNL1	ENSCAFP00000017303
*Caenorhabditis elegans (*nematode*)*	ATRN/ATRNL1	NP_001024625
*Ciona intestinalis (*tunicate*)*	ATRN/ATRNL1	ENSCINP00000013249
*Ciona savignyi (*tunicate*)*	ATRN/ATRNL1	ENSCSAVP00000008291
*Drosophila melanogaster (*fruit fly*)*	ATRN/ATRNL1	NP_651571.3
*Drosophila melanogaster (*fruit fly*)*	MEGF8	NP_609180.2
*Gallus gallus (*chicken*)*	ATRN	ENSGALP00000025782
*Gallus gallus (*chicken*)*	ATRNL1	ENSGALP00000014887
*Gasterosteus aculeatus (*stickleback*)*	ATRN	ENSGACP00000005821
*Gasterosteus aculeatus (*stickleback*)*	ATRNL1	ENSGACP00000015076 ENSGACP00000008795
*Homo sapiens (*human*)*	ATRN	ENSP00000262919
*Homo sapiens (*human*)*	ATRNL1	ENSP00000347152
*Macaca mulatto (*rhesus macaque*)*	ATRN	ENSMMUP00000029333
*Macaca mulatto (*rhesus macaque*)*	ATRNL1	ENSMMUP00000002545
*Monodelphis domestica (*opossum*)*	ATRN	ENSMODP00000005644
*Monodelphis domestica (*opossum*)*	ATRNL1	ENSMODP00000012047
*Monosiga brevicollis (*choanoflagellate protist*)*	MEGF8	XP_001748540.1
*Mus musculus (*mouse*)*	ATRN	NP_033860.2
*Mus musculus (*mouse*)*	ATRNL1	ENSMUSP00000076514
*Mus musculus (*mouse*)*	MEGF8	NP_001153872.1
*Oryzias latipes (*medaka*)*	ATRN	ENSORLP00000022537
*Oryzias latipes (*medaka*)*	ATRNL1	ENSORLP00000004353 ENSORLP00000006305
*Pan troglodytes (*chimpanzee*)*	ATRN	ENSPTRP00000022608
*Pan troglodytes (*chimpanzee*)*	ATRNL1	ENSPTRP00000039368
*Rattus norvegicus (*rat*)*	ATRN	ENSRNOP00000028847
*Rattus norvegicus (*rat*)*	ATRNL1	ENSRNOP00000023414
*Takifugu rubripes (*pufferfish*)*	ATRN	SINFRUP00000144197
*Takifugu rubripes (*pufferfish*)*	ATRNL1	SINFRUP00000156274 SINFRUP00000128200
*Tetraodon nigroviridis (*pufferfish*)*	ATRN	GSTENT00019974001
*Tetraodon nigroviridis (*pufferfish*)*	ATRNL1	GSTENP00018764001 GSTENP00034986001
*Trichoplax adhaerens (*placozoan*)*	MEGF8	XP_002112184.1
*Xenopus tropicalis (*frog*)*	ATRN	ENSXETP00000009491
*Xenopus tropicalis (*frog*)*	ATRNL1	ENSXETP00000051348

F1 pups mated back to the appropriate *Atrn* mutant strain. One founder did not transmit the transgene, a second founder probably did not express the transgene (no rescued phenotypes were evident in pups from this founder) and was not characterized further, and the third, B4, was used for all experiments as it bred well, transmitted the transgene, and rescued *Atrn* mutant phenotypes.

Histology

Brains were collected into cold phosphate-buffered saline and fixed in phosphate-buffered 4% paraformaldehyde or 10% formalin. Dehydrated tissues were embedded in paraffin and 5-μm sections stained with hematoxylin and eosin (H&E). Myelination was assessed by Luxol fast blue staining on 10-μm spinal cord sections following a standard protocol (Sheehan and Hrapchak, 1980).

Northern blot verification of Atrnl1 overexpression

RNA was prepared from brains of transgenic and non-transgenic $Atrn^{Gt(PST112)Byg/+}$ mice by Trizol extraction and run on a denaturing MOPS/formaldehyde agarose gel. RNA was transferred to charged nylon membrane (Immobilion) and hybridized with a ^{32}P-dCTP-labeled probe complementary to a ~500bp sequence of *Atrnl1* (IMAGE clone 1616940 and a probe amplified using primers AGTGAGGGGTAACGAGACCGT and GTGACGTTGCCATCACTGGT).

Results

Evolution of the Atrn gene family

The *Atrn* family of genes is widely conserved in the eumetazoa, indicating an ancient origin. Comparison of their domain organization reveals that the ancestral structural arrangement of all ATRN family members is a CUB domain flanked by

EGF repeats, followed by kelch repeats, PSI motifs, a second set of EGF repeats, and a transmembrane helix (Figure 2.3). "Short-form" family members such as mouse ATRN and ATRNL1 consist of a single instance of this basic pattern. In the case of "long-form" members of the family such as mouse MEGF8, the basic sequence is repeated (except for the transmembrane helix) as a tandem array. Remarkably, genomes from every eumetazoan phylum examined -- from chordates, to cnidarians, to the most primitive extant multicellular animal, *Trichoplax* -- contain a protein-coding gene with essentially the same domain organization as *Megf8*. This universal distribution indicates that a "long-form" *Megf8*-like gene was present in the last eumetazoan common ancestor. The basic architecture of this founding member of the *Atrn* family appears to have been invented by a common ancestor of the eumetazoa and their closest protozoan sister group, the choanoflagellates, as a more distant homolog of *Megf8* is recognizable in the genome of the choanoflagellate *Monosiga*, and not in any other protistan phylum (Figure 2.4).

The tandem structure of the ancestral eumetazoan *Megf8* gene may have made it susceptible to homology-mediated deletion of one of the tandem repeats. Such an event seems likely to be responsible for the appearance of the "short-form" subclass of ATRN family members. This innovation apparently occurred very early in metazoan evolution, prior to the divergence of the Bilateria from the radially symmetrical animals such as sea anemones. The resulting two-member gene family, comprising a single "long-form" *Megf8*-like gene and a single "short-form" *Atrn/Atrnl1*-like gene, is the ancestral arrangement for all modern eumetazoan phyla except, possibly, *Trichoplax* (Figure 2.4). It is retained in diverse organisms including the starlet anemone *Nematostella*, arthropods such as the fruit fly *Drosophila*, and in primitive chordates including the lancelet *Branchiostoma* and the tunicate *Ciona*. The nematodes *Caenorhabditis briggsae* and *C. elegans* lack the *Megf8*-like member of the

Figure 2.3. ATRN family proteins across eukaryotic phyla. Representations are to scale, except for the large MEGF8-like protein of *Monosiga*, which is shown at 50% of scale.

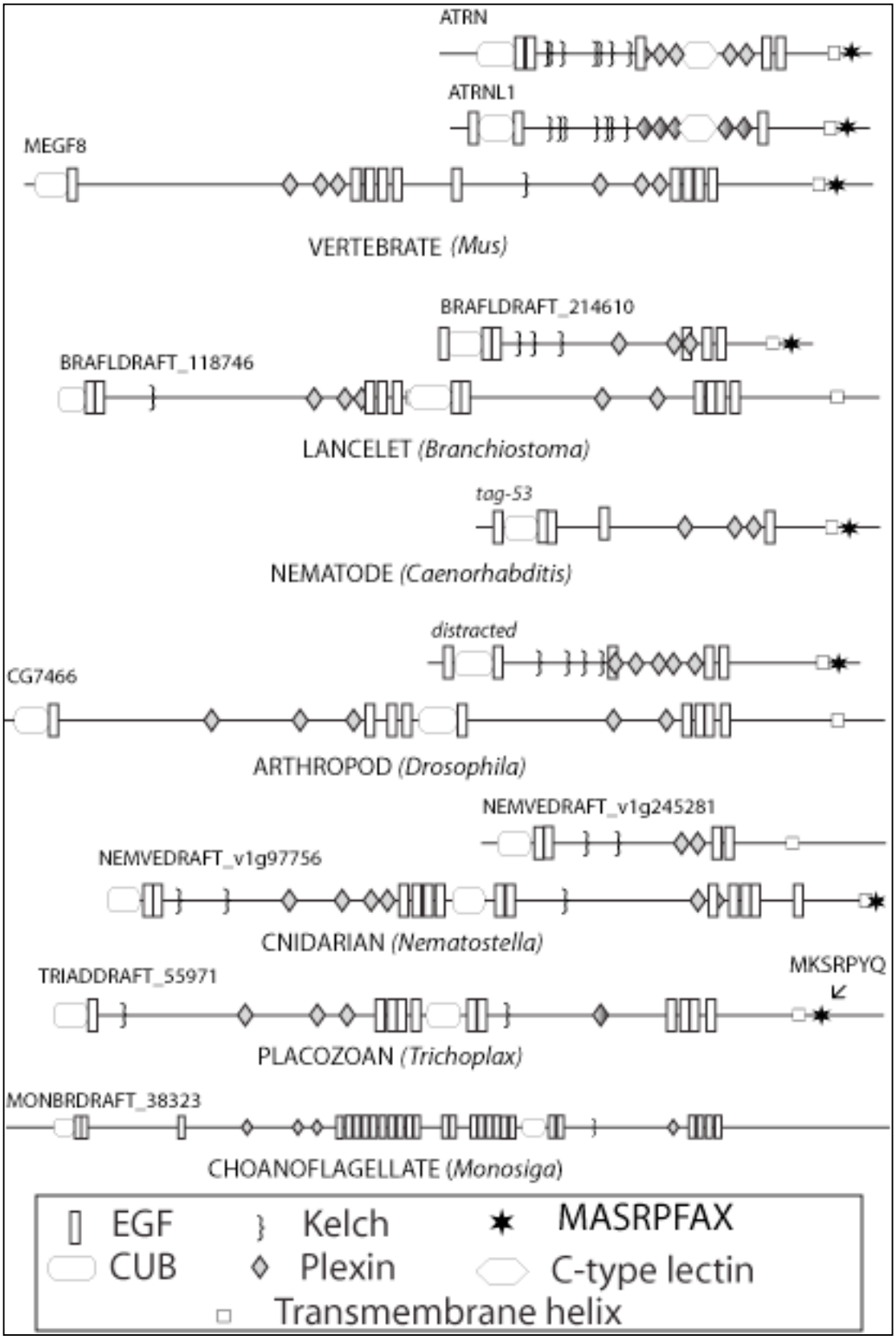
ATRN
ATRNL1
MEGF8
VERTEBRATE (Mus)
BRAFLDRAFT_214610
BRAFLDRAFT_118746
LANCELET (Branchiostoma)
tag-53
NEMATODE (Caenorhabditis)
distracted
CG7466
ARTHROPOD (Drosophila)
NEMVEDRAFT_v1g245281
NEMVEDRAFT_v1g97756
CNIDARIAN (Nematostella)
TRIADDRAFT_55971
MKSRPYQ
PLACOZOAN (Trichoplax)
MONBRDRAFT_38323
CHOANOFLAGELLATE (Monosiga)
EGF
Kelch
MASRPFAX
CUB
Plexin
C-type lectin
Transmembrane helix

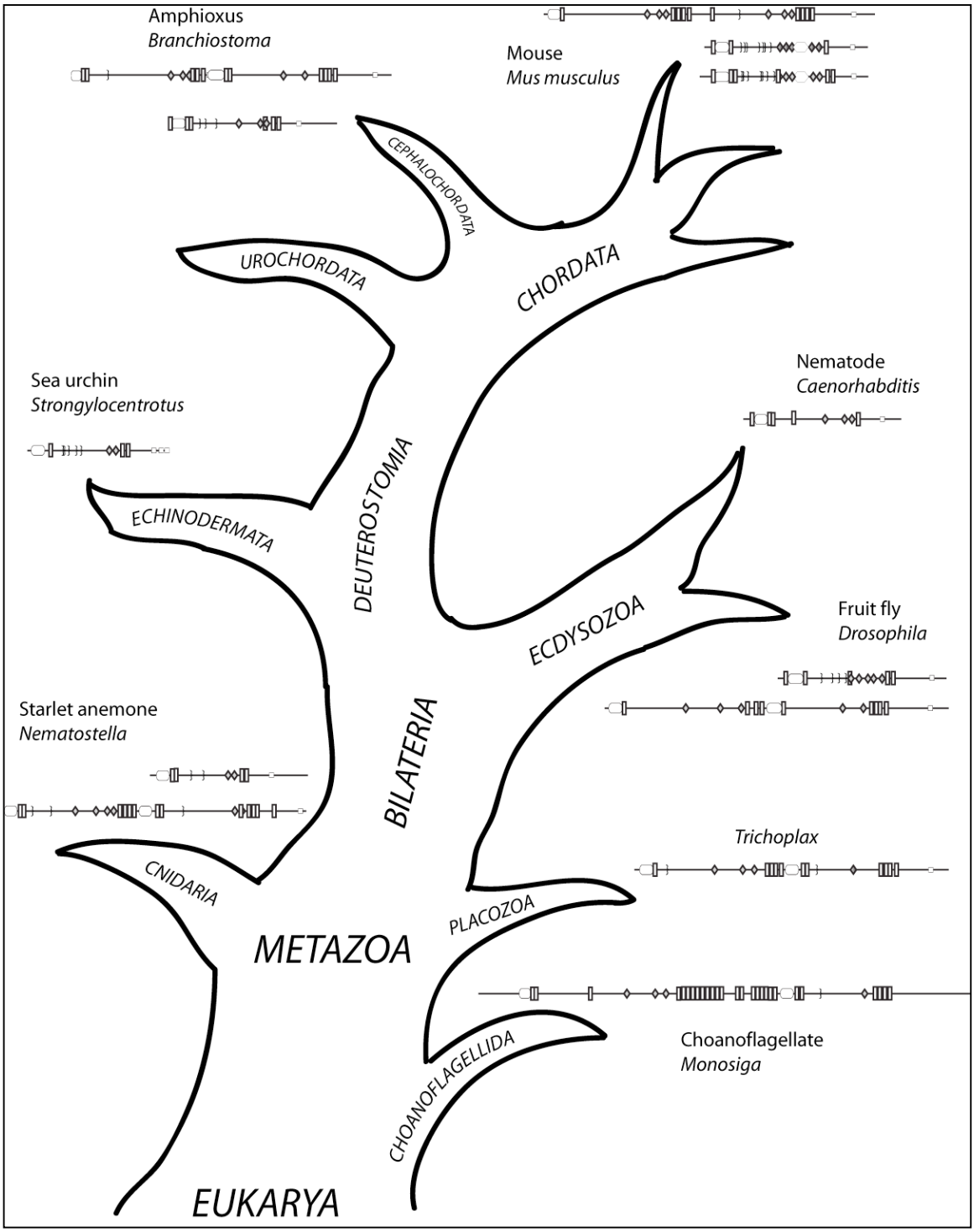

Figure 2.4. Innovations in the ATRN family on the tree of life. Eumetazoan branches for which genomic data are not available are omitted.

family, which has apparently been secondarily lost in this lineage.

While hemichordates (acorn worms) and primitive chordates retain the ancestral two-member complement of *Atrn* family members, several notable innovations appeared specifically in the vertebrate clade. A new feature, the C-type lectin domain, was added to the ancestral "short-form" family member, while the "long-form" protein lost one of its two CUB domains. At about the same time, a segmental duplication event occurred at the genomic locus of the shorter family member, splitting the ancestral gene into a pair of paralogs, the descendants of which are the modern vertebrate *Atrn* and *Atrnl1*.

Sequence analysis of Atrn and Atrnl1

As expected for genes that arose from an ancient duplication event, *Atrn* and *Atrnl1* are each embedded in a small block of paralogous sequence, with each gene occurring immediately adjacent to a glial cell line-derived neurotrophic factor family receptor alpha homolog (*Gfra4* and *Gfra1*, respectively, in non-fish vertebrates). The named domains and motifs are highly conserved across vertebrates, and they are very similar between the two paralogs within each species (Figure 2.5).

Because the cytoplasmic tail region of the proteins contains no named domains but is likely to mediate important interactions with cytoplasmic proteins, I examined this region at the sequence level. Figure 2.6 shows a multiple alignment of the primary sequence of mouse ATRN and ATRNL1, with fruit fly and roundworm ATRN cytoplasmic tail. This analysis reveals that the cytoplasmic tails of ATRN and ATRNL1 can be divided into 4 regions. The most membrane-proximal 40 amino acids of mouse ATRN and ATRNL1 differ at only five residues and include the highly conserved MASRPFAXVXV sequence also shared by fly and worm ATRN. There follows a short stretch of low sequence conservation from residues 41-52, and then a

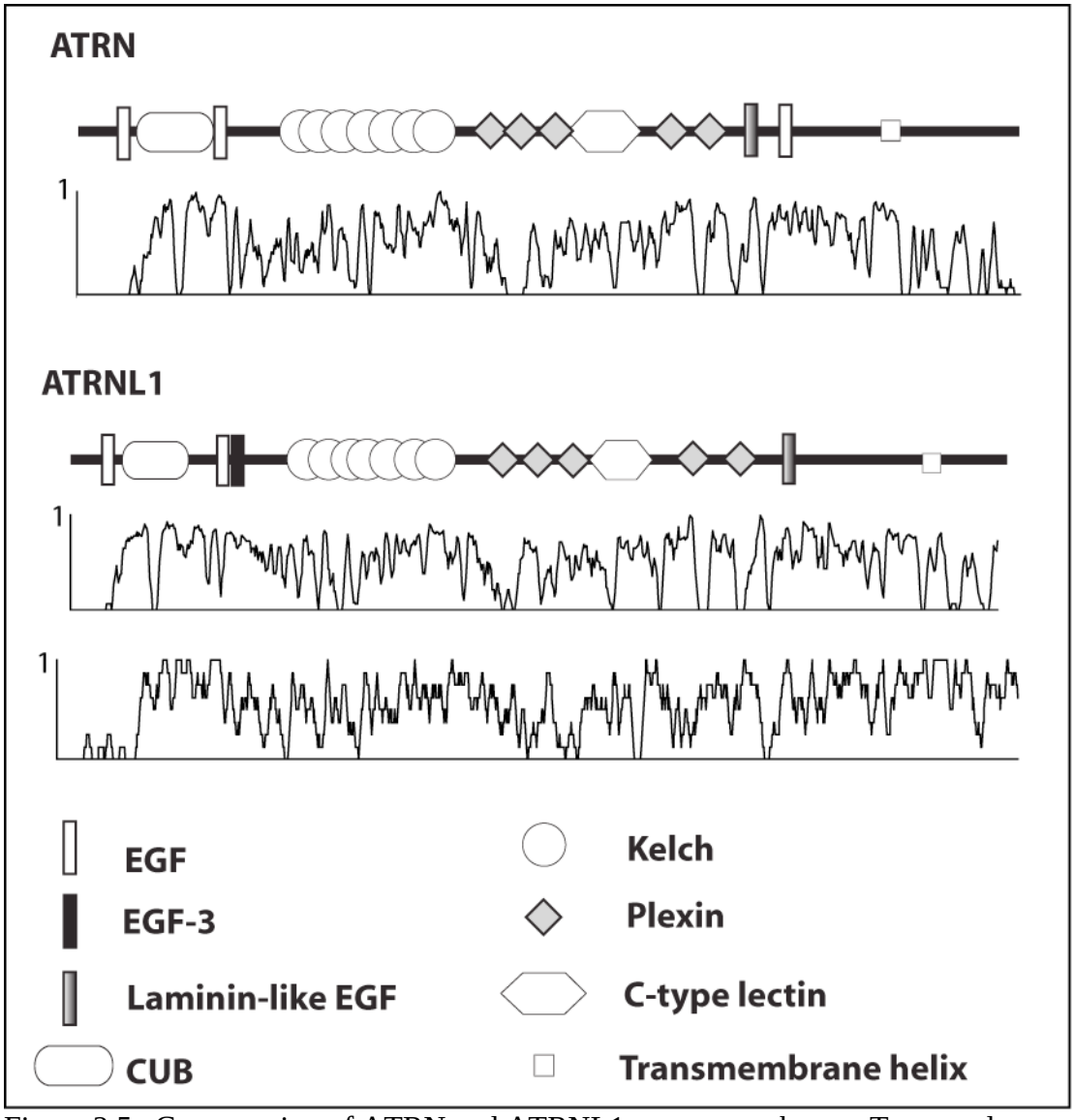

Figure 2.5. Conservation of ATRN and ATRNL1 across vertebrates. Top panel: Schematic figure of murine ATRN and conservation trace showing amino acid conservation across a multiple alignment of vertebrate species. Middle panel: schematic figure of murine ATRNL1 and conservation trace showing amino acid conservation across a multiple alignment of vertebrate species. Bottom panel: Conservation trace showing sequence similarity between murine ATRN and ATRNL1.

second region of high conservation at residues 53-104. This region is made up of two conserved groups of hydrophobic residues, each of which is flanked by evolutionarily conserved prolines. The two hydrophobic stretches each contain a conserved serine or threonine, and are connected by a glycine-rich linker sequence. As indicated in Figure 2.6, the sequence downstream of MASRPFAXVXV in ATRNL1 contains two regions which are each sufficient to confer the ability to interact with the MC4R cytoplasmic tail (Haqq *et al.*, 2003); the second of these MC4R interaction domains of ATRNL1 corresponds to the first set of conserved proline-flanked hydrophobic residues (53-76) of ATRN. Following this conserved region, the C-terminal ends of mouse ATRN and ATRNL1 have little sequence similarity and are not evolutionarily conserved. COILS analysis of the cytoplasmic tail regions shows that the conserved membrane-proximal regions of ATRN and ATRNL1 are each predicted to participate in the formation of a

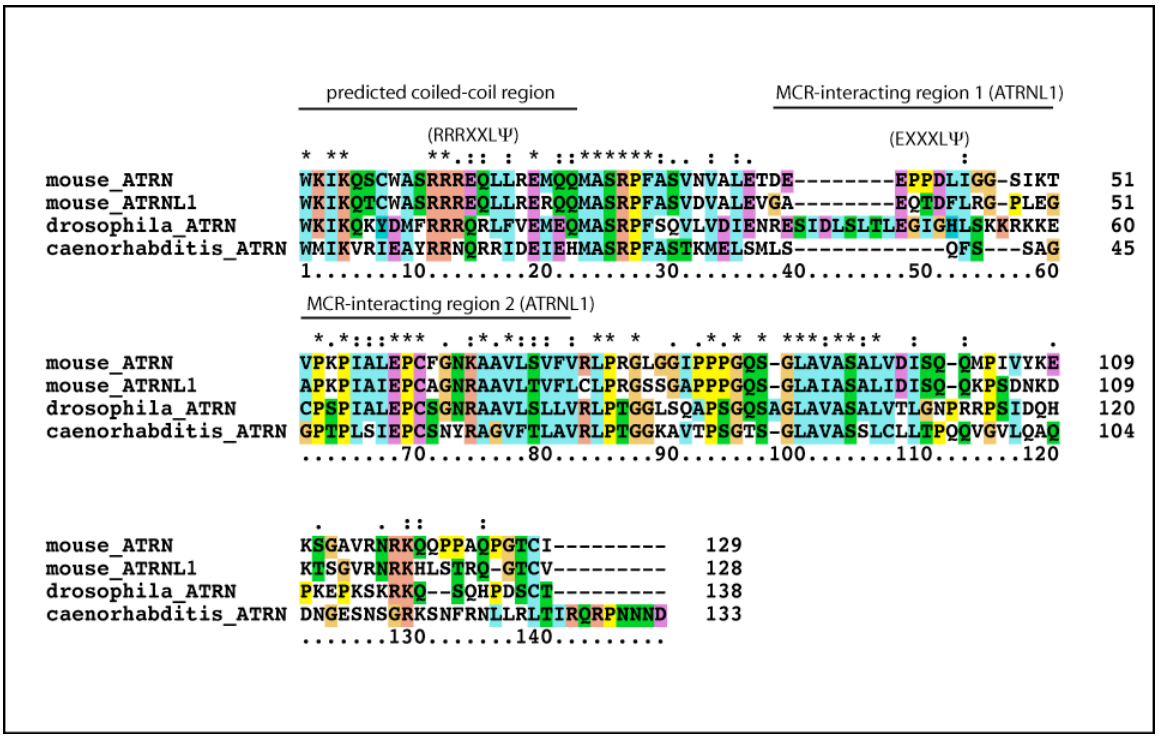

Figure 2.6. Multiple alignment of ATRN family cytoplasmic tail sequences, showing proposed functional motifs.

coiled-coil motif. The ELM motif recognition tool identifies a pair of endosomal/lysosomal targeting motifs (EPPDLI and RRREQLL) in ATRN, the latter of which is also present in ATRNL1. As the high overall similarity of ATRN and ATRNL1 suggests that the two proteins might exhibit functional redundancy (perhaps enabling a dissection of the structure/function relationships of ATRN by enabling the assignment of rescued phenotypes to regions of the protein displaying high inter-paralog sequence similarity). I therefore tested whether overexpression of *Atrnl1* construct could rescue *Atrn* mutant phenotypes.

Rescue of Atrn mutant phenotypes by Atrnl1 overexpression

I mated *Tg(Atrnl1)B4Tmg* mice (which express mouse *Atrnl1* from the human β-actin promoter) to two different *Atrn* mutants on two different genetic backgrounds. The *Atrn* coat color phenotype was completely rescued in $Atrn^{PST112/PST112}$; *Tg(Atrnl1)B4Tmg* animals, while $Atrn^{mg\text{-}3J/mg\text{-}3J}$*; Tg(Atrnl1)B4Tmg* mice only displayed a partial rescue, having ‘‘dark agouti’’ hairs (Figure 2.7 and Table 2.2). The difference in the extent of coat color rescue by the *Atrnl1* transgene is most likely caused by genetic differences between the C3H and the 129 strain backgrounds (upon which the $Atrn^{mg\text{-}3J}$ and $Atrn^{GT(PST112)Byg}$ alleles are maintained, respectively) as previous phenotypic and molecular studies indicate that both alleles are null (Gunn *et al*., 2001).

To ascertain whether *Atrnl1* over-expression could also compensate for loss of *Atrn* in the CNS, brains of 3-month-old transgenic and nontransgenic *Atrn* mutants were examined histologically. Nontransgenic mice homozygous for either the $Atrn^{GT(PST112)Byg}$ or $Atrn^{mg\text{-}3J}$ allele showed pronounced spongiform vacuolation, while age-matched *Atrn* mutants carrying the *Atrnl1*transgene showed robust rescue of this phenotype with only sparse, scattered vacuoles evident in their brains (Figure 2.7 and

Figure 2.7. Ubiquitous over-expression of *Atrnl1* compensates for loss of ATRN. (A,B) Overexpression of *Atrnl1* rescues the pigmentation defect of *Atrn* mutant mice. Although the pigmentation phenotype of 129S1/SvImJ; $Atrn^{GT(PST112)Byg}$ mutants was rescued completely (A), C3H/HeJ; $Atrn^{mg\text{-}3J}$ mutants expressing the transgene were darker than wild-type agouti mice but not as dark as $Atrn^{mg\text{-}3J/mg\text{-}3J}$ mice (B), consistent with a strain background-dependent effect on pigment type switching. (C-R) Overexpression of *Atrnl1* in the brains of *Atrn* null mutant mice protects against spongiform neurodegeneration. High-magnification views of H&E-stained sections from 3- and 6-month-old $Atrn^{mg\text{-}3J/mg\text{-}3J}$ mice (left panel) and $Atrn^{mg\text{-}3J/mg\text{-}3J}$; *Tg(Atrnl1)B4Tmg* mice (right panel) showing cerebral cortex (C,D,K,L), hippocampus (E,F), cerebellum (G,H,O,P), pons (I,J,Q,R) and thalamus (K,L). Although nontransgenic $Atrn^{mg\text{-}3J/mg\text{-}3J}$ mutants showed extensive, progressive spongiform changes, $Atrn^{mg\text{-}3J/mg\text{-}3J}$; *Tg(Atrnl1)B4Tmg* mice showed no significant vacuolation at 3 months of age and only mild, scattered vacuolation at 6 months of age. (S–U) Partial rescue of hypomyelination of $Atrn^{mg\text{-}3J}$ mutants. Representative Luxol fast blue stained sections from 1-month-old mice showing normal myelination in spinal cord from *Atrnl1* mice (S), hypomyelination in $Atrn^{PST112/PST112}$ mutants (T), and an intermediate level of myelination in $Atrn^{PST112/PST112}$; *Tg(Atrnl1)B4Tmg* mice (U). (V) Northern blot analysis confirmed significant overexpression of *Atrnl1* in the brains of mice carrying *Tg(Atrnl1)B4Tmg* relative to nontransgenic mice. Upper panel: *Atrnl1* (probe against exons 4–8). Transgenic (4.4 kb) and endogenous (6.1 kb) transcripts are indicated. The endogenous transcript was more apparent with a longer exposure. A small, non-specific band was observed in all samples. Lower panel: β-actin (*Actb*) probe, used to verify equal RNA loading.

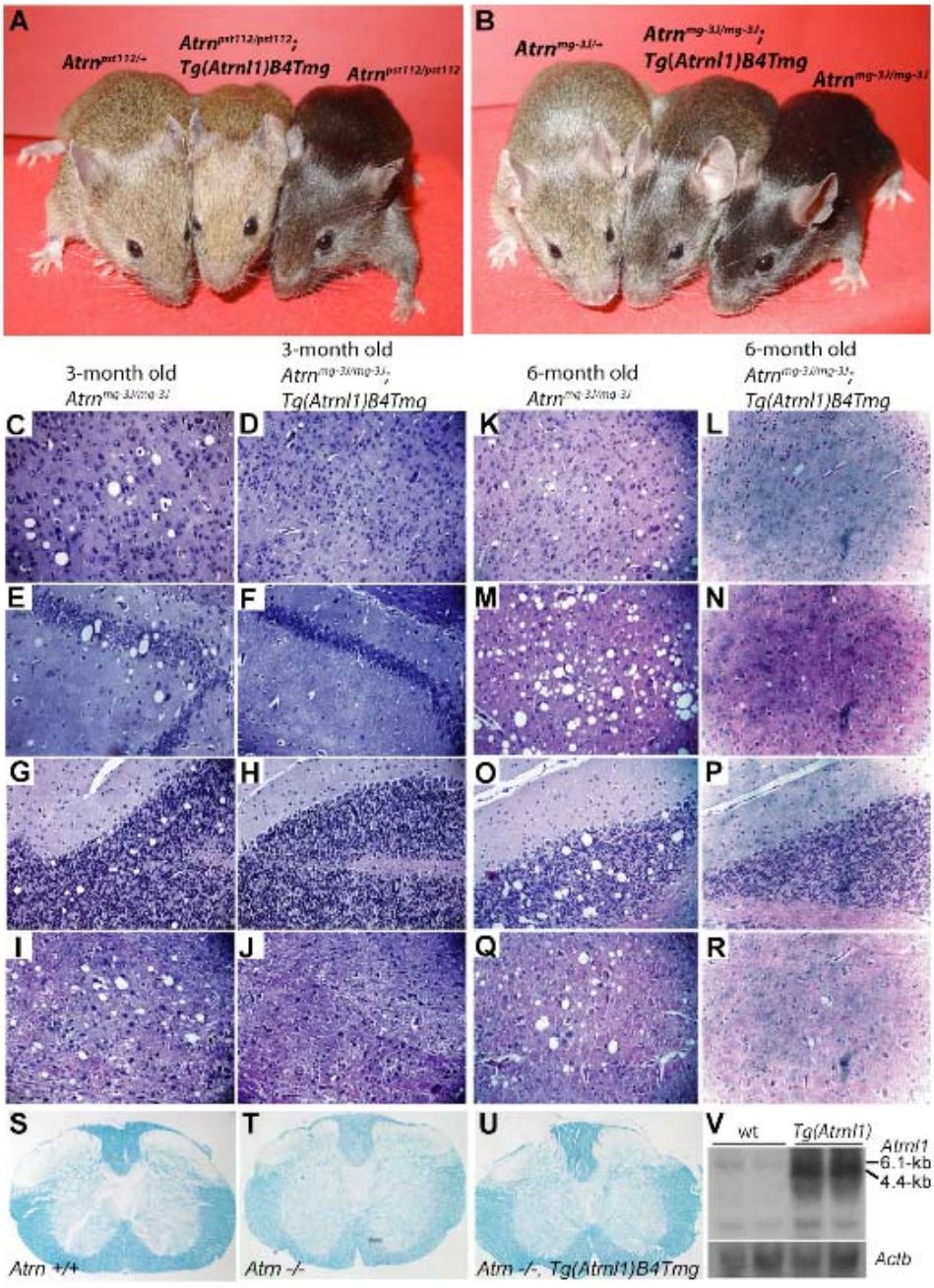
A
Atrnpst112/+
Atrnpst112/pst112;
Tg(Atrnl1)B4Tmg
Atrnpst112/pst112
B
Atrnmg-3J/-
Atrnmg-3J/mg-3J;
Tg(Atrnl1)B4Tmg
Atrnmg-3J/mg-3J
3-month old
Atrnmg-3J/mg-3J
3-month old
Atrnmg-3J/mg-3J;
Tg(Atrnl1)B4Tmg
6-month old
Atrnmg-3J/mg-3J
6-month old
Atrnmg-3J/mg-3J;
Tg(Atrnl1)B4Tmg
C
D
K
L
E
F
M
N
G
H
O
P
I
J
Q
R
S
T
U
V
wt
Tg(Atrnl1)
Atrnl1
6.1-kb
4.4-kb
Actb
Atrn +/+
Atrn -/-
Atrn -/-; Tg(Atrnl1)B4Tmg

Table 2.2. Rescue of *Atrn* mutant phenotypes by *Atrnl1* transgene.

Genotype	**Coat color**	**CNS pathology at 3 months**	**CNS pathology at 6 months**
Atrn$^{pst112/pst112}$	5/5 Black	3/3 Widespread vacuolation	2/2 Extensive vacuolation
Atrn$^{pst112/pst112}$; *Tg(Atrnl1)B4Tmg*	7/8 Agouti, 1/8 Dark agouti	5/5 no significant vacuolation	3/3 Sparse to mild vacuolation
Atrn$^{mg\text{-}3J/mg\text{-}3J}$	6/6 Black	2/2 Widespread vacuolation	2/2 Extensive vacuolation
Atrn$^{mg\text{-}3J/mg\text{-}3J}$; *Tg(Atrnl1)B4Tmg*	8/8 Dark agouti	5/5 No significant vacuolation	3/3 Sparse to mild vacuolation

Table 2.2). Rescue of the spongiform neurodegeneration phenotype was similarly robust for both *Atrn* mutant alleles, indicating that strain background effects do not detectably influence the onset or progression of vacuolation in this study. A similar phenomenon has been observed in the case of C3H/HeJ and C57BL/6J mice; *Atrn*$^{mg\text{-}3J}$ homozygotes are darker on the former compared with the latter background, but the extent of vacuolation is identical on both backgrounds (Teresa Gunn, personal communication). To determine whether overexpression of *Atrnl1* prevented spongiform neuropathology in *Atrn* mutants altogether or only delayed its appearance, a second cohort of mice was examined at 6 months of age. Profound spongiform vacuolation was observed in most regions of the brains of nontransgenic *Atrn* mutants, while *Atrn* mutants carrying the *Atrnl1* transgene showed some areas of mild-to-moderate vacuolation (Figure 2.7 and Table 2.2). Thus, the onset of spongiform neuropathology in *Atrn* mutants was significantly delayed but not completely prevented by overexpression of *Atrnl1*. I also examined whether overexpression of *Atrnl1* ameliorated the hypomyelination observed in *Atrn* mutants by performing Luxol fast blue staining on sections of spinal cord from 1-month-old mice. Staining levels in *Atrn*$^{GT(PST112)Byg}$ mutants carrying the *Atrnl1* transgene were intermediate to those of nontransgenic *Atrn*$^{GT(PST112)Byg}$ mutants and control mice (Figure 2.7).

As transgenic overexpression of *Atrnl1* compensated for loss of *Atrn* in the skin and the brain despite the fact that both genes are normally expressed in these tissues (Walker *et al.*, 2007), I hypothesized that abnormally high levels of *Atrnl1* expression may be required to compensate for loss of *Atrn*. I performed Northern hybridization of brain RNA from transgenic and nontransgenic *Atrn* mutants. *Atrnl1* expression was significantly elevated over endogenous levels in *Tg(Atrnl1)B4Tmg* mice (Figure 2.7V).

Discussion

Function of attractin family genes in evolutionary history

As I have described, homologous genes with the distinctive domain organization of *Atrn* and its close relative, *Megf8*, appear to be nearly universal features of eumetazoan genomes. From its conservation in such a diverse assemblage of phyla, we can infer that *Atrn* has been a part of the basic eumetazoan "genomic toolbox" since very close to the origin of animal multicellularity, over 600 million years ago. Given these ancient origins, it is ironic that *Atrn* is currently best understood for its role as a modulator of signaling by melanocortin receptors, which are a comparatively recent innovation restricted to the vertebrate lineage. Obviously, *Atrn*'s co-option into the melanocortin signaling pathway is a relative evolutionary novelty. It is interesting to speculate about what the "original" function of *Atrn* was, given what we know about the phenotypes of *Atrn* family mutants in modern organisms. In mammals, *Atrn* clearly plays roles in maintaining nervous system function, modulating melanocortin signaling, energy homeostasis, and immune function. In invertebrates the consequences of *Atrn* mutations are not well-studied, but some phenotypic information is available for fruit flies and in *C. elegans*. The *Atrn* homolog in the *Drosophila* genome is known as *distracted* and its loss causes neurological abnormalities in adult flies: in a fascinating similarity to the neurological phenotype of *Atrn* null mice,

distracted fruit flies develop vacuolated neurons in the optic and antennal lobes of their CNS (Thomas, 2005). The occurrence of spongiform neurodegeneration in *Atrn/distracted* mutant mice and flies suggests that *Atrn* plays a deeply conserved role necessary for maintaining neuronal integrity. While *Atrn* (tag-53) mutant *C. elegans* have not been studied in detail, they have been reported to display an uncoordinated phenotype, which may indicate a neurological defect. The other overt phenotypes of *Atrn* mutant *C. elegans* are "dumpy" morphology, high rate of egg infertility, and the abnormal vulval morphology (Wormbase website, www.wormbase.org. Release WS213, April 24 2010).

Phenotypic overlap between Mgrn1 and Atrn-family mutations indicates an ancient functional relationship between Mgrn1 and Atrn family members

In the mouse, *Atrn* and *Mgrn1* null mutants are remarkable for their significant degree of phenotypic overlap. Both mutants develop spongiform neurodegeneration, and both have a defect in pigment-type switching, which indicates that their gene products may cooperate as part of a molecular mechanism that is deployed in both the pigment cell and the neuron. Because *Mgrn1* apparently participates both in *Atrn's* "modern" role in melanocortin receptor signaling and its more ancient role in the neuron, it is interesting to ask whether the association between the two genes is unique to mammals, or an ancient legacy of the evolutionary past. Unlike ATRN, MGRN1 lacks an easily recognizable signature sequence of protein domains. Also, the major bioinformatically identifiable feature of *Mgrn1*, its RING domain, is shared by hundreds of other E3 ligases, making the confident identification of *Mgrn1* orthologs across distantly related phyla somewhat more difficult than is the case with *Atrn*. However, *Mgrn1* orthologs can be identified in both *C. elegans* and *Drosophila melanogaster* by reciprocal best-hit protein-protein BLAST (data not shown).

Remarkably, worms with mutations in the *Mgrn1* ortholog, C11H1.3, demonstrate complete phenotypic overlap with *Atrn* (tag-53) mutant worms. Both mutants display uncoordinated movement, "dumpy" morphology, low fertility, and the "P-vulva" phenotype (Wormbase website, www.wormbase.org. Release WS213, April 24 2010). Thus *Atrn* and *Mgrn1* are linked by a notable correspondence of pleiotropic overlap both in mice and in worms, suggesting that a functional relationship between the two genes may have been established very early in eumetazoan evolution. If this is the case, one might predict that the neurological defects seen in *distracted* fruit flies will be present in *Drosophila Mgrn1* mutants as well. To date, the only phenotypic information available concerning the physiological function of the D*rosophila Mgrn1* ortholog, CG9941, came from an RNAi study that revealed a role in heart development (Kim *et al.,* 2004).

It also will be of interest to determine whether *Mgrn1* orthologs have a functional relationship with orthologs of the other major member of the *Atrn* gene family, *Megf8.* To date, nothing is known about the phenotypic consequences of loss of fly Megf8, and the rich genomic resources in the *C. elegans* model system not informative because worms in this genus appear to lack a *Megf8* ortholog. In the mouse, however, there are striking similarities between the left-right (L-R) patterning and cardiac defects reported in *Mgrn1* null mutants and a syndrome of abnormal L-R patterning and heart defects that was recently reported in mice homozygous for an ENU-induced mutation in *Megf8* (Cota *et al.*, 2006, Aune *et al., 2008;* Zhang *et al.*, 2009). Both mutations appear to disrupt left-right patterning downstream of the initial symmetry break at the embryonic node. In wild-type embryos, asymmetric expression of *Nodal* at the embryonic node is the initial symmetry-breaking developmental event, which leads to expression of *Nodal* in the left lateral plate mesoderm (LPM) and a left-side specific activation of the "leftness" identity-establishing transcription factors *Lefty1*, *Lefty2,* and *Pitx2* (Shiratori and Hamada, 2006). In both *Mgrn1* and *Megf8*

mutant embryos, the initial symmetry break by *Nodal* at the node occurs normally, but apparently fails to propagate correctly to the LPM, leading to aberrant expression of *Lefty1, Lefty2,* and *Pitx2.* In *Megf8* mutants, normal expression of *Nodal* in the left LPM is also disrupted. The consequences of these defects in early embryonic patterning are similar in both mutants, which exhibit elevated rates of embryonic death due to heart defects, and cardiac malformations characteristic of heterotaxy with elevated frequencies of *situs inversus.* This situation is highly reminiscent of the phenotypic overlap seen between *Mgrn1* and *Atrn* mutants in mouse and nematodes, which is likely to stem from a conserved functional relationship between MGRN1 and ATRN proteins. Given the high similarity between ATRN and MEGF8, and the similarity of the L-R patterning phenotypes of *Megf8* and *Mgrn1* mutations, it seems reasonable to speculate that MGRN1 and MEGF8 have an analogous functional relationship to that between MGRN1 and ATRN. If this speculation is correct, it will explain why the several phenotypes of *Mgrn1* mutant mice map so precisely onto either *Atrn* or *Megf8* mutant phenotypes (Figure 2.8).

In *C. elegans,* the phenotypes of *Mgrn1* mutants completely overlap with those of worms bearing mutations in the single nematode *Atrn* family member. In mice, *Atrn* and *Megf8* mutants phenocopy different subsets of M*grn1* mutant phenotypes. The implication is that MGRN1 and ATRN family members share a conserved functional relationship. If this functional relationship is mediated by a direct physical interaction between MGRN and ATRN-family proteins, it is likely that the interaction occurs between a conserved region of MGRN1 and the cytoplasmic tail of ATRN/MEGF8. By examining the alignment of mouse ATRN, mouse MEGF8, and worm ATRN, it may be possible to predict which regions of the cytoplasmic tail are important for this hypothesized interaction, based on their conservation of sequence across these three proteins. As shown in Figure 2.9, the MASRPFAXVXV motif is an excellent candidate motif for this hypothesized interaction with *Mgrn1*.

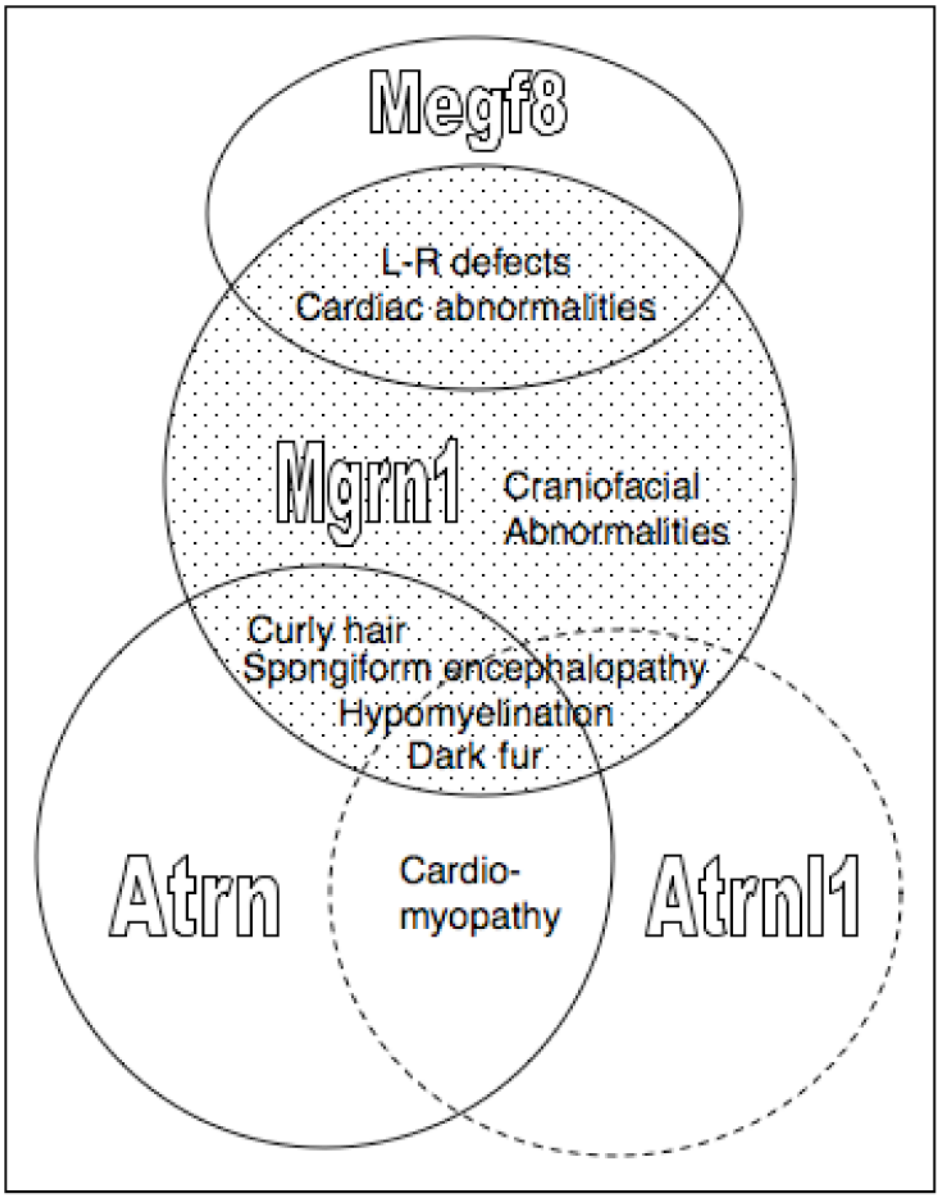

Figure 2.8. Phenotypic overlap of mouse *Mgrn1* and *Atrn* family members. *Megf8* and *Mgrn1* mutants share similar L-R patterning defects and developmental cardiac abnormalities, suggesting cooperation between their gene products in an unknown developmental mechanism. Similarly, the correspondence of mutant phenotypes in *Mgrn1* and *Atrn* suggests a functional relationship between the proteins encoded by these two genes. While no phenotypes of *Atrnl1* single mutants have been reported, ATRNL1 appears to be able to act similarly to ATRN in these pathways if overexpressed, and *Atrn/Atrnl1* double mutants have a cardiomyopathy that likely reveals a redundant function of these two proteins which is not dependent on *Mgrn1*.

Figure 2.9. Conserved cytoplasmic tail sequence across murine and nematode *Atrn*-family genes identifies the highly conserved MASRPFAXVXV sequence as a candidate MGRN1-interaction motif.

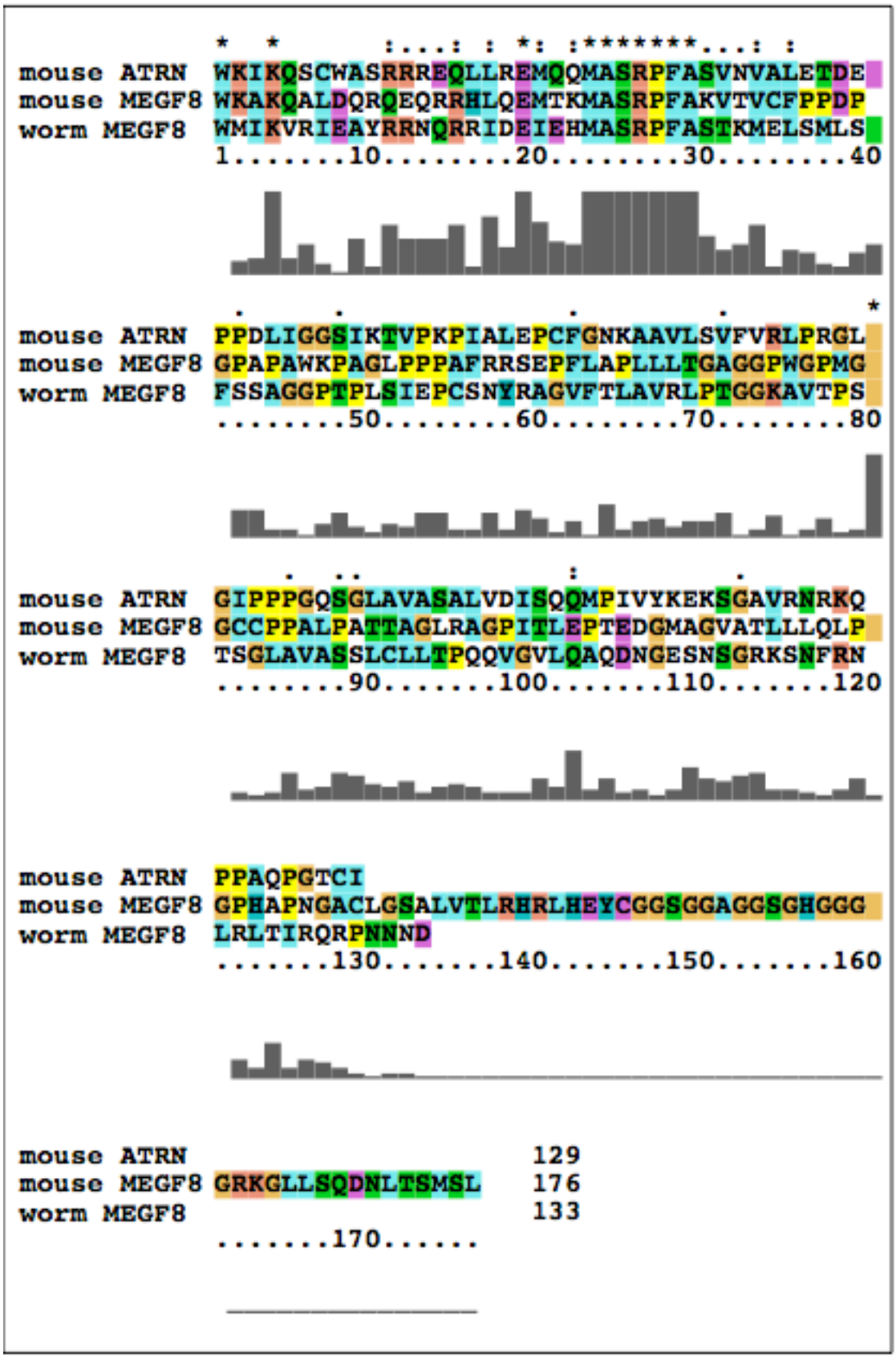
mouse ATRN WKIKQSCWASRRREQLLREMQQMASRPFASVNVALETDE
mouse MEGF8 WKAKQALDQRQEQRRHLQEMTKMASRPFAKVTVCFPPDP
worm MEGF8 WMIKVRIEAYRRNQRRIDEIEHMASRPFASTKMELSMLS
1.....10.....20.....30.....40
mouse ATRN PPDLIGGSIKTVPKPIALEPCFGNKAAVLSVFVRLPRGL
mouse MEGF8 GPAPAWKPAGLPPPAFRRSEPFLAPLLLTGAGGPWGPMG
worm MEGF8 FSSAGGPTPLSIEPCSNYRAGVFTLAVRLPTGGKAVTPS
.....50.....60.....70.....80
mouse ATRN GIPPPGQSGLAVASALVDISQQMPIVYKEKSGAVRNRKQ
mouse MEGF8 GCCPPALPATTAGLRAGPITLEPTEDGMAGVATLLLQLP
worm MEGF8 TSGLAVASSLCLLTPQQVGVLQAQDNGESNSGRKSNFRN
.....90.....100.....110.....120
mouse ATRN PPAQPGTCI
mouse MEGF8 GPHAPNGACLGSALVTLRHRLHEYCGGSGGAGGSGHGGG
worm MEGF8 LRLTIRQRPNNND
.....130.....140.....150.....160
mouse ATRN 129
mouse MEGF8 GRKGLLSQDNLTSMSL 176
worm MEGF8 133
.....170.....

The role of Atrnl1

Paralogous genes often have partly or wholly redundant functions, a fact that is frequently a source of frustration to geneticists: redundant components of a genetic pathway are difficult to identify by forward genetic approaches, and pathways made robust by redundant components are difficult to disable by reverse genetic approaches. *Atrnl1* and *Atrn* present an unusual case study of paralogous proteins. From the standpoint of gain-of-function mutations, the two paralogs are redundant, as overexpression of ATRNL1 largely rescues the pigmentation and neurodegenerative defects of *Atrn* mutants. However, from the standpoint of loss-of-function mutations, the paralogs are non-redundant, as the presence of endogenous levels of ATRNL1 does not mask or ameliorate either the coat color phenotype or the neurodegenerative syndrome of *Atrn* mutants. As endogenous ATRNL1 is widely expressed with similar tissue-level patterns of expression to ATRN (Walker *et al.*, 2007), and since ATRNL1 protein is clearly capable of compensating for ATRN when overexpressed, one might expect that endogenous ATRNL1 would mask the loss of endogenous ATRN. Obviously, this is not the case. The simplest explanation of these observations is that endogenous levels of ATRNL1 may simply be too low (at least in the relevant cell types) to have a detectable effect on pigment type switching or neurodegeneration. Interestingly, *Atrn*$^{-/-}$*; Atrnl1*$^{-/-}$ double mutants were reported to develop a progressive cardiomyopathy that is not exhibited by either single mutant (Walker *et al.*, 2007), indicating that ATRN and ATRNL1 may both be required in cardiac tissue to promote normal function. No progressive cardiomyopathy has been reported in *Mgrn1* mutant mice, suggesting that this function of ATRN/ATRNL1 is *Mgrn1*-independent (Figure 2.8). This conclusion has one caveat, however: it is possible that some functions of *Mgrn1* may be masked in *Mgrn1* mutants by the potentially redundant function of the vertebrate-specific *Mgrn1* paralog, ring finger protein 157 (*Rnf157)*.

ATRNL1 was identified by yeast two-hybrid screen as an interactor of the cytoplasmic tail of MC4R, leading to the suggestion that ATRNL1 might mediate anorexigenic AGRP-dependent signaling through this receptor, analogous to the apparent mediation by ATRN of ASP-dependent signaling through the MC1R (in wild type melanocytes) and MC4R (in hypothalamic neurons of *lethal yellow* mice ectopically expressing ASP). This hypothesis is appealing, but it is challenged by my results. Because ATRNL1 overexpression rescues the pigmentation phenotype of *Atrn* mutants, it seems likely that ATRNL1 interacts with ASP, and yet endogenous ATRNL1 is not sufficient to support obesity in $Atrn^{-/-}$, A^{Y} mice. This suggests that despite fairly widespread expression of ATRNL1 in MC4R+ neurons, ATRNL1 may not be expressed in the critical MC4R+ neuron population involved in energy homeostasis. (In light of this observation, it would be interesting to determine whether *Atrn* null mice overexpressing both *agouti* and *Atrnl1* become obese.) Furthermore, no overt energy homeostasis phenotype has been reported for *Atrnl1* mutants to date. The conclusive experiment will be to test *Atrnl1* null animals (and *Atrn/Atrnl1* double mutants) for resistance to AGRP-induced obesity.

I have suggested that the MASRPFAXVXV motif common to all ATRN family members may be a MGRN1 interaction motif. Given that the neurodegenerative, coat color, curly hair, L-R patterning, and cardiac development phenotypes of *Mgrn1* mutant mice are phenocopied by mutations in either *Atrn* or *Megf8*, an obvious question of interest is whether the craniofacial abnormalities of *Mgrn1* mice might appear in *Atrnl1* mutants, thereby indicating that these phenotypes could be assigned to a functional interaction between *Mgrn1* and this third member of the murine *Atrn* gene family. This is not the case (Walker *et al.,* 2007), meaning that an explanation of these phenotypes of *Mgrn1* mutants must be sought elsewhere.

The apparent functional exchangeability of ATRN and ATRNL1 *in vivo* is

useful for predicting which regions of ATRN are important for its function in the skin and CNS. Although many protein domains are conserved in ATRN homologs across vertebrate and invertebrate genomes, the C-type lectin domain is a vertebrate-specific motif found in both ATRN and ATRNL1. One possibility is that this motif facilitates interactions with melanocortin receptors, which arose in the vertebrate lineage at approximately the same time as the split of the ancestral *Atrn* into two paralogs. As this domain typically mediates interactions with N-linked glycosyl groups, and both ASP and MC1R are reported to be glycosylated (Willard *et al,* 1995; Sanchez *et al.,* 2002), this seems a possibility worthy of investigation. Because the MC4R-interacting region of ATRNL1 has been mapped, it is possible to make predictions regarding a likely MC1R-interacting region of ATRN. The MC4R-interacting region of ATRNL1 spans the 36 amino acid residues immediately following the MASRPFAXVXV motif (Haqq *et al,* 2003). The second half of this region is almost identical between ATRNL1 and ATRN, suggesting that any interaction between ATRN and the cytoplasmic tail of MC1R is likely to be mediated by this region.

Predictions regarding functional regions of the ATRN cytoplasmic tail

The bioinformatic and genetic analysis of ATRN homologs presented in this chapter underlies several hypotheses concerning putative functional sequences in the cytoplasmic tail of ATRN. These include a coiled-coil-forming juxtamembrane region, which is potentially a dimerization motif; the MASRPFAXVXV motif, hypothesized to be a MGRN1 interaction region; and a likely site of interaction with MC1R, homologous to the MC4R-interaction region of the ATRNL1 cytoplasmic tail. These proposed interactions form the basis of a mechanistic explanation of the genetic interactions of *Atrn, Mgrn1, Mc1r,* and *agouti.* The next chapter will explore the cell biology, colocalization, and interactions of ATRN, MGRN1, and MC1R.

CHAPTER THREE

CELL BIOLOGY AND MOLECULAR INTERACTIONS OF ATTRACTIN, MAHOGUNIN RING-FINGER 1, AND MELANOCORTIN RECEPTOR 1

Chapter Overview

This chapter describes experiments testing the hypotheses derived from the bioinformatic and genetic analyses of Chapter Two. Specifically, data are presented demonstrating physical interactions between ATRN and both MGRN1 and MC1R, and tagged ATRN and MC1R are shown to colocalize and to traffic through the endosomal/lysosomal pathway in transiently transfected HEK293T cells. These observations suggest that ATRN may function as a MGRN1- and ASP-dependent lysosomal targeting factor for MC1R, a hypothesis that will be further investigated in the melanocyte model in Chapter Four.

Introduction to Melanocortin Receptor 1 biology

To place the data of this chapter in context, it will be useful to have in mind a brief overview of G-protein-coupled receptor (GPCR) signaling biology. The canonical view of GPCR signaling imagines the receptor as occupying an equilibrium state between "active" and "inactive" conformations, where agonist binding stabilizes the active conformation and inverse agonist binding stabilizes the inactive conformation. The active conformation allows the receptor to interact with a G protein α (Gα) subunit in a way that promotes GDP-GTP exchange and causes the release of the GTP-bound Gα from the G protein heterotrimer. Downstream events depend on the Gα subunit binding specificity of the receptor in question; for MC1R, signaling occurs through the stimulatory Gαs molecule, which functions in the melanocyte to activate adenylyl cyclase. Because MC1R has a high constitutive rate

of signaling, this receptor stimulates cAMP production even in the absence of the agonist, αMSH.

Signaling from GPCRs is limited by several fairly well-understood processes (Figure 3.1). First, the GTP-bound G-protein α subunits produced by GPCR activity have an intrinsic GTP hydrolysis ability that limits the signaling lifetime of each individual activated G protein. In addition, ligand binding causes many GPCRs to be removed from the plasma membrane into early endosomes, which in many cases promotes dissociation of the GPCR from its ligand due to the relatively low pH of the endosomal lumen. At this point, internalized GPCRs are subject to desensitization, which canonically occurs when agonist-bound GPCRs are phosphorylated by G-protein-coupled receptor kinases (GRKs), recruiting arrestins which decouple them from their G proteins and render them temporarily insensitive to further stimulation (reviewed by Moore, Milano, and Benovic, 2007). MC1R has been shown to undergo desensitization upon phosphorylation by GERK2 and GERK6 (Sanchez-Mas *et al.*, 2005). From the early endosome, internalized GPCRs can follow a "fast" recycling pathway directly back to the plasma membrane, or a "slow" recycling pathway that leads to the plasma membrane by way of a large tubulovesicular sorting station, the Rab11-positive endosomal recycling complex (ERC). Recycled GPCRs are thus returned to the plasma membrane and made available for a second round of ligand binding and G protein-coupled signaling. However, some GPCRs follow an alternative pathway from the Rab5-labeled early endosome and are sorted towards the lysosome for degradation. The critical decision point in this process occurs at the surface of incipient late endosomes, referred to as multivesicular bodies (MVBs) due to their complex "vesicles within a vesicle" morphology. There, receptors and other transmembrane proteins destined for lysosomal degradation are recognized by proteins of the Endosomal Complex Required for Transport (ESCRT) machinery, frequently on

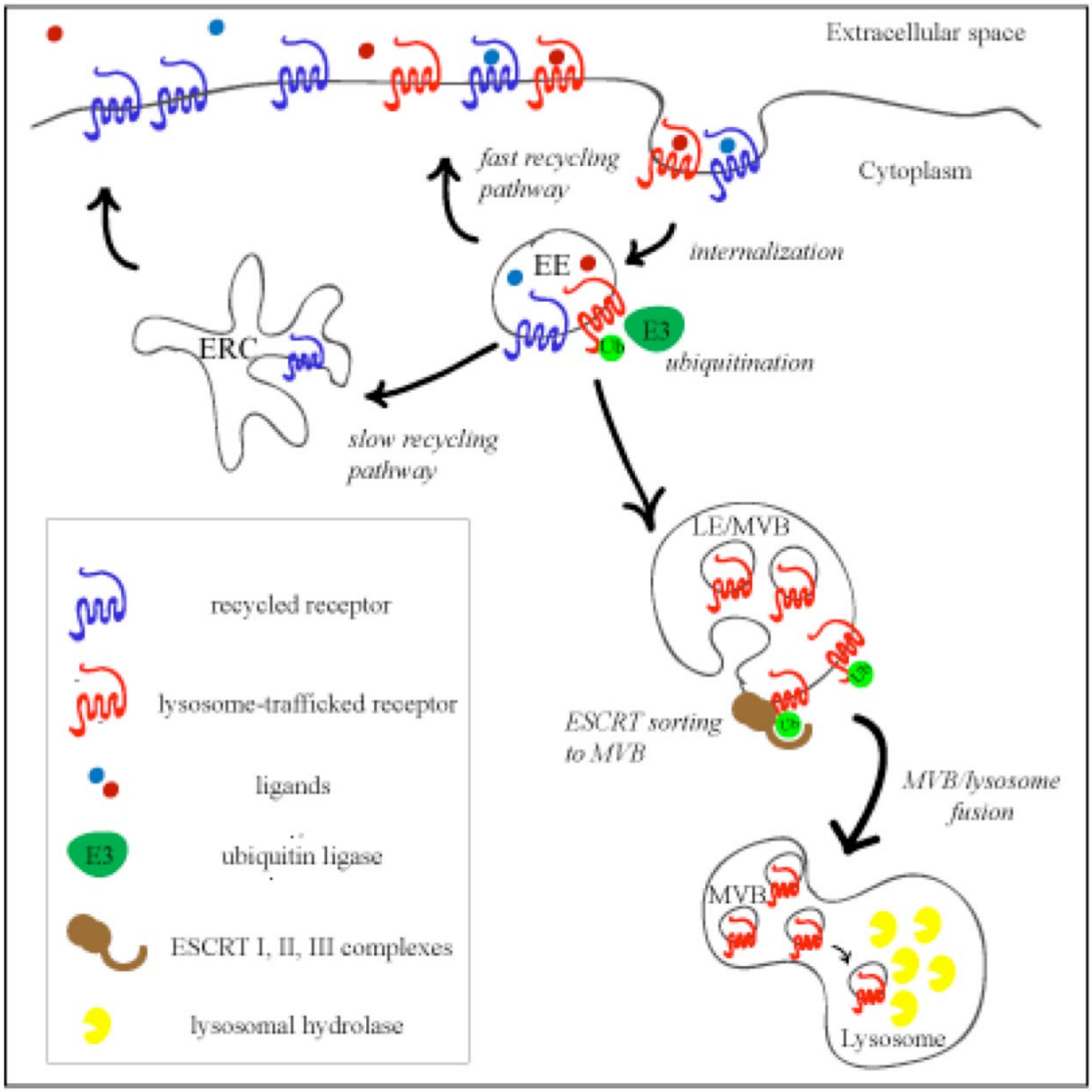

Figure 3.1. GPCR recycling and lysosomal trafficking. Endocytosed GPCRs in early endosomes (EEs) may recycle to the plasma membrane directly through the fast endosomal recycling pathway, or indirectly through the endosomal recycling complex (ERC). Monoubiquitinated receptors may be recognized by proteins of the ESCRT complex and sorted into the intracisternal vesicles of late endosomes/multivesicular bodies (LEs/MVBs). Fusion of the MVB with the lysosome delivers ESCRT cargo to lysosomal hydrolases for degradation.

the basis of a monoubiquitin tag attached to a lysine residue of the target protein. Proteins so recognized are handled sequentially by three major complexes of ESCRT proteins (ESCRT I-III) and sorted into the intracisternal vesicles of the MVB, topologically sequestering any active receptors from their effectors and effectively silencing them. The limiting membrane of the mature MVB then fuses with a lysosome, releasing the intracisternal cargo into the lysosomal lumen for degradation by lysosomal hydrolases. This highly effective mechanism of receptor downregulation is well-characterized for the yeast α mating pheromone receptor, the GPCR Ste2p. Ligand-bound Ste2p is ubiquitinated by the Nedd4 family E3 ubiquitin ligase Rsp5p, causing the receptor to be sorted by ESCRT proteins into the intracisternal vesicles of the MVB, leading to the lysosomal trafficking and degradation of the receptor (Hicke and Reizman, 1996; Dunn and Hicke, 2001; for a review of ubiquitin-mediated receptor downregulation through the endolysosomal pathway see Katzmann, Odorizzi, and Emr, 2002). Compared to the first two mechanisms, lysosomal degradation is an especially potent, irreversible means of limiting GPCR signaling. Whether MC1R undergoes a regulated lysosomal trafficking event as part of the agouti-mediated pigment-type switching mechanism is not known, but it is interesting to note that ASP treatment has been reported to induce a reduction in MC1R protein levels in cultured melanocytes and in rat skin (Rouzaud *et al.,* 2003; Yang *et al.,* 2004). If this reduction requires active MC1R protein degradation (as opposed to decreased MC1R biogenesis and unaltered protein turnover rates), it is probable that this degradation occurs via the lysosomal degradative pathway.

These canonical modes of GPCR signaling regulation are relatively well understood, at least for model GPCRs such as the yeast mating pheromone receptors. However, recent lines of investigation have revealed additional levels of complexity in signaling of some GPCRs. It has been recognized that many, if not most, GPCRs

form dimers or higher-order oligomers, and that this oligomerization may be important for their function (Reviewed in Milligan 2007; Gurevich and Gurevich 2008). Analysis of the functional importance of GPCR oligomerization is complicated by the fact that some GPCRs actually participate in GPCR "heteromers" made up of more than one type of GPCR (*e.g.,* Harikumar *et al,* 2008; Pello *et al.,* 2008; Vidi *et al.,* 2008.) MC1R is known to form homodimers (and probably higher-order oligomers), which appear to form from domain-swapping interactions between the subunits (Zanna *et al.,* 2008). These oligomers are stabilized by the presence of conserved cysteines and are reducible with β-mercaptoethanol, indicating that intermolecular disulfide bonds probably contribute to their structure. Furthermore, the dimerization of MC1R appears to be critical for its function, as non-dimerizing mutants fail to localize to the plasma membrane. Whether the oligomerization state of MC1R is affected by ASP treatment or by interaction with ATRN or MGRN is not known.

Another emerging theme in GPCR signaling is that signaling from the receptor is not necessarily confined to plasma membrane-localized GPCRs. It has recently become apparent that so-called "signaling endosomes" containing active GPCRs, G proteins, and effectors can be internalized from the plasma membrane and persist as signaling centers in the cytoplasm over long periods of time (e.g., see Calebiro *et al.,* 2009). In some cases, coupling of GPCR signaling to downstream signaling pathways may be dependent on GPCR internalization to endosomes, suggesting that the details of post-endocytosis GPCR trafficking may be important in determining the physiological effects of ligand binding (reviewed in Jalink and Moolenaar, 2010). This realization potentially adds a new layer of complexity to interpretations of ASP signaling, raising the possibility that ASP-bound MC1R may not merely be "turned off" with respect to cAMP production but could also have altered coupling to a non-cAMP-mediated signaling pathway. This scenario is one possible explanation of the

curious observation that ASP-overexpressing mice are actually yellower than *Mc1R* null animals (Jackson *et al.*, 2007; Ollmann *et al.*, 1998), which is difficult to explain if ASP is strictly an inactivator of MC1R signaling.

Another interesting development in GPCR signaling biology is the growing list of transmembrane receptor accessory proteins that act as modulators of GPCR function. A particularly pertinent example are the Melanocortin Receptor Accessory Proteins (MRAPS), which are single-pass transmembrane proteins that act as bidirectional trafficking regulators of melanocortin receptors (Chan *et al.*, 2009). Signaling from the melanocortin 2 receptor is profoundly reduced in the absence of MRAPS. Another GPCR, the calcitonin receptor (CTR), interacts with a trio of glycosylated single-pass transmembrane proteins, the Receptor Accessory Membrane Proteins (RAMPS) (Parameswaran and Spielman, 2006) which affect the CTR's cellular localization, signaling efficiency, and even its substrate specificity. Both of these examples underscore the importance of proper intracellular trafficking for regulation of signaling, and demonstrate that receptor accessory proteins can be important modifiers of such trafficking events.

If a single theme emerges from the considerations outlined above, it is that understanding how a GPCR is trafficked may be helpful to understanding the regulation of its signaling. Post-internalization trafficking events can lead to the recycling of GPCRs to the plasma membrane, the transfer of signaling GPCRs to signaling endosomes, or to the lysosomal trafficking and degradation of the GPCRs. Interactions with receptor accessory proteins and ubiquitination by E3 ligases can be decisive in sending a GPCR down one trafficking pathway or another, suggesting that interacting with ATRN and/or MGRN1 could affect MC1R signaling by altering its trafficking fate.

When specific antibodies are not yet available for a protein of interest (as was

true for both ATRN and MC1R when I began this project), the use of fluorescently tagged expression constructs can be a powerful approach for gaining insight into the protein's interactions and cellular behavior. The tags can be used as epitope "handles" for coimmunoprecipitation assays, and the tagged proteins can be observed under the confocal microscope to determine their location within the cell, their dynamic trafficking behavior, and whether they colocalize with other proteins of interest. While both the presence of the tag and the overexpression of the protein introduce caveats to the interpretation of the results, the ease of generation of the tagged constructs and the wide variety of data that can be gathered using them make this approach especially valuable for initial characterization of proteins of interest. To begin my exploration of the molecular interactions and behavior of ATRN, MGRN1, and MC1R, I used fluorescent-tagged forms of these proteins to characterize their colocalization, intracellular trafficking, and physical interactions.

Materials and Methods

Construction of tagged ATRN and MC1R expression plasmids

All cloned cDNAs and partial cDNAs were amplified using the iProof high-fidelity *Pfu* DNA polymerase (Bio-Rad, Hercules, CA). The full-length murine *Atrn* coding sequence (CDS) (excepting the stop codon) was amplified from a cDNA clone using primers CACCAGCACTGATTGGCCTAC and AATGCAGGTTCCAGGC. The gel-purified PCR product was recombined into the pENTR/DTOPO entry vector (Invitrogen, Carlsbad, CA) and sequence verified to generate clone DTOPO-AtrnCDS-7. The full-length (single exon) *Mc1R* CDS was amplified directly from genomic DNA of a C57Bl/6J mouse using primers CACCATGTCCACTGAGGAGCC and CCAGGAGCACAGCAGCACCTCC and recombined with the pENTR/DTOPO vector to generate sequence-verified clone

DTOPO-Mc1r 23. The *Atrn* cytoplasmic tail was amplified using forward primer CACCATGTGGAAGATCAAGCAGAGCTGT and reverse primer AATGCAGGTTCCAGGC. A series of truncated *Atrn* cytoplasmic tail constructs were made using the same reverse primer and the forward primers CACCATGCAACAGATGGCCAG (AtrnCytoΔ1), CACCATGACAGATGAAGAACCTC (AtrnCytoΔ2), or CACCATGAGGCTCCCTCGAGGAC (AtrnCytoΔ3), using DTOPO-ATRN-CDS7 as template.

The fluorescent protein-encoding plasmids pEGFP-N1 and pdsRed-monomer-N1 (Clontech, Mountain View, CA) were modified by insertion of an in-frame Gateway cassette to make destination vectors pDEST-EGFP and pDEST-dsRed. The entry vectors described above were recombined with the destination vectors using LR clonase (Invitrogen, Carlsbad, CA) to generate C-terminal tagged expression constructs.

Other plasmids

GFP-tagged Rab5 and Rab7 plasmids were the kind gift of Cecilia Bucci, and have been described previously (Deinhadt *et al.*, 2006). YFP-Rab11 was created by Craig Roy as described in Guignot *et al.* (2004). Lamp1-DsRed and CD63-dsRed have been described (Sherer *et al.*, 2003) and were kindly supplied by Volker Vogt. The MGRN1-GFP and MGRN1(AVVA)-GFP plasmids have been described in Jiao *et al.*, 2009a; the MGRN1(AVVA) sequence differs from wild type by the conversion to alanines of two conserved cysteines in the RING domain, which results in a MGRN1 protein without E3 ubiquitin ligase activity.

Transfection and cell culture

HEK293T cells and Neuro2A cells were cultured under 5% CO2 in DMEM supplemented with L-glutamine, 10% FBS, and penicillin/streptomycin (all medium components from Gibco [Invitrogen], Carlsbad, CA), and transfected by the calcium phosphate method (Kingston, Chen, and Rose, 2003). Cells to be transfected were passaged 1:6 or 1:8, approximately 18 hours before transfection, and given fresh medium 2 hours before transfection. For a 6cm plate of cells, 4 ug total DNA was added to 10 uL of filter-sterilized 2.5 M CaCl2 and brought to 100 uL with sterile water. A DNA-hydroxyapatite precipitate was produced by the addition of 100 uL of filter-sterilized 2X HBS (50 mM HEPES, 280 mM NaCl, 1.5 mM NaPO4), allowed to incubate for 1-5 minutes until fine precipitate was visible at 10x magnification, then added to culture plates. For evaluation of lysosomal trafficking by live-imaging confocal microscopy, Lysotracker Red (Molecular Probes, Eugene, OR) was applied to cells at 200nM for 30 minutes prior to imaging. Lysosomal inhibition was carried out overnight using 50 mM ammonium chloride or 100μM chloroquine (Sigma-Aldrich, St. Louis, MO). Results presented are representative of at least two independent replicate experiments.

Confocal microscopy

Transiently transfected HEK293T cells were inspected using a Zeiss LSM510 Meta confocal microscope and the LSM510 software package. For comparisons of signal intensity between experimental and control conditions, imaging was performed under identical microscope settings and any post-processing of images was applied to all images equally.

Western blotting

Cells were collected 24-72 hours after transfection and lysed in solubilization buffer (50uM Tris-HCl pH 8.0, 1 mM EDTA, 10 mM iodoacetamide, 1% Igepal CA-630) containing Complete protease inhibitor cocktail (Roche). Lysates were centrifuged at 13,000 rpm in a benchtop microcentrifuge for 5 minutes to pellet debris, and the protein concentration of the cleared supernatant was measured by bicinchonic acid assay (Pierce). Loading samples were made by addition of a 3X SDS sample buffer (180 mM Tris-HCl pH 6.8, 15% glycerol, 9% SDS, .075% bromophenol blue, with or without 3M β-mercaptoethanol), and 10-50 ug protein/lane of each sample was run on polyacrylamide gels under standard Laemmli conditions (Laemmli, 1970) prior to wet electrophoretic transfer to Immobilon P membrane (Millipore). Samples were routinely heated before loading at 95^{o}C for 5 minutes, except for samples for demonstration of MC1R-GFP, which were not heated as heating irreversibly denatures this protein and inhibits blotting. Blots were blocked in 5% dry milk in TBS/T (100 mM Tris-HCl pH 7.5, 150 mM NaCl, 0.1% Tween-20) prior to incubation with antibodies.

Antibodies

Polyclonal rabbit anti-GFP antibody A11122 was obtained from Invitrogen (Carlsbad, CA) and used for Western blot at a dilution of 1:2000. Anti-HA mouse antibody HA.11 (used for Western at 1:1000) was from Covance. The anti-ATRN[60] rabbit polyclonal (used for Western at 1:1000) was raised against an epitope from the extracellular domain of mouse ATRN and is from the lab of Dr. Gregory Barsh. The rabbit anti-human MGRN1 polyclonal #11285 (used for Western at 1:600) was obtained from ProteinTech (Chicago, IL). Horseradish peroxidase (HRP)-conjugated goat anti-mouse secondary antibody was from BD Biosciences (San Jose, CA).

Coimmunoprecipitation

Cells were collected 48 hours after transfection, rinsed with PBS, and lysed in Cytobuster protein extraction reagent (Novagen, Madison, WI). Cells were precleared with protein A/G agarose beads and mouse IgG (Santa Cruz Biotechnology, Santa Cruz, CA) before immunoprecipitation with 1 ug anti-HA antibody and binding to 40 uL protein A/G agarose beads (Novabiochem). Non-complexed proteins were removed by filtration over an agarose-binding mini spin column (Novagen, Madison, WI) and washed with GrabIt buffer (Novagen) before elution in 1X SDS buffer (Novagen).

Results

ATRN-GFP forms oligomers and occupies endosome-like structures.

ATRN-GFP expressed in HEK293T cells occupies mobile, punctate, endosome-like structures within the cell (Figure 3.2AA). ATRN has also been shown to occupy endosome-like structures in neurons of the rat CNS by immunohistochemistry (Nakadate, Sakakibara, and Ueda; 2008), suggesting that the tagged ATRN retains at least some of the trafficking features of the native protein. When visualized by western blot using an antibody against the C-terminal GFP tag, ATRN-GFP forms a band of the expected molecular weight (~240 kD), representing monomeric ATRN-GFP (Figure 3.2D). A secondary band at high molecular weight, and a very high molecular weight "smear" of ATRN-GFP signal are observable when non-reducing electrophoretic conditions are used, and are likely to represent oligomeric species of ATRN. These high-molecular-weight bands collapse into a single band at monomeric size if β-mercaptoethanol is included in the sample loading buffer, suggesting that intermolecular disulfide bonds contribute to the structure of the oligomeric species. This single band can be resolved into a doublet under longer gel separation times, reflecting an unknown difference in post-translational modification. Besides the

signal coming from full-length ATRN-GFP, some GFP signal is also visible at approximately 30kD in western blots from ATRN-GFP-transfected cells (data not shown). This is approximately the molecular weight of native GFP, suggesting that some subset of the ATRN-GFP molecules are subject to a cleavage event near the end of the cytoplasmic tail of ATRN or else within the primary sequence of the GFP tag itself.

Colocalization of fluorescent-tagged ATRN, MC1R, and MGRN1 proteins

I examined HEK293T cells co-transfected with ATRN-dsRED and GFP-tagged MC1R to determine whether these proteins co-localize. GFP-tagged MC1R forms several bands by western blot (Figure 3.2E), presumably due to oligomerization of the receptor as reported by Zanna *et al.* (2008). Under the confocal microscope, tagged MC1R primarily localized to endosome-like structures, similar in appearance to those occupied by ATRN (Figure 3.2B). Tagged ATRN and MC1R proteins clearly colocalized in a substantial proportion of endosome-like structures when cotransfected into HEK293T cells (Figure 3.2E). As MGRN1 has been reported to decorate the surface of endosomes (Kim *et al.*, 2007), I attempted similar colocalization experiments with MGRN-GFP. Unambiguous demonstration of meaningful colocalization of this construct with ATRN-dsRed was problematic, as the MGRN-GFP fusion protein produces GFP signal both on punctate, apparently membrane-bound structures and diffusely in the cytosol. Furthermore, cotransfection with MGRN1-GFP seemed to cause a marked reduction in ATRN-dsRed levels, making it impossible to get satisfactory images of ATRN-dsRed and MGRN-GFP. Interestingly, this apparent reduction of ATRN-dsRed levels was not seen when ATRN-dsRed was cotransfected with the catalytically inactive MGRN(AVVA)-GFP construct (data not shown).

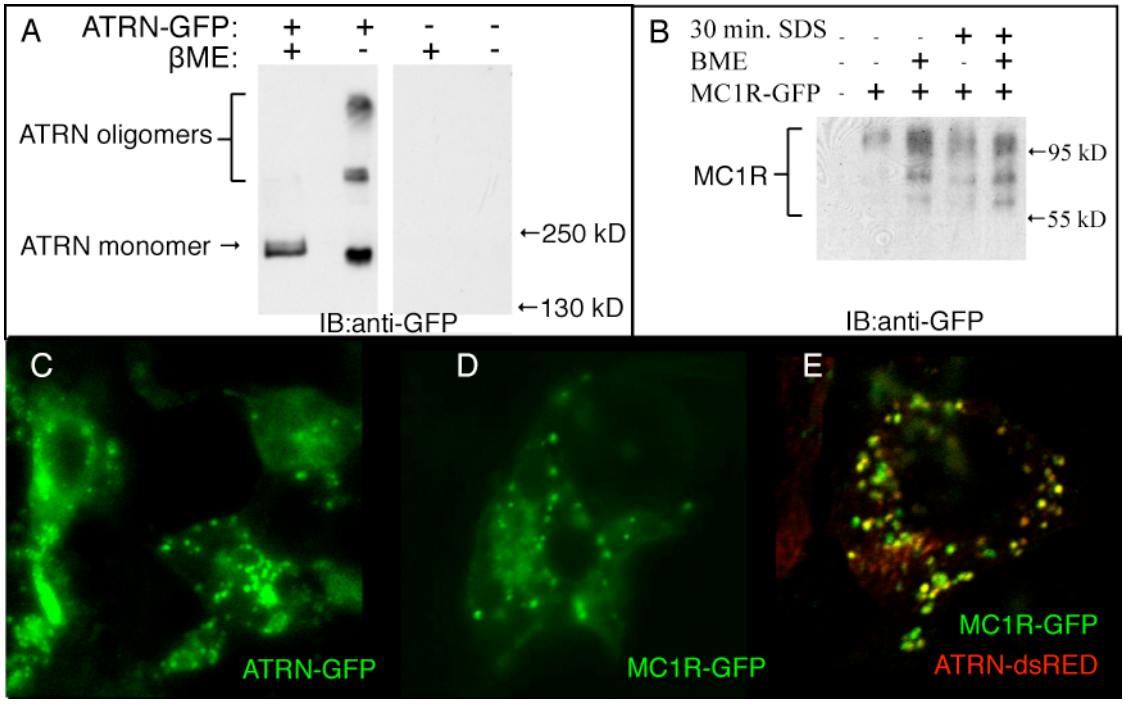

Figure 3.2. Expression and colocalization of fluorescent-tagged ATRN, MC1R, and MGRN1. ATRN-GFP (A) and MC1R-GFP (B) are detectable by western blot using an antibody against GFP. ATRN-GFP (C) and MC1R-GFP (D) signal decorates endosome-like structures in transfected HEK293T cells. ATRN-GFP colocalizes with MC1R-dsRed in a subset of endosomes (E).

ATRN-GFP traffics through the endosomal/lysosomal pathway

That ATRN colocalizes with both MGRN1 and MC1R in endosome-like structures suggests that this subcellular location may be important for the ordinary functions of these proteins in the pigment-type switching pathway. To further characterize this endosome-like subcellular compartment, I cotransfected tagged ATRN with fluorescent markers of endosomes, lysosomes, and the trans-Golgi apparatus. Tagged ATRN showed little colocalization with the early endosome marker RAB5-GFP, but clearly occupied late endosomes marked with the late endosome marker RAB7-GFP, and also colocalized extensively with the lysosome marker Lysotracker Red (Figure 3.3 A-C). Under the confocal microscope, ATRN-GFP-labeled endosome-like structures were clearly observed trafficking to and fusing with Lysotracker Red-labeled late endosomes/lysosomes over a time scale of seconds to minutes. By time-lapse confocal imaging, transient occupation of the RAB11-YFP-labeled endosomal recycling compartment by tagged ATRN was also observed (time-lapse data not shown). MC1R was observed in RAB5-GFP-labeled early endosomes, and occupied some RAB7-GFP-labeled late endosomes and CD63-dsRed-labeled late endosomes/lysosomes (Figure 3.3 D-F). Interestingly, RAB7-GFP coexpression appeared to cause a marked intensification of MC1R-dsRed signal at the plasma membrane (Compare 3.3E and 3.3 D or F).

ATRN-GFP accumulates in cells treated with lysosomal protease inhibitors

The observation of ATRN in late endosomes and lysosomes suggested that ATRN may traffic to the lysosome for degradation by lysosomal proteases. To test this hypothesis, I used confocal microscopy to examine ATRN-GFP-transfected cells that had been treated overnight with 45 uM chloroquine or 25 mM NH_4Cl to inactivate lysosomal proteases. Either treatment caused the accumulation of ATRN-GFP in

Figure 3.3. Tagged ATRN and MC1R traffic through the endosomal/lysosomal pathway. ATRN shows little colocalization with the early endosome marker RAB5-GFP (A), but is visible occupying late endosomes marked with RAB7-GFP (B, arrow) and extensively colocalizes with the late endosome/lysosome marker, Lysotracker Red (C). MC1R-dsRed occupies early endosomes marked with GFP-RAB5 (D, arrow), late endosomes marked with RAB7-GFP (E, arrow), and late endosomes/lysosomes labeled with CD63-dsRed (F, arrow. CD63-dsRed signal is false-colored grey in this image).

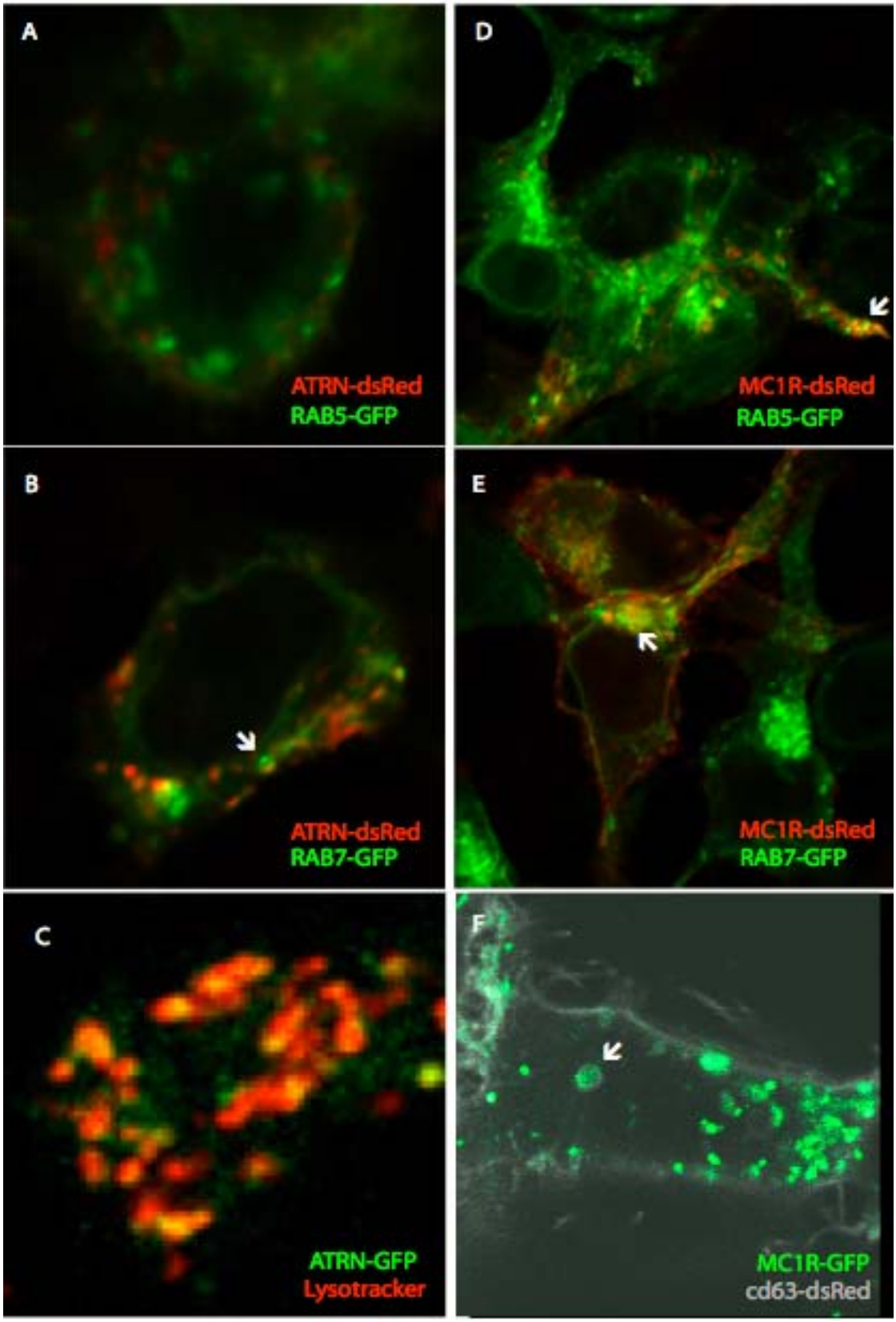
A
ATRN-dsRed
RAB5-GFP
D
MC1R-dsRed
RAB5-GFP
B
ATRN-dsRed
RAB7-GFP
E
MC1R-dsRed
RAB7-GFP
C
ATRN-GFP
Lysotracker
F
MC1R-GFP
cd63-dsRed

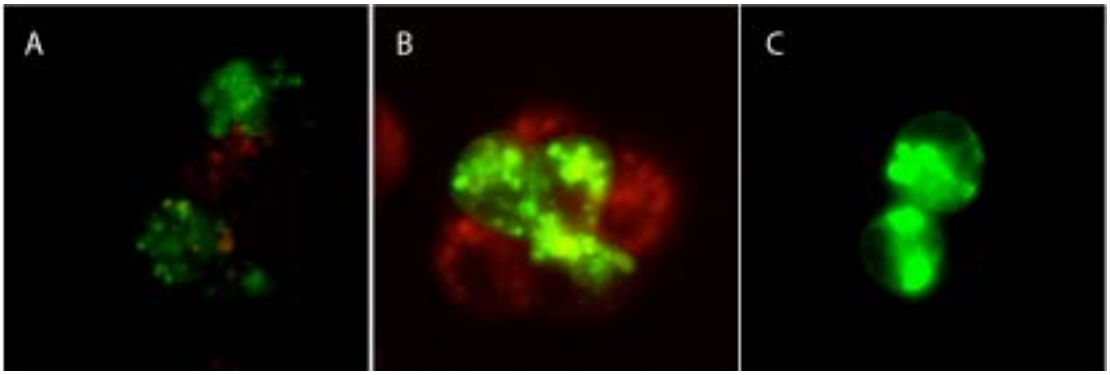

Figure 3.4. Lysosomal inhibition causes accumulation of ATRN-GFP. Representative cells imaged under identical conditions show increased ATRN-GFP signal in cells treated with the lysosomal inhibitors chloroquine (B) or ammonium chloride (C) compared to control cells (A). Red signal is Lysotracker Red. (Note that the lysosomal deacidifier, ammonium chloride, inhibits efficient labeling of lysosomes with the acidotrophic dye Lysotracker Red.)

large, bright vesicular structures, with a strong increase in GFP signal relative to control cells (Figure 3.4). While treatment with 25mM NH_4Cl deacidifies late endosomes/lysosomes to the point that they are no longer labeled by Lysotracker Red (note lack of Lysotracker Red signal in Figure 3.4 panel C), Lysotracker Red still labels late endosomes/lysosomes in cells treated with 45 μM chloroquine (Figure 3.4, panel B). Colocalization of Lysotracker Red with ATRN-GFP signal in chloroquine-treated cells confirmed that the large, bright vesicles full of ATRN-GFP are swollen late endosomes or lysosomes. (Accumulation of ATRN-GFP in chloroquine-treated cells was confirmed by Western blot by Caroline Wee, an undergraduate in the lab, as part of her honors thesis project – data not shown). The accumulation of ATRN-GFP after treatment with lysosome inhibitors suggests that ATRN-GFP is normally degraded by lysosomal proteases.

ATRN and MGRN1 physically interact

The colocalization of ATRN and MGRN1, along with the genetic interactions between *Atrn* and *Mgrn1* outlined in the first chapter, suggested that ATRN and MGRN1 might physically interact. Therefore, reciprocal coimmunoprecipitation experiments were performed using Neuro2A mouse neuroblastoma cell line lysates, which strongly expresses endogenous ATRN and MGRN1. As shown in Figure 3.5, ATRN and MGRN1 coimmunoprecipitated.

ATRN and MC1R cytoplasmic tails physically interact

As discussed in Chapter One, several lines of evidence suggest that MC1R and ATRN may physically interact with each other and that this interaction would be likely to involve their cytoplasmic tails. I tested this hypothesis by cotransfecting ATRN-Cyto-GFP and HA-tagged MC1R-Cyto-GFP into HEK293T cells and

Figure 3.5. ATRN physically interacts with MGRN1 and MC1R. (A) Endogenous ATRN from N2A cells is coimmunoprecipitated by an anti-MGRN1 antibody, but not by non-specific control γ-immunoglobulins (IgG) or by the IgG-binding column without IgG. (B) Endogenous MGRN1 coimmunoprecipitates with an anti-ATRN antibody, but not by non-specific control IgG of by the IgG-binding column without IgG. (C) GFP-tagged ATRN cytoplasmic domain (ATRN-CYTO-GFP) coimmunoprecipitates with HA-tagged MC1R cytoplasmic domain (HA-MC1R-CYTO).

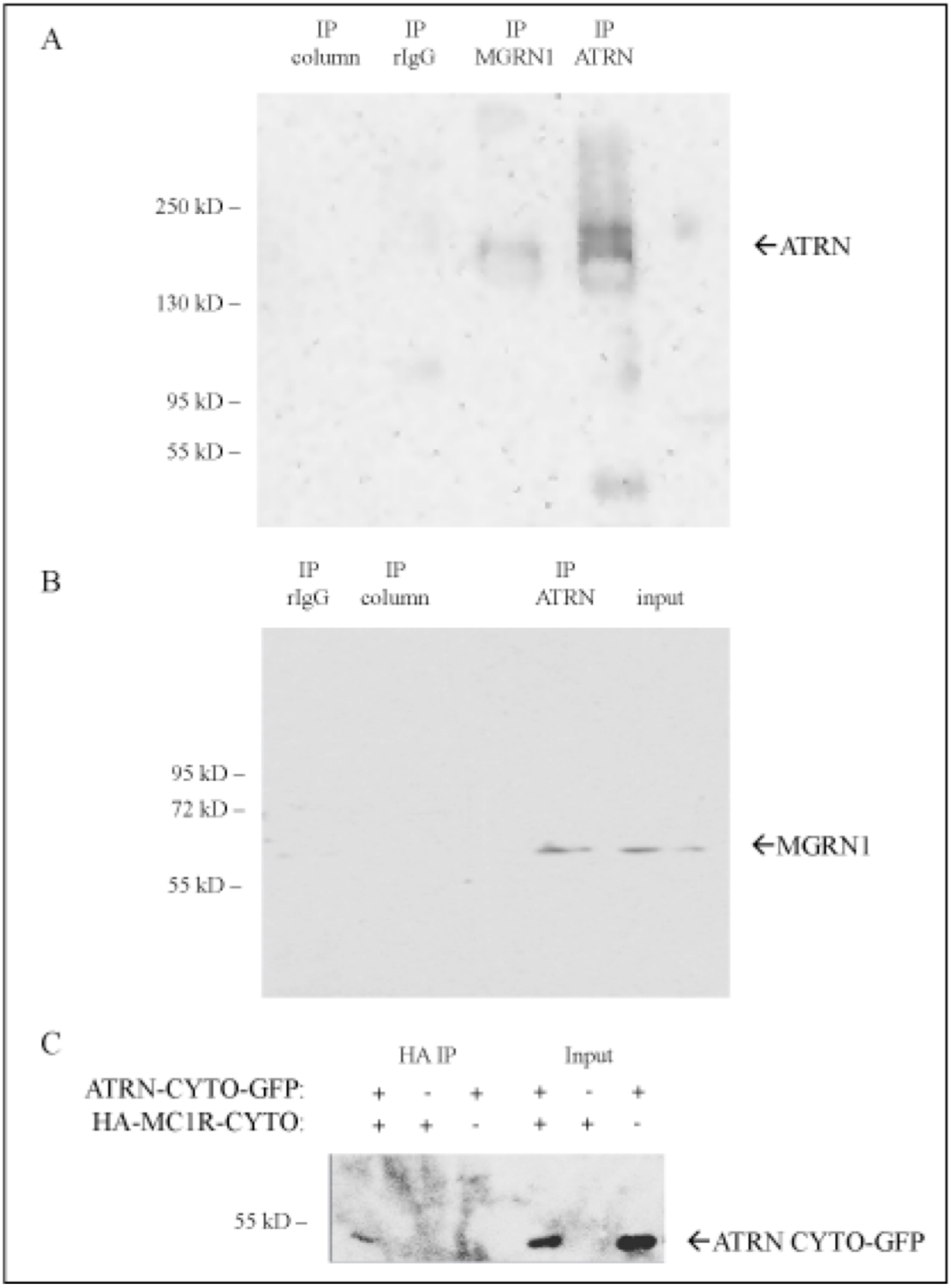
A
IP column
IP rIgG
IP MGRN1
IP ATRN
250 kD –
130 kD –
95 kD –
55 kD –
←ATRN
B
IP rIgG
IP column
IP ATRN
input
95 kD –
72 kD –
55 kD –
←MGRN1
C
HA IP
Input
ATRN-CYTO-GFP: + - + + - +
HA-MC1R-CYTO: + + - + + -
55 kD –
←ATRN CYTO-GFP

performing co-immunoprecipitation experiments using an anti-HA antibody. (The reciprocal experiment was not performed, as the small size [~3 kD] of the HA-MC1R-CYTO peptide makes it unsuitable for immunoblotting.) As shown in Figure 3.5, ATRN-Cyto-GFP coimmunoprecipitated with the HA-tagged MC1R cytoplasmic tail.

MGRN1-sensitive punctate localization of the cytoplasmic tail domain of ATRN

As suggested in the previous chapter, the conserved MASPFAXVXV sequence of the ATRN cytoplasmic tail is an attractive candidate to be the MGRN1-interacting region. In addition, by analogy to the demonstrated MC4R/ATRNL1 interaction, the interaction between MC1R and ATRN is likely to be mediated by the 37 residue sequence immediately C-terminal to the MASRPFAXVXV. Finally, the predicted coiled-coil region of the ATRN cytoplasmic domain is a possible dimerization motif. To create tools for future dissection of the interacting domains of the ATRN cytoplasmic tail, I built a series of ATRN-CYTO truncation constructs (presented schematically in Figure 3.6E). Surprisingly, even though it lacks a transmembrane helix, the AtrnCYTO-GFP fusion protein showed a distinctly punctate distribution within HEK293T cells (Figure 3.6A). This punctate distribution was dependent on the sequence QQMASRPFAXVNVALE, as AtrnCYTOΔ1, but not AtrnCYTOΔ2 or AtrnCYTOΔ3, also showed a punctate cellular distribution (Figure 3.6B-D). Because comparative genomic analysis (see Chapter One) suggested that the conserved MASRPFAXVNV sequence may be a MGRN1-interacting motif, I cotransfected ATRN-GFP with HA-MGRN1 and with the RING mutant HA-MGRN1(AVVA) construct, which is expected to act as a dominant negative MGRN1 mutant. Overexpression of either of the wild-type or mutant protein caused a redistribution of AtrnCYTO-GFP signal from its native, punctate localization to a diffuse cytoplasmic localization, similar to the cellular distribution of AtrnCYTO deletion mutants lacking

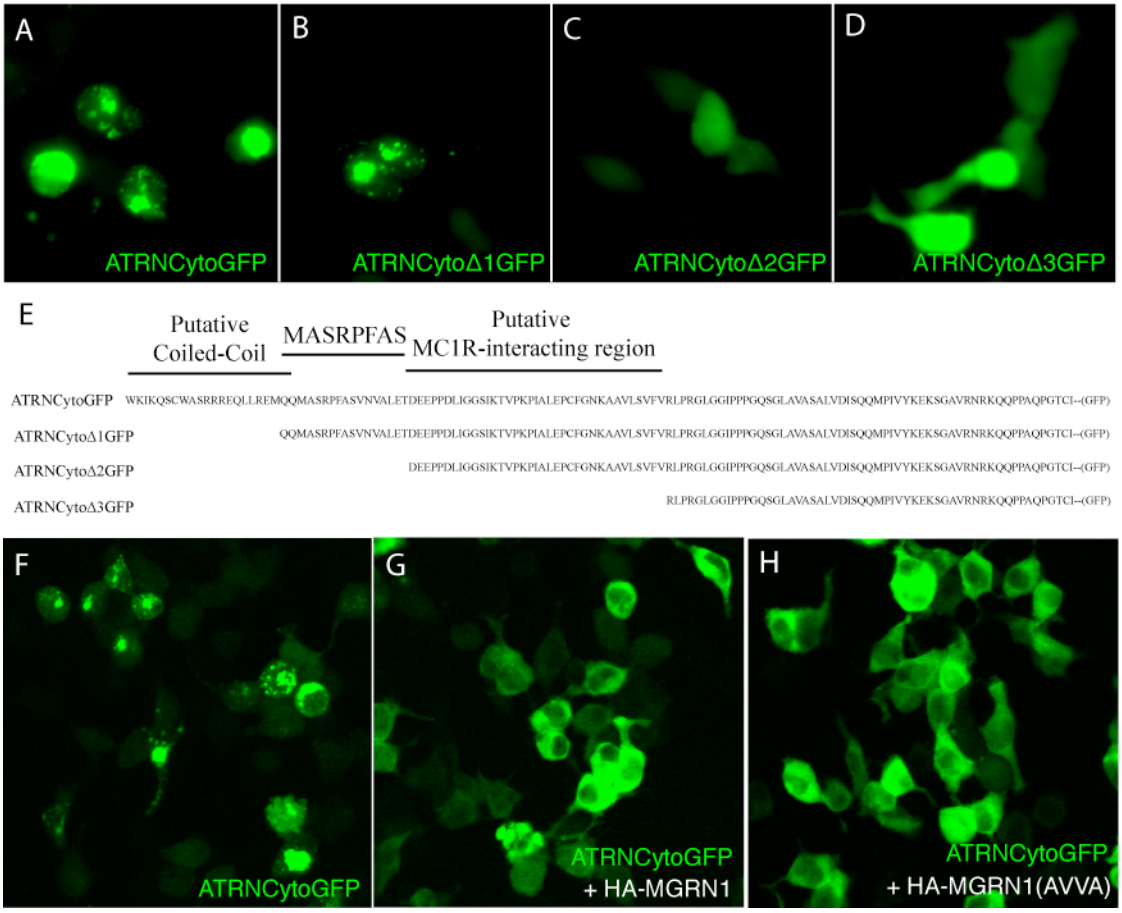

Figure 3.6. Punctate localization of the ATRN cytoplasmic domain is dependent on the QQMASRPFASVNVALE sequence and is ablated by overexpression of MGRN1. Top: the ATRN Cyto-GFP and CytoΔ1 constructs (A & B), but not the CytoΔ2 and CytoΔ3 constructs (C & D), localize to punctate cytoplasmic foci in HEK293T cells. Middle: schematic of the ATRN cytoplasmic tail deletion series (E). Bottom: Punctate distribution of AtrnCytoGFP in HEK293T cells (F) is lost upon cotransfection with HA-MGRN1 (G) or HA(AVVA)MGRN1 (H). Images are representative of three independent replicate experiments.

the QQMASRPFAXVNVALE sequence (Figure 3.6 F-H).

Discussion

While the genetic interactions of ATRN, MC1R, and MGRN1 have long prompted speculation that these proteins are physical interaction partners, the data in this chapter are the first reported evidence of a physical interaction between ATRN and the other two proteins. Combining these newly mapped interactions with the report of a MGRN1-MC1R interaction by Perez-Oliva *et al.* (2009), I propose a model whereby ATRN, MGRN1, and MC1R interact in a ternary complex (see figure 3.7). In this model, the ATRN cytoplasmic tail mediates an interaction with the cytoplasmic tail of MC1R, possibly by an analogous interaction to that reported for the cytoplasmic tails of ATRNL1 and MC4R (Haqq *et al.,* 2003). The coordinated binding of ASP by both ATRN and MC1R may strengthen the association of the two membrane proteins to activate the pigment-type switching mechanism. While I have not demonstrated that the MGRN1-interacting motif of ATRN is in the cytoplasmic tail, the cytoplasmic tail is presumably the only portion of ATRN that is topologically accessible to MGRN1, as indicated in Figure 3.7.

As expected for interacting proteins, fluorescent-protein-tagged ATRN and MC1R colocalize. Interestingly, this colocalization was observed within the cell in endosomal compartments, rather than at the plasma membrane. This suggests that ATRN does not function merely to promote binding of ASP over αMSH at the cell surface, as might be expected if ATRN were "only" an accessory receptor for a classical antagonist. Instead, ATRN's effect on MC1R signaling seems likely to occur within the endosomal trafficking system.

The most striking behavior of tagged ATRN observed in this study is its high rate of trafficking along the endosomal/lysosomal pathway. In conjunction with my

Figure 3.7. Model of ATRN interactions with MC1R and MGRN. (A): The cytoplasmic tail of ATRN interacts with MGRN1 and with the cytoplasmic tail of MC1R. The three proteins are shown in a ternary endosomal complex, with MGRN1 also interacting with MC1R as reported by Perez-Oliva *et al.* (2007). The interaction of ATRN and MC1R is presumably strengthened by their mutual binding of ASP. Note that while proteins are shown singly for clarity, ATRN and MC1R are likely to occur as dimers or higher-order oligomers. (B): Hypothetical function of ATRN as a trans-acting ubiquitinated lysosomal sorting signal for MC1R. Ubiquitinated ATRN is shown being recognized by the ubiquitin-interacting motif of the ESCRT I protein, TSG101, triggering ESCRT sorting of ATRN/MC1R into the intracisternal vesicles of an incipient MVB, leading to lysosomal degradation of ATRN/MC1R. MGRN1 is portrayed in a hypothetical role as the E3 ligase responsible for ubiquitination of ATRN. (C): Alternative or additional roles for MGRN1 in promoting lysosomal trafficking of the ATRN/MC1R complex. As MGRN1 is known to localize to endosomal membranes through its interaction with the ESCRT I protein TSG101, MGRN1's interactions with ATRN and MC1R may directly recruit ATRN/MC1R to sites of ESCRT activity. In addition, MGRN1 monoubiquitination of TSG101 has been reported to promote normal ESCRT function (Kim *et al.*, 2007) and may be an important prerequisite for lysosomal trafficking of ATRN/MC1R.

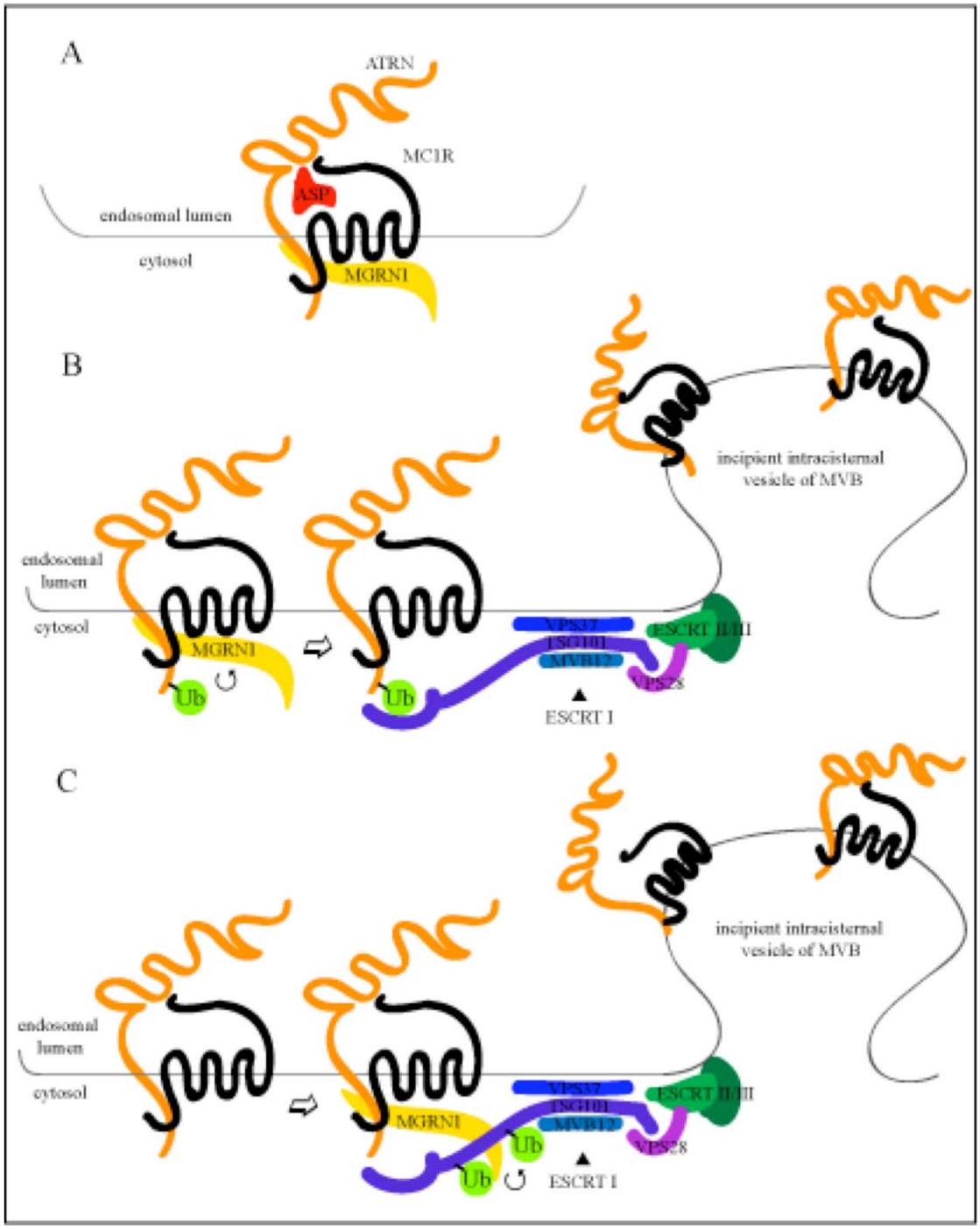
A
ATRN
MC1R
ASP
endosomal lumen
cytosol
MGRN1
B
incipient intracisternal vesicle of MVB
endosomal lumen
cytosol
MGRN1
Ub
VPS37
TSG101
MVB12
ESCRT II/III
VPS28
ESCRT I
C
incipient intracisternal vesicle of MVB
endosomal lumen
cytosol
MGRN1
Ub
Ub
VPS37
TSG101
MVB12
ESCRT II/III
VPS28
ESCRT I

observations of ATRN/MC1R interaction and endosomal colocalization, this behavior suggests a mechanism by which pigment-type switching could occur. Coordinated binding of ASP by ATRN and MC1R would be likely to promote the interaction of their cytoplasmic tails, and perhaps also promote interactions between their extracellular/lumenal domains. The strengthened MC1R/ATRN interaction could tie the trafficking fate of MC1R to that of ATRN, leading to the lysosomal trafficking and degradation of MC1R and a strong reduction of MC1R signaling (Figure 3.7B). This proposed mechanism is consistent with observations by other groups (Rouzaud *et al.*, 2003; Yang *et al.*, 2004) that ASP treatment causes a reduction in MC1R protein levels. If the lysosomal trafficking of ATRN and MC1R does underlie pigment-type switching, the genetic interactions discussed in Chapter One suggest that MGRN1 facilitates this trafficking event. There are several plausible mechanisms by which MGRN1 could promote lysosomal trafficking of ATRN/MC1R. The simplest possibility is that MGRN1 could monoubiquitinate ATRN to provide the signal directing ATRN to the lysosome. MC1R seems unlikely to be a direct target of monoubiquitination by MGRN1 as an interaction between MGRN1 and MC1R has been reported but this interaction did not result in the ubiquitination of MC1R (Perez-Oliva *et al.*, 2009). Monoubiquitination of membrane proteins is a canonical means of targeting them to the lysosome, as the monoubiquitin tag is recognized by the HRS/STAM complex (sometimes referred to as “ESCRT 0”) which initiates sorting of the monoubiquitinated proteins into the intracisternal vesicles of the incipient multivesicular body (MVB). Monoubiquitination of ATRN by MGRN1 could therefore provide a trans-acting lysosomal sorting signal for ATRN-associated MC1R. It is interesting to note that a related GPCR, the delta opioid receptor [DOR], has been reported to be lysosomally degraded in a ubiquitin and ESCRT-dependent manner, without being ubiquitinated itself (Tanowitz and Von Zastrow, 2002; Hislop, Marley,

and Von Zastrow, 2004). This apparent paradox could be explained if the DOR is escorted into the lysosomal trafficking pathway by a trans-acting ubiquitinated sorting factor.

Since MGRN1 is localized to (presumptive) late endosomal membranes by its own interaction with the ESCRT I protein TSG101 (Kim *et al.,* 2007), another possibility is that MGRN1 could promote the lysosomal trafficking of ATRN/MC1R by directly recruiting it to the site of ESCRT activity, perhaps delivering ATRN/MC1R directly to the ESCRT processing machinery. My observations on the punctate distribution of the ATRN cytoplasmic tail are of interest with regard to this possibility. As discussed in Chapter 2, genomic analysis suggests that the MASRPFAS sequence in the ATRN cytoplasmic tail may be a conserved MGRN1 binding motif. I observed that inclusion of this sequence confers a punctate distribution on ATRN-CYTOΔ1-GFP, suggesting that direct recruitment of ATRN-CYTO-GFP by MGRN1 through MASRPFAS may be responsible for the punctate cellular distribution I observed. It will be interesting to determine whether ATRN-Cyto-GFP is being recruited to the same endosomal site of TSG101/MGRN1 interaction reported by Kim *et al.* (2007). Direct recruitment of ATRN by MGRN1 is also compatible with my observation that HA-MGRN overexpression disperses ATRN-CYTO-GFP diffusely into the cytoplasm. Presumably, overexpressed MGRN1 saturates the endogenous endosomal binding sites on Tsg101, leaving an excess of free cytoplasmic MGRN1 to compete with normally localized MGRN1 for ATRN-CYTO-GFP binding. Interactions with this free cytoplasmic MGRN1 may underlie the dispersal of ATRN-CYTO-GFP by overexpression of MGRN1. Finally, even if MGRN1 does not directly ubiquitinate ATRN or deliver it to the ESCRT machinery, MGRN1 may be important for ATRN/MC1R lysosomal trafficking simply because of its functional relationship with its known ubiquitination target, the

TSG101. MGRN1-depleted cells have impaired ESCRT-dependent lysosomal trafficking of the epidermal growth factor receptor (EGFR), suggesting that loss of MGRN1 may cause a general defect in lysosomal trafficking (Kim *et al.,* 2007).

As useful as GFP-tagged constructs are for investigating intracellular trafficking, there are important caveats for their use in degradation studies. For example, the normal, physiologically relevant, degradative pathways involved in regulating levels of a protein of interest may become saturated upon overexpression of the tagged protein, leading to loss of sensitivity in assays designed to measure the physiologically normal route of degradation and perhaps leading to the processing of "excess" tagged proteins through physiologically atypical channels. In addition, the presence of the tag itself may be sufficient to alter the trafficking behavior or degradative dynamics of the proteins of interest. These considerations make it of paramount importance to examine the behavior of endogenous proteins whenever possible. In the case of the molecules of the pigment-type switching system, the use of pigment cells rather than heterologous cell types may also be especially important as the mechanism of pigment type switching is tightly regulated and may be dependent on unknown details of melanocyte biology. I will therefore turn to an investigation of ATRN, MGRN1, and MC1R in the melanocyte in the next chapter.

CHAPTER FOUR

STUDIES OF ATRN, MGRN, AND MC1R IN MELANOCYTES

Chapter Overview

Following up on the observations of tagged ATRN and MC1R in HEK293T cells reported in the previous chapter, Chapter Four extends the studies of ATRN, MGRN1, and MC1R to endogenous proteins and to the physiologically relevant cell type, the melanocyte.

Introduction

Melanocytes are the major pigment-producing cells of the mammalian skin, occurring in hair follicles and scattered throughout pigmented epidermis. Melanocytes differentiate from neural-crest-derived precursors, migrating into their final locations during embryogenesis and maturing into highly dendritic cells specialized for the production and transfer of melanosomes to recipient keratinocytes. The first mouse melanocyte lineages to be cultured *in vitro* were aggressively malignant cells derived from melanomas (Fidler, 1975), but methods were later developed for the culture of melanocyte precursors (melanoblasts) and eventually for the culture of mature melanocytes isolated from neonatal skin (Bennett, Cooper, and Hart, 1987). Mature melanocytes can be immortalized by culturing with cholera toxin and the tumor inducer 12-O-tetradecanoylphorbol-13-acetate (TPA), allowing the establishment of immortal lines of melanocytes from different strains. Melanocyte lines have been established from a wide selection of mouse pigmentation mutants, providing a rich resource for researchers wishing to use the pigment cell as a model system (Sviderskaya, Kallendar, and Bennett, 2010). To investigate my hypothesis that ATRN functions as a MGRN1-dependent, *trans*-acting lysosomal sorting factor for MC1R, I

studied ATRN, MGRN1, and MC1R in wild type and mutant melanocytes.

Materials and Methods

Melanocyte culture

Wild-type melan-a melanocytes (originating from C57Bl/6J mice and described in Bennett *et al*, 1987) were a gift from Dr. Dorothy Bennett. Mutant melanocytes bearing null mutations in *Atrn* (melan-mg1, $Atrn^{mg\text{-}3J/mg\text{-}3J}$), *Mgrn1* (melan-md2, $Mgrn1^{md\text{-}nc/md\text{-}nc}$) and *Mc1r (melan-e, $Mc1r^{e/e}$)* were generated by Dr. Elena Sviderskaya at the Wellcome Trust Functional Genomics Cell Bank, in collaboration with Drs. Gregory Barsh and Dorothy Bennett, and have been described (Hida *et al*., 2009). Cells were maintained under conditions described by Sviderskaya *et al.* (1997) with modifications for low CO_2 culture. Briefly, cells were grown in 5-6% CO_2 in RPMI1640 culture medium supplemented with 10% fetal bovine serum (FBS), 2mM glutamine, 100 U/ml penicillin, and 0.1 mg/ml streptomycin. FBS was obtained from SAFC Biosciences (Lenexa, Kansas). RPMI and culture medium supplements were obtained from Cellgro (Manassas, VA). Culture medium pH was adjusted to 7.0 with hydrochloric acid, and 200 nM TPA (Sigma-Aldrich, St. Louis, MO) was added before use.

ASP and αMSH treatment of melanocytes

Purified recombinant agouti protein was a generous gift from Drs. Elodie Le Pape and Vincent Hearing. Its production has been described by Le Pape *et al.* (2008). ASP was added to culture medium at a dosage of 5 μl/ml, which was sufficient to cause a morphological change in recipient melanocytes (as also observed by Le Pape *et al.* [2008]). αMSH was purchased from Sigma-Aldrich and applied at 100nM.

Transfection of melanocytes

Melanocytes were transfected using Lipofectamine 2000 (Invitrogen, Carlsbad, CA) at a ratio of 9 μl Lipofectamine / 3μg DNA (for one well of a 6-well plate; quantities were scaled for other culture vessel sizes). The plasmids used are described in Chapter Three. Transfection efficiency ranged from 2-10%.

Confocal microscopy

Melanocytes were imaged using a Zeiss LSM510 Meta confocal microscope and images were collected using the LSM510 software package. For visualization of lysosomes, melanocytes were treated with Lysotracker Red (Invitrogen, Carlsbad, CA) at 50-100 nM. Cells were imaged 48 hours after transfection.

Antibodies

The rabbit anti-mouse ATRN polyclonal antibodies αATRN-60 and αATRN-1408 were produced against peptides from the cytoplasmic and extracellular region of ATRN, respectively; these antibodies were generous gifts from Dr. Gregory Barsh. All ATRN westerns depicted below were performed using the αATRN-60 antibody unless otherwise noted. A rabbit anti-rat ATRN polyclonal was generously provided by Dr. Shuichi Ueda (Described in Nakadate *et al.,* 2009), and Dr. Vincent Hearing kindly shared the pep-19 rabbit anti-mouse MC1R antibody (Rouzaud *et al.,* 2003). Anti-ATRN antibodies were used for western blotting at 1:1000 dilution. Other antibodies were purchased from commercial sources, including rabbit anti-MGRN1 (Proteintech, Chicago, IL), the FK2 mouse monoclonal anti-ubiquitin (Biomol, Plymouth Meeting, PA), rabbit anti-SUMO1 (Cell Signaling Technologies, Beverly, MA), and the goat anti-MC1R polyclonals N-19 and L20 (Santa Cruz Biotechnology, Santa Cruz, CA).

Western Blotting

Confluent 10 cm plates of melanocytes were scraped and lysed in 200 uL of a cell lysis buffer (50 mM Tris-HCl, pH 8.0; 1% Igepal CA-630; 1 mM EDTA; 10 mM iodoacetamide), frozen and thawed once, and spun at 2000 rpm in a benchtop microcentrifuge for 5 minutes at 4^{o}C to pellet cell debris. The protein concentration of the cleared supernatant was measured by bicinchonic acid (BCA) assay (Pierce) using a Nanodrop spectrophotometer, and 10 ug total protein was combined with a 3X SDS sample buffer (180 mM Tris-HCl pH 6.8, 15% glycerol, 9% SDS, 0.075% bromophenol blue). Samples were routinely boiled before loading, unless MC1R was to be visualized, and β-mercaptoethanol was omitted from samples for anti-ATRN immunoblot as it greatly reduced the strength of the signal. Samples were run under standard SDS-PAGE conditions (Laemlli, 1970) in 8-15% polyacrylamide gels and transferred electrophoretically to Immobilion-P membrane (Millipore, Billerica, MA). After blocking for one hour with 5% dry milk in TBS/T (100 mM Tris, pH7.5; 0.9% NaCl; 0.1% Triton X-100), primary antibodies were applied diluted in TBS/T for 1-3 hours. After incubation with horseradish-peroxidase (HRP) conjugated secondary antibodies and washing in TBS/T, blots were visualized using SuperSignal West Pico or Dura chemiluminescent substrates (Pierce Biotechnology, Rockford, IL).
For deglycosylation of proteins, cleared cell lysates prepared as for western blotting were denatured at 95 ^{o}C for 5 minutes in 1% SDS. 1% NP-40 and 1.5 U/μg peptide N-glycosidase (PNGase F; New England Biolabs, Ipswich, MA,) were added and the lysates were incubated at 37 ^{o}C for three hours. SDS sample buffer was added and the samples were heated to 95 ^{o}C for 5 minutes before separation by SDS-PAGE and analysis by Western blot.

Results

ATRN-GFP traffics through the endosomal/lysosomal pathway in melanocytes

Melan-a cells were transfected with ATRN-GFP in order to observe the trafficking behavior of ATRN in this physiologically relevant cell type. ATRN-GFP in melanocytes exhibited a primarily endosomal distribution, similar to that seen in HEK293T cells. The low transfection efficiency obtained in melanocytes made cotransfection with compartment-specific marker proteins impracticable; however, treatment with Lysotracker Red revealed significant colocalization of ATRN-GFP signal with late endosomes/lysosomes. Time-lapse images recorded ATRN-GFP-labeled endosomes fusing with late endosomal/lysosomal compartments (Figure 4.1A). Trafficking of ATRN-GFP was not unidirectional; in some instances, ATRN-GFP signal could be observed fusing transiently with late endosomes/lysosomes and then withdrawing, suggesting that ATRN-GFP may occupy the limiting membrane of MVBs rather than the intralumenal vesicles.

Lysosomal targeting of ATRN-GFP is lost in MGRN1-null melanocytes.

As described in Chapter Three, overexpression of MGRN1 caused a relocalization of the GFP-tagged ATRN cytoplasmic tail construct, suggesting that MGRN1 may be required for normal late endosomal/lysosomal trafficking of ATRN. Therefore, I transfected *Mgrn1* null (melan-md2) cells with ATRN-GFP and compared the lysosomal trafficking of ATRN-GFP in these cells with that of wild-type cells, using Lysotracker Red. In melan-a cells, ATRN-GFP-labeled endosomes were observed actively trafficking to and fusing with Lysotracker Red-labeled structures over a time scale of minutes (Figure 4.1A). In melan-md2 cells this trafficking was lost; rather than occurring in small endosomes that trafficked to lysosomes, ATRN-GFP was localized to large, amorphous compartments that were static over the time scale observed (3 minutes) and did not colocalize with Lysotracker Red (Figure 4.1B).

Appearance of ATRN by Western blot

Because artifacts associated with overexpression of tagged constructs can cause trafficking abnormalities, it is desirable to examine the behavior of the endogenous protein using an appropriate antibody. To that end, I characterized several available antibodies generated against fragments of the ATRN protein. A commercial rabbit anti-mouse ATRN polyclonal (Abcam) and a rabbit anti-rat ATRN polyclonal kindly shared by Shuichi Ueda and used by his lab for extensive characterization of ATRN protein expression in the rat brain (Nakadate, Sakikibara, and Ueda, 2008) failed to produce specific signal (that is, signal not also evident in extracts from *Atrn*$^{mg\text{-}3J/mg3J}$ cells) in my hands, and failed to label ATRN-GFP in extracts from cells transfected with the tagged construct (data not shown). Better results were seen with the rabbit polyclonal antibody αAtrn-60, which was raised against a peptide from the extracellular/lumenal domain of ATRN and which specifically labels a ~220-240 kD

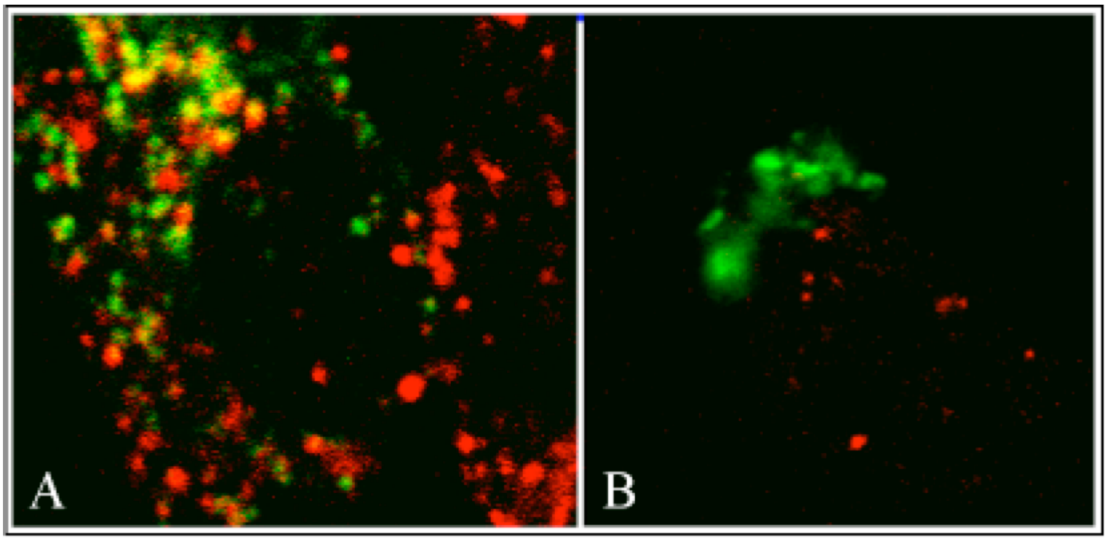

Figure 4.1. A. ATRN-GFP traffics to lysosomes in wild-type melanocytes. Frame from a representative time-lapse image showing rapid trafficking of ATRN-GFP-labeled endosomes to lysosomes labeled with Lysotracker Red. B. Loss of lysosomal trafficking of ATRN in *Mgrn1*$^{md\text{-}nc/md\text{-}nc}$ melanocytes. Frame from a representative time-lapse image showing ATRN-GFP in large, amorphous, static compartments that do not traffic to lysosomes in *Mgrn1*- deficient cells.

doublet in wild-type melan-a cells (Figure 4.2). The appearance of the doublet is reminiscent of the doublet seen for ATRN-GFP and presumably represents a difference in the post-translational modification state of some of the ATRN molecules. An identical set of bands was seen on blots probed with the anti-ATRN antibody αATRN-1408, which was raised against a peptide from the cytoplasmic tail of ATRN (data not shown). For unknown reasons, the inclusion of β-mercaptoethanol in the sample-loading buffer greatly reduced signal intensity (data not shown). As was seen for the ATRN-GFP tagged construct (see Chapter Three), a high-molecular-weight smear was visible in anti-ATRN western blots of unreduced lysates, suggesting that

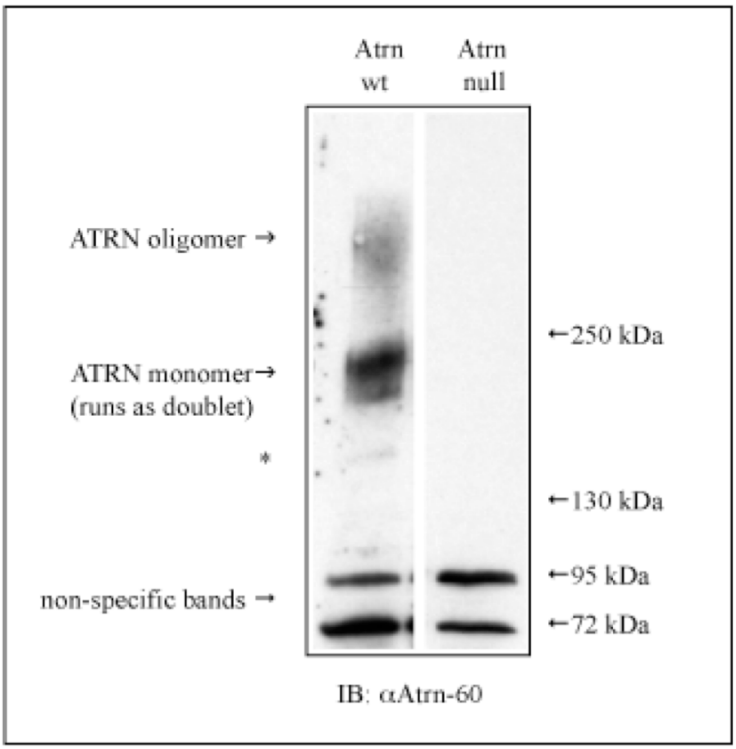

Figure 4.2. Appearance of ATRN by Western blot of melanocyte lysates. Most ATRN signal occurs as a doublet of approximately 220-240 kD. Higher molecular weight signal is likely to represent an ATRN dimer or oligomer. Asterisk marks faint ATRN signal at approximately 160 kD, near the predicted mass of the unmodified native protein (158 kD) and perhaps representing nascent ATRN without post-translational modifications.

dimerization or oligomerization of ATRN is a feature of the native protein and not an artifact caused by the GFP tag. A faint specific band at approximately 160 kD was sometimes observed. As this is near the predicted molecular weight (158 kD) of the unmodified ATRN peptide, this band may represent nascent ATRN without post-translational modifications.

Melanosomal ATRN does not accumulate during lysosomal inhibition

Because ATRN-GFP can be observed trafficking to lysosomes in melanocytes, I expected that endogenous ATRN would accumulate if lysosomal proteases were inhibited by addition of chloroquine to the culture medium. Contrary to this expectation, overnight chloroquine treatment (100uM) reduced levels of endogenous ATRN protein (Figure 4.3A). Chloroquine treatment disproportionately affected the lower band of the ATRN doublet, causing its near disappearance.

Melanosomal ATRN does not accumulate during lysosomal inhibition

Because ATRN-GFP can be observed trafficking to lysosomes in melanocytes, I expected that endogenous ATRN would accumulate if lysosomal proteases were inhibited by addition of chloroquine to the culture medium. Contrary to this expectation, overnight chloroquine treatment (100uM) reduced levels of endogenous ATRN protein (Figure 4.3A). Chloroquine treatment disproportionately affected the lower band of the ATRN doublet, causing its near disappearance.

Behavior of ATRN upon ASP and αMSH treatment

To determine whether either of the ligands of the mouse MC1R have an effect on ATRN protein levels or post-translational modification, I treated melan-a cells with recombinant murine ASP (1:100 dilution) or αMSH (100nM) overnight. Neither

Figure 4.3. Response of endogenous ATRN to lysosomal inhibition and treatment with ligands of the MC1R. All lanes represent independent replicates. Each experiment was performed twice with similar results. A. Upper panel: ATRN protein levels were reduced after 12 hour treatment with 100μM chloroquine, with an especially pronounced reduction of the lower band of the monomer doublet. Lower panel: a lower region of the blot showing several non-specific bands to demonstrate even loading. B. Upper panel: overnight treatment with 10 μl/ml ASP caused no change in ATRN protein levels but appeared to increase the intensity of ATRN signal at high molecular weight. Lower panel: lower region of blot stained with Ponceau S red to demonstrate even loading. C. Upper panel: modest reduction in ATRN protein levels after overnight treatment with 100 nM αMSH. Lower panel: GAPDH loading control.

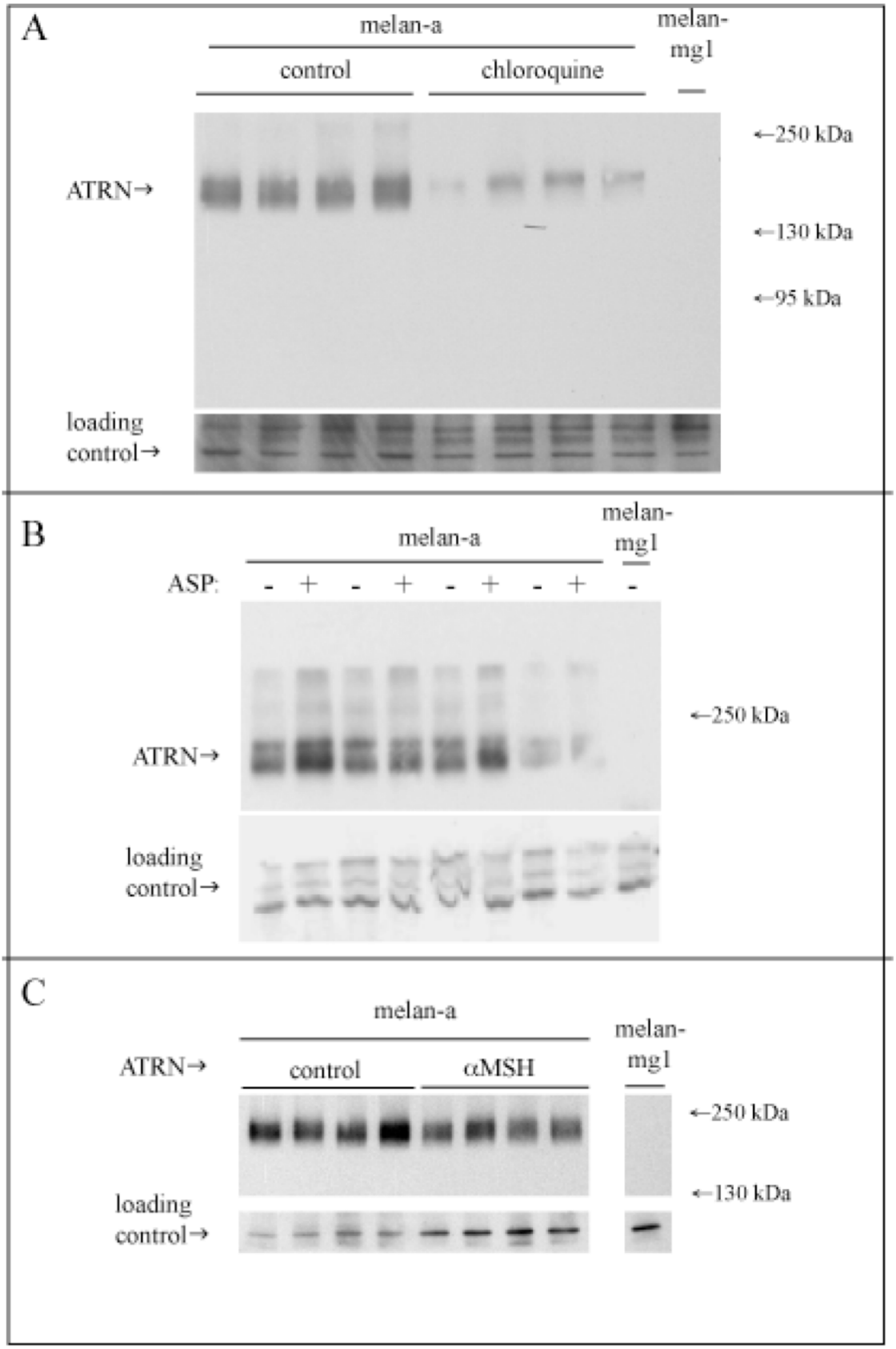
A
melan-a
melan-mg1
control
chloroquine
ATRN→
loading control→
←250 kDa
←130 kDa
←95 kDa
B
melan-a
melan-mg1
ASP: - + - + - + - + -
ATRN→
loading control→
←250 kDa
C
melan-a
melan-mg1
ATRN→
control
αMSH
loading control→
←250 kDa
←130 kDa

treatment caused an obvious change in the appearance of the ATRN doublet, and ASP did not affect the level of ATRN protein in treated cells (Figure 4.3B). αMSH treatment resulted in a slight decrease in ATRN protein levels (Figure 4.3C). Treatment with ASP appeared to increase the relative intensity of ATRN signal at high molecular weight, perhaps reflecting an increase in formation of ATRN oligomers.

N-linked glycosylation of ATRN is abnormal in Mgrn1 mutant melanocytes

Since lysosomal inhibition caused a change in the relative intensity of the bands of the ATRN doublet, it seemed possible that the loss of MGRN1-directed lysosomal trafficking of ATRN might also cause a change in the post-translational modification state of ATRN. To test this possibility, extracts of melan-a and melan-md2 cells were run on SDS-PAGE gels side-by-side and blotted for ATRN. MGRN1-deficient cells showed a decrease in ATRN protein levels as well as a decrease in the apparent molecular weight of the ATRN bands (Figure 4.4a). Instead of forming a normal ATRN doublet at 220-240 kD, the majority of ATRN signal in melan-md2 cells was seen at an apparent molecular weight of ~160 kD. To determine whether direct ubiquitin ligase or SUMO ligase activity of MGRN1 might contribute to the observed size difference, ATRN was immunoprecipitated from melan-a and melan-md2 cells and SDS-PAGE-separated proteins from the immunoprecipitations were immunoblotted with antibodies against SUMO1 and ubiquitin. No ubiquitinated or sumoylated ATRN was observed (data not shown). As human ATRN has been reported to be N-glycosylated (Duke-Cohan *et al.,* 1995) I treated extracts of melan-a, melan-md2, and melan-mg1 cells with peptide N-glycosidase F (PNGase F) to remove N-linked polysaccharides. Upon PNGase F treatment, the appearance of deglycosylated ATRN in melan-a and melan-md2 cells was identical, demonstrating that the difference in apparent molecular weight of ATRN in MGRN1-deficient cells

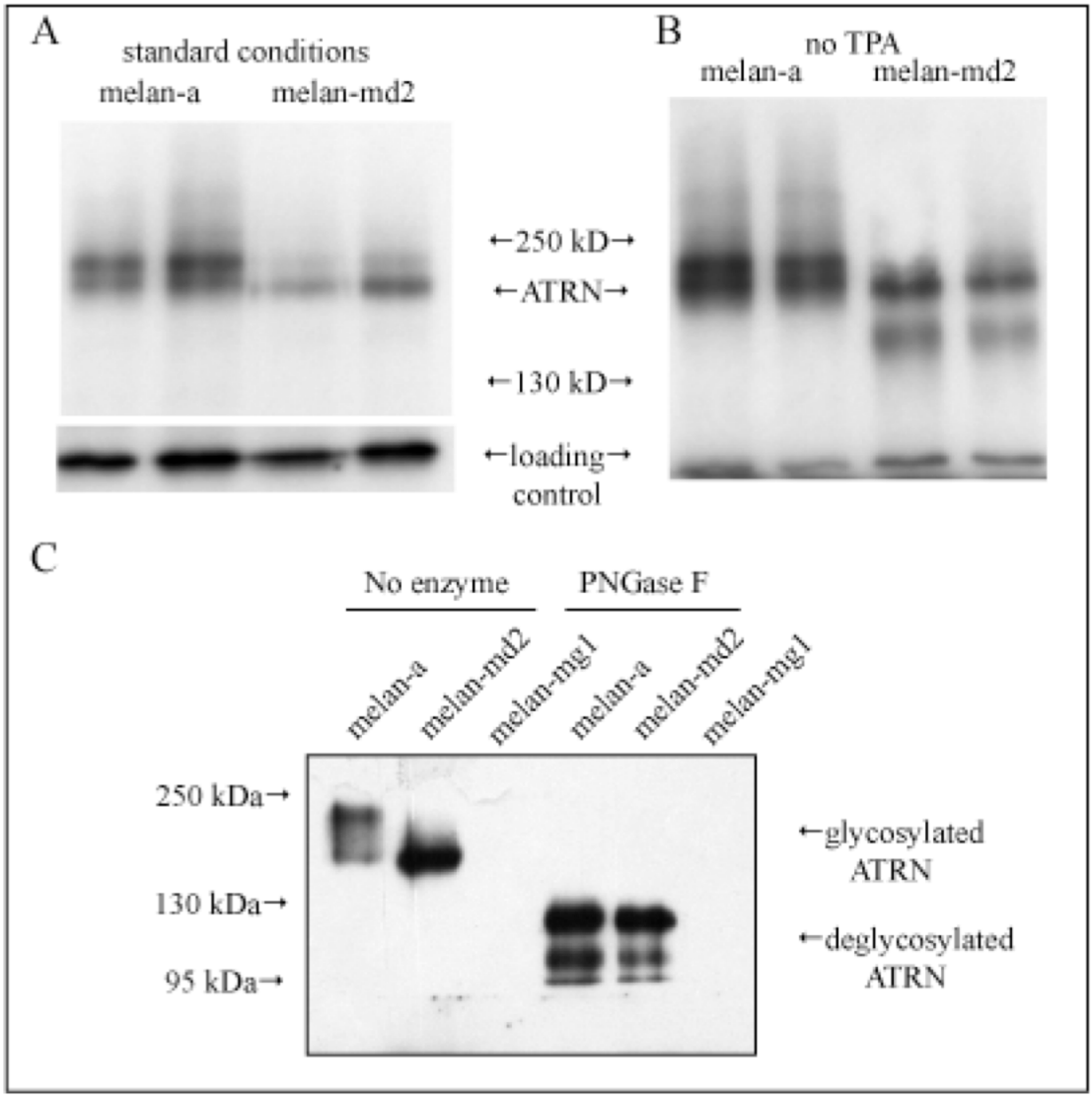

Figure 4.4. ATRN is abnormally glycosylated in *Mgrn1* null melanocytes. A & B. melan-md2 cells lose most of the higher m.w. band of the ATRN doublet and have reduced ATRN levels overall. Withdrawal of TPA from the culture medium promotes strong appearance of the ~160 minor ATRN band in melan-md2 cells. C. Size differential of ATRN bands disappears after PNGase F treatment. Blots are representative examples of at least three independent replicate experiments.

was due to aberrant or incomplete N-linked glycosylation. Upon deglycosylation, the ATRN signal in either cell type appears at an apparent molecular weight of ~130 kD, with additional bands at ~110 and ~100 kD (Figure 4.4C). I observed that the intensity of the ~160 kD ATRN band in melan-md2 cells was sometimes especially pronounced on blots made using quiescent cells. Withdrawal of TPA (which stimulates proliferation of melanocytes by activation of adenylyl cyclase) for 24 hours similarly increased the intensity of the 160 kD band (Figure 4.4B). If the 160 kD band represents nascent peptide that is not yet fully glycosylated, the increase in the intensity of this band in melan-md2 cells grown without TPA suggests that proliferating melanocytes downregulate the production of ATRN, and also suggests a delay in maturation of nascent ATRN in *Mgrn1* mutant cells.

MC1R-GFP traffics to lysosomes in melanocytes.

As described in the previous chapter, MC1R-GFP transiently expressed in HEK293T cells trafficked through the endosomal/lysosomal pathway. To determine whether this behavior also occurs in melanocytes, MC1R-GFP-transfected melan-a cells

were treated with Lysotracker Red and imaged by confocal microscopy (Figure 4.5A). Some colocalization of MC1R-GFP with lysosomes was visible in control cells,

control cells, and MC1R-GFP labeled vesicles were observed trafficking to and fusing with lysosomes. Colocalization of MC1R-GFP signal with Lysotracker Red was prominent in many cells treated with ASP for four hours prior to imaging (Figure 4.5). However, the high degree of variability in MC1R-GFP expression from cell to cell made it difficult to determine whether the apparent increase in colocalization was real, or an artifact of different transfection efficiencies from plate to plate.

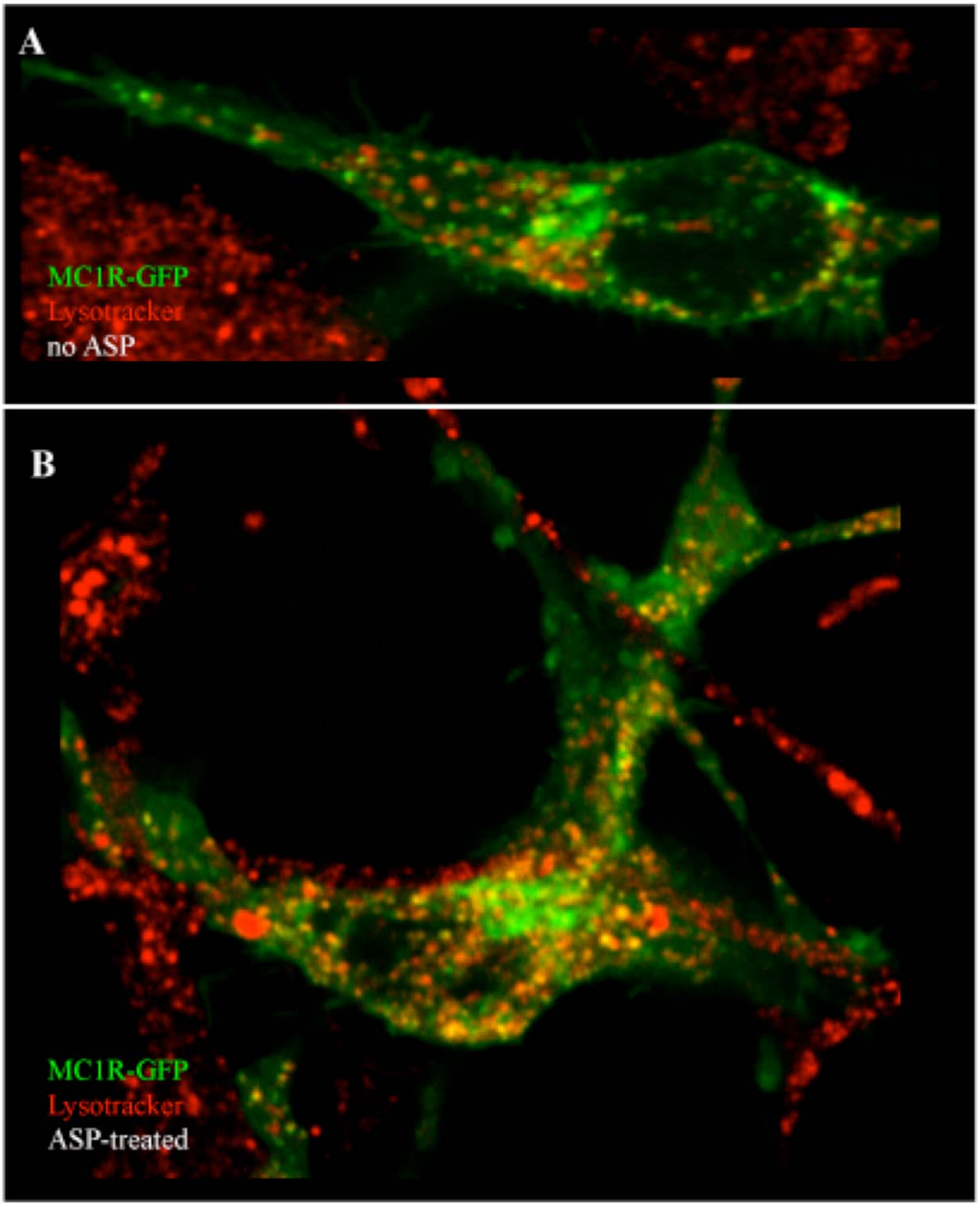

Figure 4.5. MC1R-GFP traffics to late endosomes/lysosomes in melanocytes. A. Melan-a cells were transfected with MC1R-GFP and acidic organelles were labeled with Lysotracker Red. Note colocalization of MC1R-GFP signal with Lysotracker Red signal. B. Melan-a cells transfected with MC1R-GFP were treated with recombinant ASP for 3 hours prior to Lysotracker Red treatment and visualization. Some cells were identifiable with high levels of MC1R-GFP/lysosome colocalization, although cell-to-cell variability in MC1R-GFP expression from complicates interpretation of relative colocalization rates compared to untreated control (see text).

Characterization of MC1R antibodies

That ATRN-GFP and MC1R-GFP both traffic to lysosomes in melanocytes suggests that endogenous ATRN could target MC1R to the lysosome by an ASP and MGRN1-dependent process. As transient transfection of melanocytes resulted in mostly weak and generally variable MC1R-GFP expression levels, colocalization of MC1R-GFP with lysosomes was difficult to quantify with confidence. An alternative experimental approach was therefore pursued using antibodies against endogenous MC1R. The detection of MC1R protein by western blot presents special challenges. The protein is small and consists largely of hydrophobic transmembrane helices, which make poor epitope targets for antibody generation. Furthermore, the highly hydrophobic nature of the receptor is likely to make it vulnerable to irreversible aggregation during routine pre-loading boiling of the sample, leading to inability of the MC1R aggregates to enter the electrophoretic gel and resulting in loss of signal (Sturm *et al.*, 2003; Eberle, 1988; Schioth *et al*., 1996). Unfortunately, this problem is not universally recognized in the field and several groups have reported MC1R signal from boiled lysates, sometimes without showing adequate controls to demonstrate the specificity of the band reported (*e.g.*, Chakraborty and Pawelek, 1993; Moustafa *et al*., 2002; Salazar-Onfray *et al*., 2002; Rouzaud *et al.*, 2003; Rouzaud *et al*., 2006), fueling contention in the field over the question of what tissue types express MC1R (*e.g.* see Roberts, Newton, and Sturm, 2007). In my hands, the use of boiled lysates resulted in the total loss of MC1R-GFP signal from anti-GFP western blots (data not shown), supporting concerns about irreversible aggregation of MC1R by heat. Two highly cited commercially available MC1R antibodies (the N-19 and L-20 goat anti-rabbit polyclonals from Santa Cruz Biotechnology) failed to detect MC1R-GFP expressed in HEK-293T cells, and the bands that they recognized on blots from melanocyte lysates were unaffected by boiling. The pep-19 rabbit polyclonal (Rouzaud *et al.*, 2003;

Rouzaud *et al*, 2004; Rouzaud *et al.*, 2006) similarly failed to recognize tagged MC1R in HEK293T lysates, or any heat-labile band in melanocyte lysates. These observations suggest that these antibodies do not recognize mouse MC1R.

Discussion

Loss of endo/lysosomal trafficking of ATRN in Mgrn1 mutant melanocytes suggests trafficking of ATRN is important for pigment-type switching and CNS integrity

As was observed for heterologous cell types in Chapter Three, ATRN-GFP traffics constitutively to late endosomes/lysosomes in wild-type melanocytes. Significantly, the data presented in this chapter demonstrate that this trafficking is lost in *Mgrn1* null mutant melanocytes. Because *Mgrn1*-null homozygotes develop similar pigmentation and neurodegeneration phenotypes to those seen in *Atrn* mutants, this observation suggests that loss of *Atrn* trafficking through the endolysosomal pathway causes hyperpigmentation and spongiform change in both *Atrn* and *Mgrn1* mutants. My observation of *Mgrn1*-dependent endolysosomal trafficking of ATRN-GFP in melanocytes is consistent with data produced by others in our laboratory, who have shown that ATRN-GFP is degraded in lysosomes of HEK293T cells, and that overexpression of a catalytically inactive mutant MGRN1 prevents lysosomal degradation of ATRN (Caroline Wee, personal communication). Unlike overexpressed ATRN in HEK293T cells, however, endogenous ATRN does not appear to be rapidly degraded in lysosomes, as inhibition of lysosomal proteases does not cause a buildup of ATRN in melanocytes. As ATRN-GFP signal could sometimes be observed trafficking out of Lysotracker Red-labeled compartments after transient fusion, it is possible that endogenous ATRN in melanocytes preferentially occupies the limiting membrane of the MVB and is recovered after lysosomal fusion via a retrograde trafficking pathway. If ATRN is a lysosomal sorting factor for

associated signaling receptors such as the MC1R, retrieval of ATRN for repeated use in the endolysosomal trafficking system would increase the efficiency with which target receptors are degraded. The well-studied cathepsin lysosomal trafficking pathway offers canonical examples of an analogous arrangement. Cathepsins are soluble lysosomal hydrolases that reach the lysosome with the assistance of transmembrane helper proteins, the best known of which are the mannose-6-phosphate receptors (M6PR) (for review see Ghosh, Dahms, and Cornfeld, 2003; Braulke and Bonifacino, 2009). These receptors recognize phosphorylated N-glycosyl groups applied to cargo molecules in the *trans*-golgi , and escort the proteins so decorated from the *trans*-Golgi to late endosomes. After delivering its cargo to the endosomal pathway, M6PR is retrieved from the late endosomal membrane and returned to the *trans*-Golgi through a retrograde trafficking pathway. The example of the M6PR and other lysosomal enzyme sorting proteins such as sortilin (Canuel *et al.*, 2008) shows that for accessory sorting proteins, traffic to the late endosome need not be a one-way trip.

The cell biology of MC1R-GFP in melanocytes is compatible with a role for ATRN as an ASP-activated, MGRN1-dependent, trans-acting lysosomal targeting factor for MC1R.

My observations of MC1R-GFP trafficking to lysosomes in melanocytes are consistent with the hypothesis of MC1R downregulation by ATRN-dependent lysosomal targeting. A model incorporating my observations with the known genetic and biochemical features of pigment-type switching is presented in Figure 4.6. As argued above, the observation that the lysosomal trafficking of ATRN is MGRN1-dependent suggests that the lysosomal trafficking of ATRN is important for

Figure 4.6. A unified model showing the proposed mechanism of action of ATRN and MGRN1 in pigment-type switching. MC1R encounters ASP at the cell surface and forms a ternary complex with ASP and ATRN either at the cell surface or in an endosomal compartment. Interactions with MGRN1 promote the sorting of both proteins to regions of ESCRT protein activity on incipient multivesicular bodies (MVBs), and ubiquitination of TSG101 by MGRN1 also promotes ESCRT function. MC1R is sorted by ESCRT activity into the intralumenal vesicles of the MVB, which fuses with lysosomes to deliver MC1R for degradation by lysosomal hydrolases. ERC: Endosome Recycling Complex. Ub: ubiquitin.

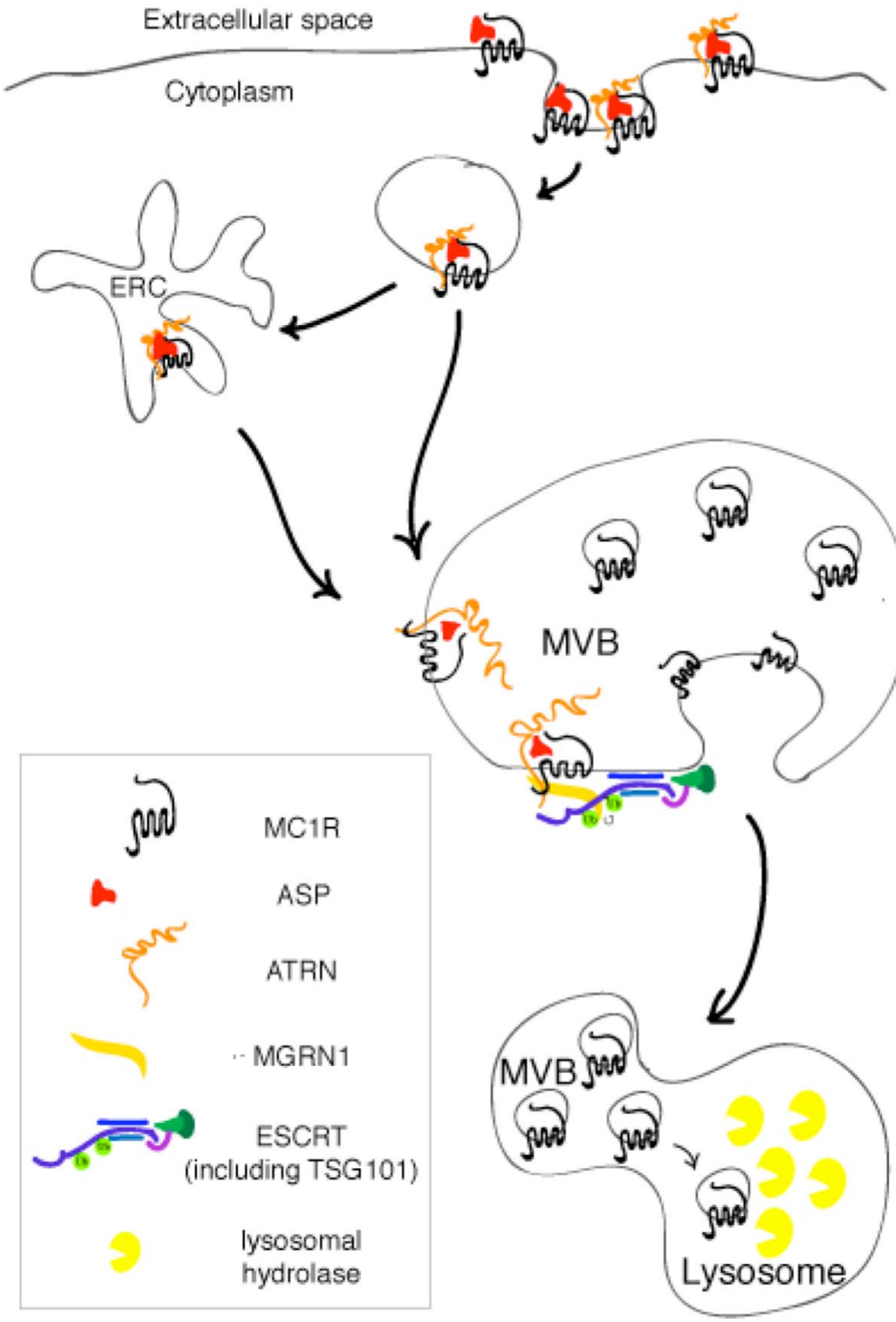
Extracellular space
Cytoplasm
ERC
MVB
MC1R
ASP
ATRN
MGRN1
ESCRT
(including TSG101)
lysosomal
hydrolase
MVB
Lysosome

downregulation of MC1R signaling. Mutual binding of ATRN and MC1R to ASP is likely to promote the demonstrated physical interaction of the ATRN and MC1R cytoplasmic tails, potentially linking the trafficking fate of MC1R to that of ATRN. MGRN1-dependent trafficking of ATRN could therefore promote MC1R delivery to the lysosome, providing a plausible explanation for the ASP, ATRN, and MGRN1-dependent nature of pigment-type switching and for observations by others that ASP administration causes a reduction in MC1R protein levels. As efforts by myself and by Perez-Oliva *et al.* (2009) have failed to show that MGRN1 ubiquitinates either ATRN or MC1R, MGRN1 is depicted in Figure 4.6 as using its known interactions with MC1R, ATRN, and TSG101 to promote both the sorting of MC1R to ESCRT, and the function of the ESCRT complex itself.

This model predicts that MC1R protein levels in wild-type melanocytes will decrease upon ASP treatment, but not upon concurrent treatment with ASP and lysosomal inhibitors such as chloroquine; conversely, lysosome-dependent MC1R degradation will not occur in ASP-treated *Atrn* or *Mgrn1* mutant cells. The major obstacle to testing these predictions is the lack of a validated antibody capable of specifically identifying endogenous MC1R from mouse melanocytes. Future efforts towards refining the model of pigment-type switching presented here should focus on overcoming this technical obstacle.

Future directions: abnormal glycosylation status of ATRN is a novel signature of MGRN1 deficiency

The data related here demonstrate an unexpected feature of ATRN in *Mgrn1* mutant melanocytes: abnormal N-linked glycosylation. Whereas wild-type cells show a doublet at 220-240 kD, in proliferating melan-md2 cells ATRN is represented primarily by the 220 kD band (with a trace of signal representing the attenuated upper

band of the doublet). In addition, the 160 kD band is intensified in melan-md2 cells under conditions of TPA deprivation. All of these protein mobility differences between ATRN in melan-a and melan-md2 cells disappear when the lysates are treated with PNGase F before electrophoresis, strongly suggesting that the difference in apparent molecular weight is due to abnormal N-linked glycosylation of ATRN in *Mgrn1* mutants.

Glycosylation is important for many aspects of function in different proteins, so there are many ways in which abnormal glycosylation might adversely affect the functionality of ATRN. Glycosylation is believed to be important for efficient protein folding in the ER because the large carbohydrate groups increase the solubility of nascent polypeptide chains, simultaneously shielding transiently unfolded hydrophobic surfaces from participating in inappropriate interactions. Incorrect glycosylation can also trigger the intervention of ER quality control machinery and inhibit protein export from the ER. Therefore, a failure of glycosylation resulting in ER retention could explain the aberrant localization of ATRN-GFP in melan-md2 cells. Outside of the biosynthetic pathway, abnormal glycosylation can adversely affect protein function by altering ligand binding specificity or avidity, or by altering interactions with components of the extracellular matrix. ATRN in *Mgrn1* mutant cells might therefore have impaired ability to bind MC1R and/or ASP. Additionally, the presence of a conserved C-type lectin carbohydrate-binding domain on ATRN suggests that interactions with glycosyl groups are important for its function, so altered glycosylation of ATRN could adversely affect its ability to participate in homo-oligomerization interactions through its C-type lectin domain. In light of this possibility, it's interesting to note that the intensity of the high molecular weight "oligomeric ATRN" smear appears to increase in intensity in cells treated with ASP (Figure 4.3 B), while consistently appearing reduced in intensity on western blots of

melan-md3 lysates (Figure 4.4 A&B). If oligomerization is important for ATRN function, these observations would suggest that ASP promotes oligomerization in a MGRN1-dependent manner.

How exactly MGRN1 deficiency causes abnormal ATRN glycosylation is an interesting question for future study. It is not obvious how MGRN1's effect on lysosomal trafficking of ATRN could feed into the canonical pathway of N-linked glycosylation, which occurs in the secretory pathway in the ER and Golgi apparatus. As endogenous ATRN appears not to be degraded in the lysosome in melanocytes, it is possible that a retrograde trafficking pathway analogous to that followed by the M6PR could be responsible for cycling ATRN back to the Golgi or trans-Golgi, where repeated exposure to Golgi-resident glycosylation-modifying enzymes could effect the glycosylation state of ATRN over repeated rounds through this compartment. A block in ATRN trafficking in *Mgrn1* mutant cells could alter this trafficking itinerary in a way that prevents formation of the higher molecular weight band of the 220-240 kD doublet. For unknown reasons, the upper band of the ATRN doublet that is lost in *Mgrn1* mutant melanocytes becomes the major ATRN band (at the expense of the lower band of the doublet) in the presence of chloroquine (Figure 4.3A). It is not clear what this means. It is interesting to note that lysosomal inhibition caused a decrease in ATRN protein levels, a counterintuitive result that may represent a downregulation of *Atrn* transcription by stressed melanocytes. Since the higher molecular-weight band of the doublet is the only remaining band in this situation, this could be interpreted as a "fully mature" form of ATRN, representing the final state of the last bolus of ATRN peptide to persist after ATRN biosynthesis shuts down. The question of how ATRN protein levels are reduced in the absence of lysosomal function is a puzzling one; as a transmembrane protein, ATRN would be expected to undergo degradation mainly through lysosomal or autophagic pathways (which also require lysosomal function).

While lysosomal inhibition does stress the cells (cell death is evident in plates of melanocytes treated with chloroquine or ammonium chloride for 24 hours), under the conditions used cell death at 12 hours did not occur. This rules out the possibility that average ATRN levels go down in chloroquine-treated plates because of selective death of cells expressing the most ATRN. Since ATRN levels fall during lysosome inhibition, it is possible that chloroquine-treated cells may reduce ATRN levels through an unexpected non-lysosome-dependent pathway such as cleavage by secretases or secretion in exosomes. Regarding this last possibility, it should be noted that melanocytes in cell culture do shed plentiful small membrane-bound structures (possibly melanosomes or exosomes) into the culture medium (data not shown). Whether these structures could act as sinks for ATRN under conditions of lysosomal inhibition is unknown.

From the melanocyte to the brain: implications for the mechanism of spongiform neurodegeneration.

This chapter presents a model of ATRN and MGRN function in the pigment-type switching pathway that attempts to explain the shared pigmentation phenotypes of *Atrn* and *Mgrn1* mutant mice. A question of major interest is whether this model can be extended to the central nervous system to explain the shared neuropathological phenotype of these mutants. The next chapter explores the implications of my studies of *Atrn* and *Mgrn1* function for the mechanism of spongiform neurodegeneration.

CHAPTER 5

NEURODEGENERATION AS A CONSEQUENCE OF ESCRT DYSFUNCTION

Chapter Overview

This chapter returns to the subject of spongiform change reviewed in Chapter One, extending the model of ATRN/MGRN1 interaction proposed for the pigment cell to hypothesize that failure of endo/lysosomal trafficking at the point of multivesicular body sorting by ESCRT proteins could cause an accumulation of abnormal intracellular membrane, thereby giving rise to the vacuoles of spongiform neurodegeneration. The literature on the consequences of neural ESCRT loss-of-function is reviewed, and a proof-of-concept experiment is described which tests this hypothesis by knocking out the ESCRT gene Tsg101 in the neurons of the adult mouse forebrain. Preliminary data supporting the hypothesis are reported. These results are integrated with the known biology of spongiform neurodegeneration in retroviral and prion-related diseases, and a unified hypothesis of spongiform change is proposed suggesting that the immediate cause of spongiform change in these diseases is ESCRT sequestration by exogenous (in the case of retrovirus-associated disease) or endogenous (in the case of prion disease) retroviral capsid proteins. This hypothesis suggests that antiretroviral therapy could be an efficacious treatment for prion diseases.

There and back again: from pigment-type switching to spongiform neurodegeneration

As discussed in Chapter One, the goal of my studies of ATRN and MGRN1 in the pigment cell model system is to understand the mechanism that, when disrupted, leads to spongiform change in the brain. In the pigment-type switching pathway, loss

of ATRN and loss of MGRN1 produce identical phenotypes. As described in Chapters Three and Four, studies of these proteins in cell culture demonstrate that MGRN1 is important for the normal lysosomal trafficking of ATRN. Taken together, these observations suggest that loss of normal lysosomal trafficking (of ATRN and perhaps also ATRN-interacting proteins such as MC1R) may be the fundamental defect underlying the shared phenotypes of *Atrn* and *Mgrn1* mutant mice. This hypothesis is supported by the recent realization that MGRN1 interacts with and ubiquitinates TSG101, a component of the lysosomal protein sorting ESCRT machinery (Kim *et al.*, 2007; Jiao *et al*., 2009a). By what mechanism might loss of ATRN's normal lysosomal trafficking underlie spongiform change in both *Atrn* and *Mgrn1* null mutants? In the melanocyte, this impairment seems likely to prevent the downregulation of signaling through the ATRN interactor, MC1R, perhaps suggesting that similar dysregulation of an unknown ATRN-interacting GPCR in the brain could underlie spongiform change in *Atrn* and *Mgrn1* mutants through an unknown pathological pathway. (Dysregulation of MC1R in the brain cannot explain spongiform neurodegeneration in these mutants, as hyperactive mutant alleles of *Mc1r* produce no overt neurological phenotypes.) A more interesting possibility is that the failure of a subset of lysosomal protein trafficking events *per se*, rather than the dysregulation of any particular GPCR, underlies spongiform neurodegeneration in these mutants. One can imagine that transmembrane proteins such as ATRN and MC1R, if unable to traffic normally to the lysosome, might simply accumulate along with their associated membrane. In long-lived, non-dividing cells (such as most neurons of the CNS), this abnormal accumulation of membrane could eventually appear as an intracytoplasmic vacuole. To the extent that such a primary defect in lysosomal protein trafficking would impede housekeeping functions such as clearance of autophagosomes (which requires autophagosomal fusion with functioning

lysosomes) or myelination and myelin maintenance (which makes tremendous demands on the membrane-trafficking machinery of oligodendrocytes in the CNS), additional membranous abnormalities could accumulate as a secondary consequence of a lysosomal protein trafficking defect.

ESCRT dysfunction and the "class E vps *compartment"*

In fungi and in mammalian cells, abnormal membranous accumulations have been shown to occur as a consequence of ESCRT protein depletion. As discussed in Chapter Three, ESCRT proteins form large complexes on the limiting membranes of incipient multivesicular bodies (MVBs), where they sort lysosomally targeted membrane proteins into intralumenal vesicles in preparation for their delivery to the lysosome (Reviewed by Saksena *et al.,* 2007). Deletion of members of this class of proteins in yeast severely disrupts normal trafficking of target proteins to the yeast vacuole (a large lysosome-like organelle) (Raymond *et al.,* 1992). The morphological consequence of this disruption is the "class E vacuolar protein sorting (*vps*) compartment," which is an accumulation of an abnormal multilamellar membranous structure within the cytoplasm (Rieder *et al.,* 1996, see Figure 5.1A) The class E *vps* compartment contains vacuole-targeted proteins such as vacuolar hydrolases and vacuolar H(+)-ATPase subunits, suggesting that it represents a "stalled" prevacuolar compartment that is unable to progress toward fusion with the yeast vacuole.

A similar aberrant compartment has been reported to form in mammalian cells depleted of the ESCRT protein (and MGRN1 ubiquitination target) TSG101 (Doyotte *et al.,* 2005; see figure 5.1B). As MGRN1 appears to be important for the normal function of TSG101 (Kim *et al.,* 2007), it is possible that *Mgrn1* mutant cells in the CNS experience ESCRT dysfunction and develop a class E *vps* compartment. Could this be the origin of the vacuoles of spongiform change in these mutants? As shown in

Figure 5.1, images of class E *vps* compartments in yeast and mammalian cells consistently show tightly laminated, concentric layers of membrane, which at first glance do not greatly resemble the more open cytoplasmic vacuoles of spongiform change. Why the class E *vps* compartment adopts this tightly laminated morphology is not understood. As these compartments are experimentally induced using RNAi transfection or temperature-sensitive yeast mutants, it is also not known whether the compact multilamellar morphology is maintained over time periods of more than a few days, or if indeed the initially compact morphology of a newly generated class E *vps* compartment is only an ephemeral stage that gives way over time to more disorganized vacuolar appearance.

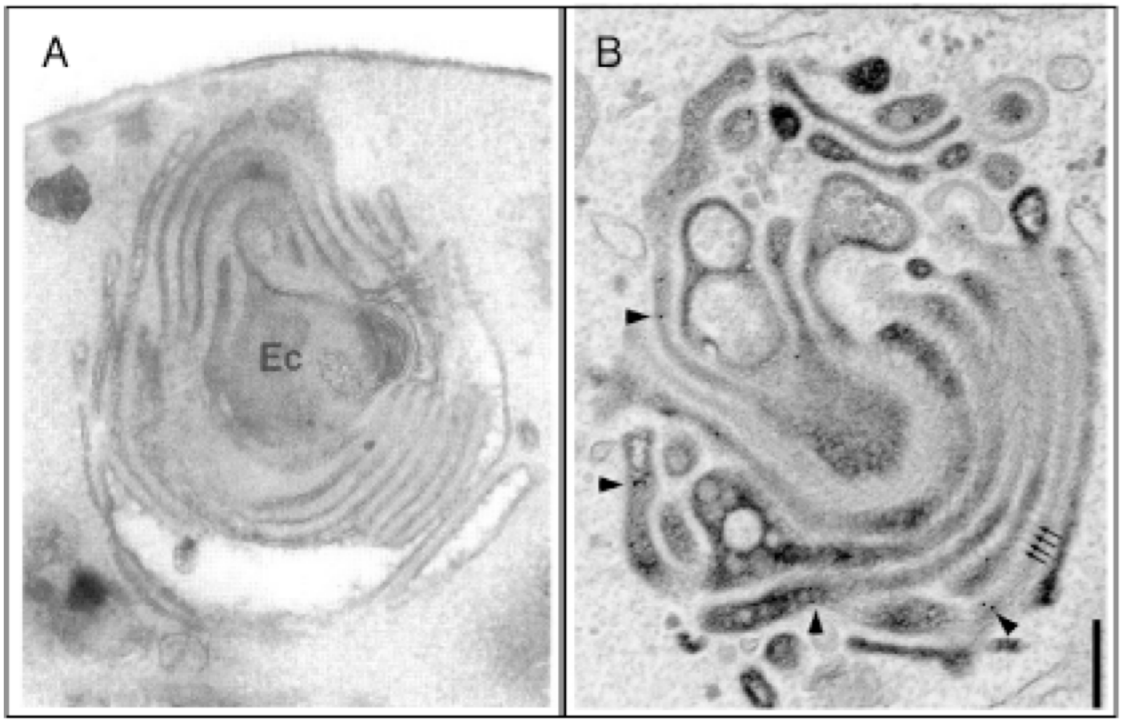

Figure 5.1. Appearance of class E *vps* compartments in yeast and mammalian cells. A. Class E *vps* compartment in *vps28* mutant yeast (Rieder *et al.,* 1996). B: Class E *vps* compartment in TSG101-depleted HeLa cells (Doyotte *et al.,* 2005). Scale bar in B is 0.5 μm. Images used by permission.

Downstream consequences of ESCRT malfunction: autophagosome accumulation provides another potential source of vacuolar membrane.

Whether or not the class E *vps* compartment directly contributes to accumulation of spongiform vacuoles, it seems clear that the consequences of ESCRT disruption can extend beyond impairment of the endosomal-lysosomal pathway to affect related pathways in the intracellular trafficking network. These downstream trafficking disruptions must also be considered as potential sources of aberrant membranous accumulations. Depletion of the ESCRT-III protein SNF7-2 causes not only the disruption of ESCRT sorting, but also the accumulation of autophagosomes in *Snf7-2* RNAi-treated neurons in culture (Lee *et al*, 2007). Along with the accumulation of morphologically identifiable autophagosomes, these neurons also develop non-compact membranous abnormalities ultrastructurally reminiscent of the spongiform vacuoles observed in *Atrn* mutants and prion diseases (Figure 5.2 B). Similar abnormalities are seen in neurons transfected with a mutant form of the SNF7-2-interacting protein CHMP2B, another member of ESCRT-III (Figure 5.2 A). The mutant form of CHMP2B, known as $CHMP2B^{exon5}$, binds avidly to SNF7-2 and inhibits the repeated rounds of ESCRT-III assembly and disassembly that are necessary for ESCRT-III function (Lee *et al.*, 2007). Depletion of SNF7-2 or transfection with $CHMP2B^{exon5}$ appears to induce autophagosome accumulation by causing a block in autophagosome maturation (Lee and Gao, 2008). As autophagosome maturation involves fusion of the autophagosome with MVBs (Lecocq and Walker, 1997; Bampton *et al*, 2005; Eskelinen 2005), it is not surprising that the disruption of MVB formation by ESCRT impairment should feed forward to impair autophagosome maturation as well. In cell culture, this accumulation of autophagosomes appears to be directly neurotoxic, as SNF7-2-depleted neurons exhibit high mortality that is partly suppressed by autophagy inhibitors (Lee, Liu, and

Gao, 2009). Given the considerable ultrastructural resemblance between the vacuoles of spongiform change and the non-compact "vacuolar" structures in ESCRT-III depleted cells, it is tempting to speculate that autophagosome accumulation downstream of a block in MVB maturation could be an additional source of spongiform vacuolar membrane. Data to support or refute this hypothesis are few; to date, neither *Snf7-2* nor *Chmp2B* disruption has been studied in the context of the whole mouse brain. Interestingly, however, the *Chmp2B*^{exon5} mutation does occur in one Danish kindred, in which it causes an autosomal dominant form of familial frontotemporal dementia (FTD) (Brown *et al.*, 1995; Skibinski *et al*, 2005; Momeni *et al.*, 2006). Available autopsy reports, while describing the major neuropathological feature of this rare form of FTD as a global cortical and central atrophy, do each briefly mention the presence of cortical "spongiosus" or "microvacuolation" (Gydesen *et al.*, 2002; Yancopoulou *et al*, 2003). The contribution of autophagosome accumulation to spongiform neurodegeneration in ESCRT mutants thus remains an intriguing possibility.

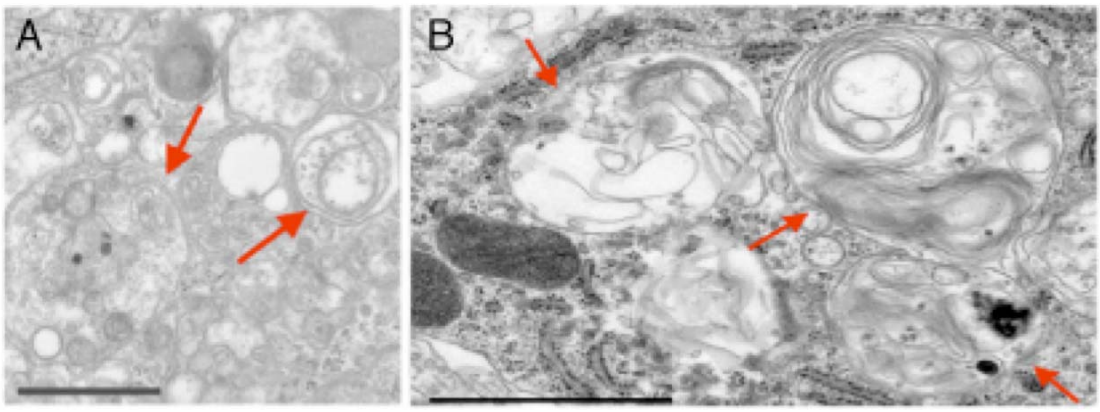

Figure 5.2. Abnormal vacuolar structures derived from accumulated autophagosomes in ESCRT-III depleted cells. A: Autophagosome accumulation in *Drosophila* neurons expressing CHMP2B^{intron5}. B: Autophagosome accumulation in cultured mouse cortical neurons expressing *Snf7-2* RNAi construct. Scale bars are 1 μm. Images from Lee *et al.*, 2007 and are used by permission.

PI(3,5)P_2 regulatory mutants display a classical spongiform pathology and impaired ESCRT function.

As discussed in Chapter One, mice with mutations in *Fig4* or *Vac14* have aberrant regulation of the endosomal signaling lipid PI(3,5)P_2, a probable resident of the late endosomal membrane which is important for multiple trafficking events centered around late endosomes. The phenotypic consequence of dysfunction at either locus is spongiform neurodegeneration (Figure 5.3; Zhang *et al.*, 2007; Chow *et al.*, 2007). Interestingly, there are clear links between PI(3,5)P_2 and ESCRT function. PI(3,5)P_2 production is essential for MVB sorting (Odorizzi, Babst, and Emr, 1998), and the ESCRT-III protein CHMP3/VPS24 has been shown to preferentially interact with PI(3,5)P_2 and can be made to accumulate on the class E *vps* compartment in a PI(3,5)P_2 – dependent fashion (Whitley *et al.*, 2003). This suggests that PI(3,5)P_2 regulatory mutants have impaired ESCRT function and that accumulation of a class E *vps*-like compartment (and/or downstream effects such as autophagosome accumulation) could underlie spongiform change in *Fig4* and *Vac14* mutants.

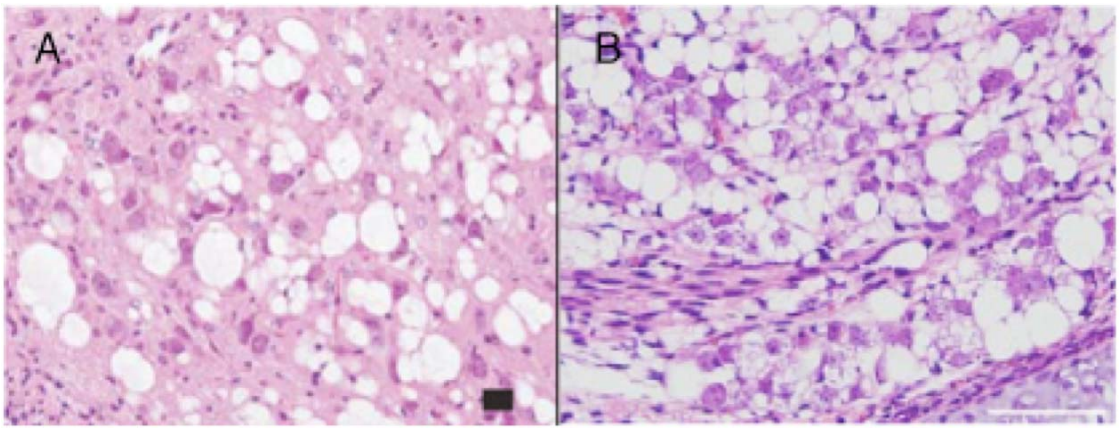

Figure 5.3. Spongiform neurodegeneration in PI(3,5)P_2 regulatory mutants. A: Spongiform vacuoles in brainstem of *Fig4*$^{-/-}$ mouse (Chow *et al*, 2007). Scale bar is 25μm. B: Spongiform vacuoles in trigeminal ganglion of *Vac14*$^{-/-}$ mouse (Zhang *et al.*, 2007). Scale bar is 100 μm. Images used by permission.

Consistent with this hypothesis, spongiform vacuoles in *Vac14* mutants contain lysosome associated membrane protein 2 (LAMP2) (Zhang *et al.,* 2007), strongly suggesting a late endosomal/lysosomal contribution.

Atrn and Mgrn1 point to MVB sorting / ESCRT dysfunction as an underlying cause of spongiform neurodegeneration

In the preceding chapters, I have provided evidence to support the hypothesis that ATRN and MGRN1 function together to accomplish the regulated endosomal/lysosomal trafficking of MC1R. As *Atrn* and *Mgrn1* null mutants also develop spongiform encephalopathy, I suggest that a similar loss of an endosomal/lysosomal trafficking event in cells of the CNS underlies the formation of spongiform vacuoles. As discussed above, impairment of the master regulators of endosomal/lysosomal trafficking (the ESCRT proteins) causes accumulation of abnormal endosomal membrane in the "class E *vps*" compartment in mammalian cells in culture and of additional membrane in cultured neurons by feeding into a defect in autophagosome clearance. ESCRT dysfunction therefore provides two fairly well-understood mechanisms for accumulation of abnormal intracellular membrane. When ESCRT dysfunction happens within cells of the CNS, does the resulting membranous accumulation develop into the characteristic vacuoles of spongiform change? The remarkably similar spongiform neurodegenerative phenotypes of *Mgrn1*, *Fig4*, and *Vac14* mutants suggest that this could be the case, as both the MGRN1-dependent ubiquitination of the ESCRT-I protein TSG101 and the *Fig4/Vac14*-dependent production of $PI(3,5)P_2$ are important for ESCRT function. These considerations motivate the following hypothesis: that the vacuoles of spongiform change are essentially neuronal or glial class E *vps* compartments induced by defects in endosomal/lysosomal trafficking, and possibly augmented by accumulation of

autophagosomal membrane secondary to impaired MVB maturation. If this is the case, deletion of a class E *vps* gene in the brain should cause spongiform neurodegeneration. To test this hypothesis, I deleted *Tsg101* within neurons of the adult mouse brain.

Practical considerations regarding Tsg101 deletion in mouse brain

Tsg101 was originally described as a tumor repressor when knockdown of the gene was discovered to cause transformation of NIH3T3 cells (Li and Cohen, 1996). As TSG101 is now known to function in the lysosomal trafficking and degradation of membrane proteins (Babst *et al.,* 2000), including growth factor receptors, impairment of TSG101 function may lead to elevated growth factor receptor signaling and consequent hyperproliferation in certain cell types. Nevertheless, TSG101 loss-of-function does not necessarily promote cell proliferation in all cellular contexts, most likely because of its importance for general "housekeeping" functions (Wagner *et al.,* 1998; Krempler *et al.,* 2002). Consequently, homozygous null *Tsg101* mouse embryos fail to develop normally and die before day 6.5 of gestation (Ruland *et al.,* 2001; Wagner *et al.,* 2003). This suggests that deletion of TSG101 in neurons of the developing embryo could result in a general failure of brain development, which would be counterproductive for a study of the development of spongiform neuropathology. Therefore, I pursued a conditional gene inactivation strategy by using a loxP-flanked *Tsg101* conditional knockout (cKO) mouse allele in combination with a tamoxifen-inducible $CreER^{T2}$ transgene under the control of the CaMKIIα promoter, which is active in neurons of the mouse forebrain (Erdmann, Schutz, and Berger, 2007). Upon administration of tamoxifen, the estrogen receptor ligand binding domain of the $CreER^{T2}$ fusion protein directs translocalization of CreERT2 from the cytoplasmic to the nucleus, where the Cre recombinase domain excises loxP-

flanked DNA sequences (Feil *et al.,* 1997; Indra *et al,* 1999). Using this approach, gene deletion can be spatiotemporally restricted to only those cells in which the CreER^{T2} promoter is active at the time of tamoxifen administration; in this case, *Tsg101* would be deleted in CaMKIIα-positive neurons of the adult mouse forebrain. The brains of these mice were inspected for spongiform neurodegeneration.

Materials and Methods

Mice

Animals used in this study were housed in standard conditions at the Animal Resources Facility of the McLaughlin Research Institute for Biomedical Sciences in Great Falls, MT. The *Tsg101* conditional knockout mouse (*Tsg101 cKO*) was the kind gift of Dr. Kay-Uwe Wagner, and has been described elsewhere (Wagner *et al.,* 2003). This allele was created and is maintained on a 129/SvJ genetic background. The cKO allele has loxP sites 3kb upstream and 230 bp downstream of the first coding exon of *Tsg101*. Cre recombinase activity at the *Tsg101* cKO allele thus results in excision of the proximal promoter region and the first exon of *Tsg101*, resulting in a null allele. Frozen CamKCreER^{T2} transgenic mouse embryos were obtained from the European Mutant Mouse Archive (EMMA) and implanted into surrogate mothers by the McLaughlin Research Institute Transgenic Mouse facility. The CamKCreER^{T2} mice were created and characterized by Erdmann, Schutz, and Berger (2007). The ROSA26 reporter strain has been described by Soriano (1999).

Genotyping

Animals were genotyped using PCR assays on tail-snip DNA isolated by a standard alkaline lysis protocol. Tail snips <5mm long were collected from mice within 7 days of weaning and lysed in tail lysis buffer (50 mM Tris [pH8], 50 mM

EDTA, 0.5% SDS, 0.1 M NaCl, with protease K [10mg/ml]) at 65 ^{o}C followed by ethanol precipitation and resuspension in water. Presence of the wild type *Tsg101* allele was demonstrated using primers GTTCGCTGAAGTAGAGCAGCCAG and CATTTCTGGAGTCCGATGCGCAG. For the floxed allele, primer sequences AGAGGCTATTCGGCTATGACTG and TTCGTCCAGATCATCCTGATC were used. CamKCreER^{T2} transgene genotyping was performed using primers GGTTCTCCGTTTGCACTCAGGA, CTGCATGCACGGGACAGCTCT, and GCTTGCAGGTACAGGAGGTAGT to produce a band for the wild type allele at 290 bp and for the transgene at 375 bp. The ROSA26 reporter transgene was detected by PCR using the common forward primer sequence AAAGTCGCTCTGAGTTGTTAT and the reverse primer sequences GGAGCGGGAGAAATGGATATG (wt) and GCGAAGAGTTTGTCCTCAACC (ROSA+). All genotyping was performed using GoTaq green polymerase (Promega, Madison, WI) and 30 cycles of PCR (95^{o}C, 30 s; 63 ^{o}C, 60 s; 72 ^{o}C, 60 s).

Activation of Cre-ER

Gene excision was induced in 6 week-old mice (with or without CreER^{T2}, either homozygous or heterozygous for *Tsg101^{cKO}*) by twice-daily intraperitoneal injection of 0.5ug tamoxifen (Sigma) for five consecutive days. Tamoxifen was dissolved to 5 ug/ml in a 1:9 mixture of absolute ethanol and pharmacopoeial grade sunflower oil (Sigma). Some animals received injections of the 1:9 ethanol:oil vehicle mixture without tamoxifen as a control treatment. Body weight data were gathered for later cohorts of injected mice; mice were weighed once daily.

Verification of Cre recombinase activity

Cre activation of LacZ expression in ROSA26 mice was visualized at 6 weeks after injection of tamoxifen. Animals were deeply anesthetized with avertin and perfused with 4% paraformaldehyde in PBS. Whole brains and coronal sections were incubated for up to 8 hours in X-gal staining solution (5mM EGTA, 2mM $MgCl_2$, 0.01% sodium deoxycholate, 10 mM potassium ferricyanide, 10 mM potassium ferrocyanide, 0.02% Triton X-100, 0.5 mg/ml 5-bromo-4-chloro-3-indolyl-b-D-galactopyranoside [X-gal] in 1x PBS) as described by Erdmann, Schutz, and Berger (2007). Cre recombinase deletion of the floxed *Tsg101* sequence was verified by PCR of genomic DNA isolated from dissected brain regions (hippocampus, cerebral cortex, cerebellum, striatum, and hindbrain posterior to pons) of vehicle- and tamoxifen-injected animals, as well as from brains of $CreER^{T2}$(-) animals as a further negative control. Presence of the *Tsg101* null allele was detected using the primer pair GATGGTCATACCTGGTTAGAAAGC and CATTTCTGGAGTCCGATGCGCAG.

Histology

Animals were humanely euthanized either by CO2 asphyxiation or by deep avertin anesthesia and transcardial perfusion with 4% paraformaldehyde in PBS, and brain tissue was postfixed in paraformaldehyde overnight. Brains were processed by standard methods and embedded in paraffin, with care taken to avoid long exposure to 70% ethanol, which is known to cause artifactual vacuolation in rodent nervous tissue (Chladny and Ehrhardt, 2000). Paraffin-embedded brains were sectioned at 6 um and stained with hematoxylin and eosin (H&E) by standard methods prior to examination for spongiform neurodegeneration under the light microscope.

Results

Activity of CamKCreER^{T2} in mouse forebrain

To verify the activity of the CamKCreER^{T2} transgene under the tamoxifen treatment regime, I crossed the transgene into the ROSA26 strain, which expresses a Cre-inducible LacZ allele under the control of a ubiquitously active promoter (Soriano, 1999). Brains of tamoxifen- and control- (ethanol/ sunflower oil vehicle only) injected mice were collected 6 weeks after initiation of tamoxifen treatment and examined for β-galactosidase expression. Upon treatment with X-gal, whole mount brain preparations of CamKCreER^{T2} (+), ROSA26 (+), tamoxifen-injected animals showed extensive CreER^{T2} activity as demonstrated by the formation of the blue β-galactosidase reaction product (Figure 5.4). X-gal staining was most intense in the hippocampus and cerebral cortex, with low levels of staining in the striatum and thalamus, and no detectable staining in the cerebellum. Vehicle-injected CamKCreER^{T2} (+), ROSA26 (+) brains showed detectable recombination at the β-galactosidase activity only in the hippocampus, reflecting a low level of tamoxifen-independent CreER^{T2} activity in this anatomical location. This pattern of CamKCreER^{T2} activity replicates that reported for this transgene by Erdmann, Schutz, and Berger (2007). As expected, ROSA26 (+) mice lacking the CreER^{T2} transgene showed no detectable blue staining after tamoxifen treatment, similar to ROSA26 (-) controls (Figure 5.4). To determine whether the CamKCreER^{T2} transgene had any activity outside of the brain, I performed X-gal staining on heart, lung, liver, spleen, stomach, gut, kidney, skin, bone, muscle, uterus, ovary, testis, and seminal vesicle of tamoxifen-injected, vehicle-injected, and Rosa26(-) animals. No β-galactosidase activity over background was observed in any of these locations (data not shown).

To visualize excision of *Tsg101* sequence in tamoxifen-injected animals, I performed PCR with primers specific for the null allele on DNA isolated from cerebral

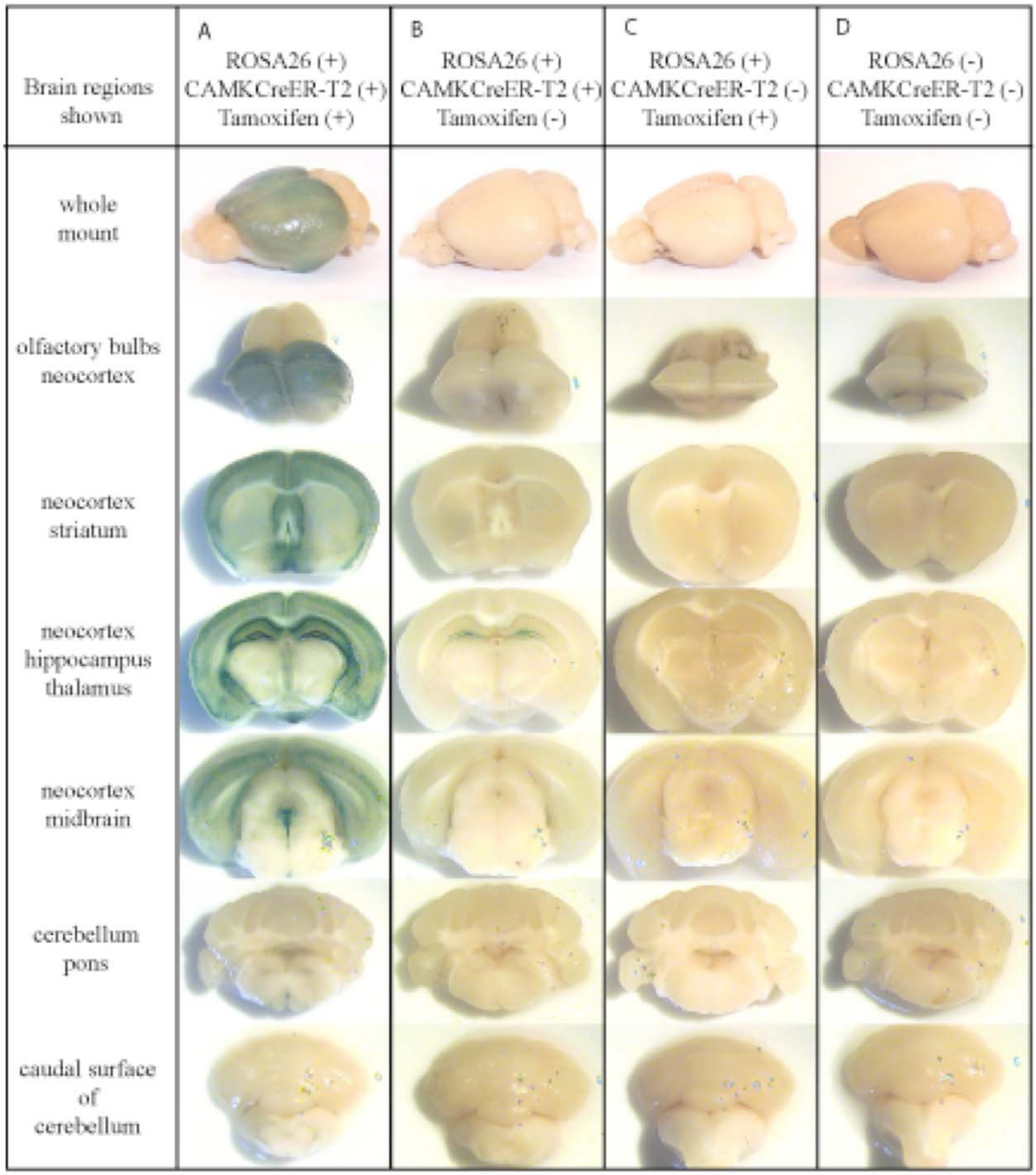

Figure 5.4. Inducible CamKCreER^{T2} activity in brains of ROSA26 mice. X-gal staining revealed robust CreER activation of ß-galactosidase in brains of tamoxifen-treated CamKCreER^{T2} (+); ROSA26(+) mice (A), but only limited CreER activity in brains of similar mice receiving control injections (B). No X-gal staining was evident in ROSA26(+) mice lacking CamKCreER^{T2} (C), or in ROSA26(-) controls (D).

cortex, hippocampus, midbrain, hindbrain, and cerebellum of tamoxifen-injected and control animals. As expected based on the pattern of Rosa26 activation seen in Figure 5.4, *Tsg101* null allele generation was not detectable in tamoxifen-injected, CamKCreER^{T2}(-) animals, but was evident in all brain areas except for cerebellum in tamoxifen-injected, CamKCreER^{T2}(+) animals (Figure 5.5). Background activity of the CamKCreER^{T2} transgene was confined to the hippocampus, as previously seen in the Rosa26 mice.

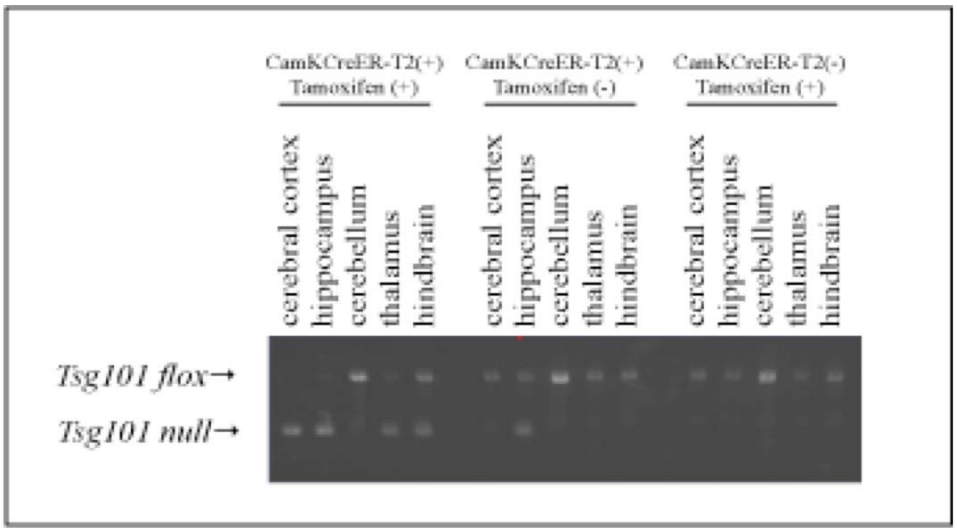

Figure 5.5. Generation of *Tsg101* null allele in different brain regions of tamoxifen-treated Tsg101 cKO/+ mice. PCR amplification of a null-allele-specific product was seen in all brain regions except cerebellum of tamoxifen-treated CamKCreER^{T2}(+) mice, (left). Only background levels of CreER^{T2} activity were seen in hippocampus of vehicle-treated CamKCreER^{T2}(+) mice (center). Generation of the null *Tsg101* allele was not detectable in the absence of the CamKCreER^{T2} transgene (right).

Response of mice to neuronal Tsg101 ablation

Tsg101 cKO/cKO, CamKCreER^{T2}(+) mice treated with tamoxifen exhibited a period of rapid weight loss beginning around the eighth day after their first treatment with the drug (Figure 5.6). By the end of the second week post-injection, these mice lost an average of 6 grams of body weight and exhibited a rough coat appearance,

kyphotic (hunched) posture, lethargy/weakness, and an abnormal "high-stepping" gait. This effect was seen only in CamKCreER^{T2}(+); *Tsg101*$^{cKO/cKO}$ mice that received tamoxifen. Control animals of the same genotype given vehicle injections only, or tamoxifen-injected animals bearing a wt *Tsg101* allele or lacking CamKCreER^{T2}, did not lose weight and did not show signs of illness (Figure 5.6 and Table 5.1).

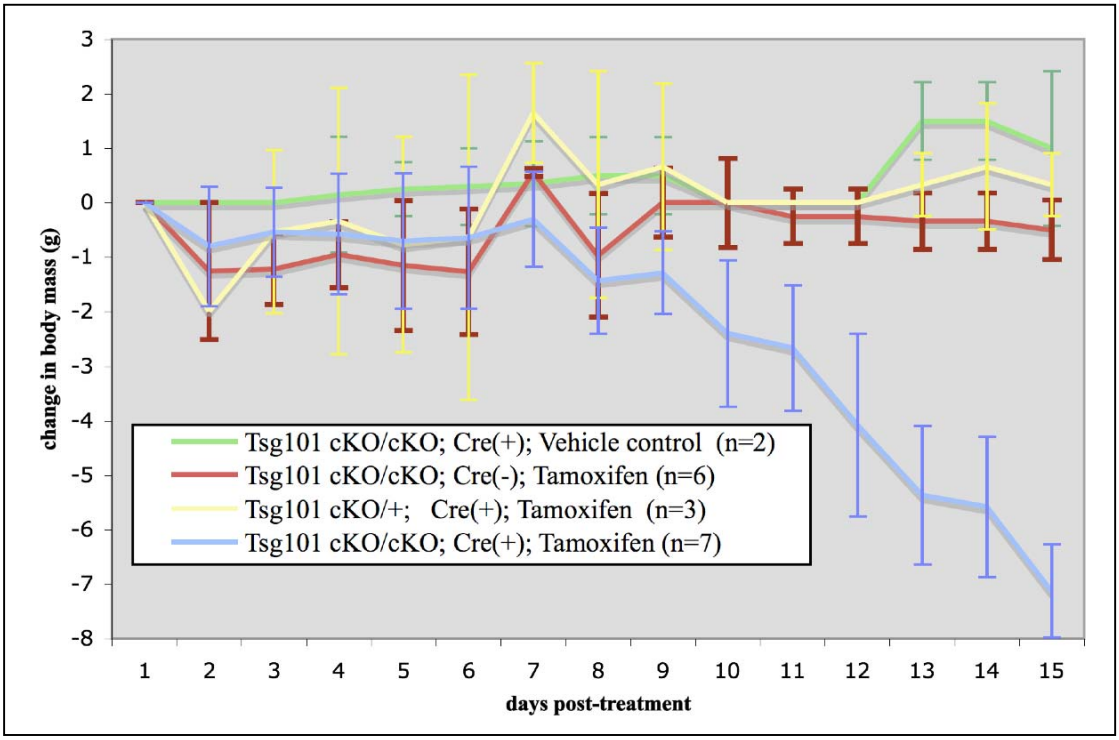

Figure 5.6. *Tsg101* deletion in forebrain neurons causes rapid weight loss. Mice received tamoxifen injection or a vehicle control during days 1-5. Reported values of *n* for each class are numbers of mice for which weight data are available. Error bars indicate one standard deviation.

The condition of these mice reached a point of crisis at approximately day 15, at which point some mice died (or were euthanized in accordance with principles of humane treatment) and other mice began to recover. The four mice that survived this crisis point (out of 17 mice that became ill from *Tsg101* gene deletion) rapidly regained their lost weight and returned to apparent health within another week. Figure 5.7 shows the patterns of weight loss and recovery experienced by the two survivors

for which body weight data were collected. Notably, these two mice had the highest starting weights recorded among all the mice that experienced acute weight loss (starting body weight ranged from 16g-26.5g), suggesting that the additional energetic reserves accompanying high body mass protects the mice from succumbing during the acute weight loss phase.

Table 5.1. Effects of *Tsg101* gene deletion in neurons of adult mouse forebrain. Mice were scored as "sick" if they displayed kyphotic posture and rough coat.

Tsg101 genotype	CamKCreER^{T2} genotype	Treatment	*n*	# sick at day 15	# alive at day 30
cKO/cKO	(+)	Tamoxifen	17	17	4
cKO/cKO	(-)	Tamoxifen	20	0	20
cKO/+	(+)	Tamoxifen	16	0	16
cKO/+	(-)	Tamoxifen	10	0	10
cKO/cKO	(+)	Vehicle	8	0	8

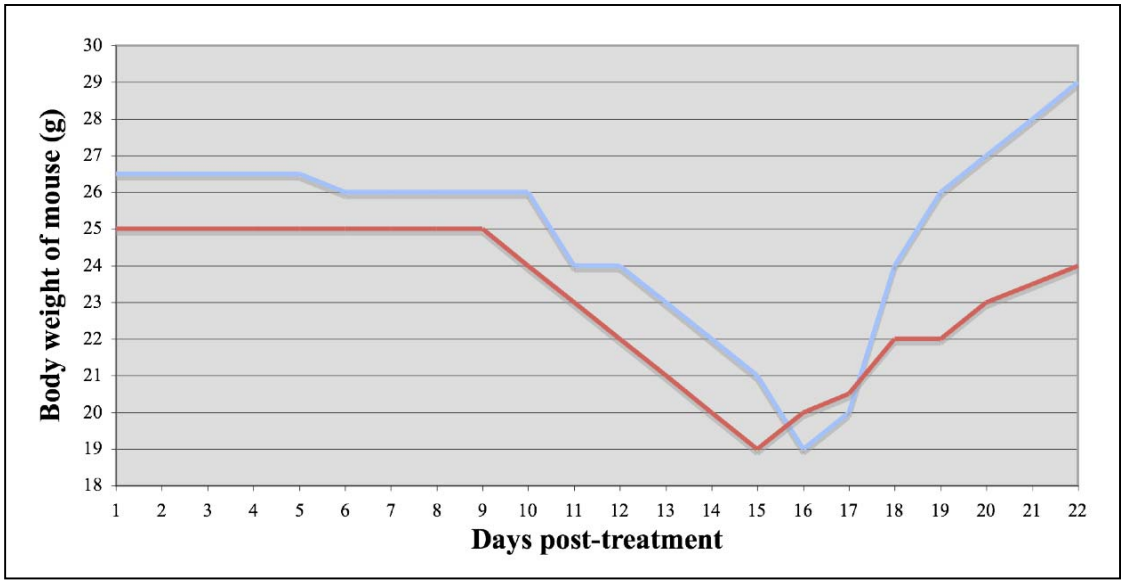

Figure 5.7. Weight loss is transient for *Tsg101*-deleted mice that survive the "day 15 crisis." Data are shown for the two individual mice for which body weight data are available beyond day 16.

Neuropathological findings

H&E-stained sections of brains from euthanized at day 14 were examined. The overall brain architecture was intact and no spongiform change was evident (data not shown). The brains of the oldest surviving tamoxifen injected *Tsg101*$^{cKO/cKO}$, *CamKCreER-T2(+)* mouse and a tamoxifen-injected *Tsg101*$^{cKO/cKO}$, *CamKCreER-T2(-)* control were examined at 8 weeks after tamoxifen injection (of the other three *Tsg101*-depleted animals that survived past the second week, two died from accidental causes and were not used for histology. The remaining animal from the most recent experimental cohort was left to age to a later time point.). This brain showed atrophy of the cerebral hemispheres on gross examination (Figure 5.8) with greatly expanded lateral ventricles and apparent thinning of the cerebral cortex apparent during sectioning. Microscopic inspection of H&E-stained 6 μm sections revealed severe hippocampal degeneration. Vacuoles similar in appearance to spongiform change were seen in the cerebral cortex (and also in the cerebellum) of the *CamKCre-T2*(+) animal which were not evident in the *CamKCre-T2*(-) control (Figure 5.9 and data not shown).

Discussion

Unexpected weight loss in TSG101-ablated mice

This study revealed an unexpected acute consequence of neuronal *Tsg101* ablation: a severe, but transient weight loss occurring during the second week following activation of CreER^{T2} to initiate *Tsg101* deletion. As the CamKCreER^{T2} allele used in this study showed no detectable activity outside of the CNS, this weight loss is apparently a consequence of *Tsg101* deletion in the brain. While I have not quantified the food intake of mice in this study, observations of mice during their acute weight-loss phase suggested that compared to their non-affected cagemates, ill

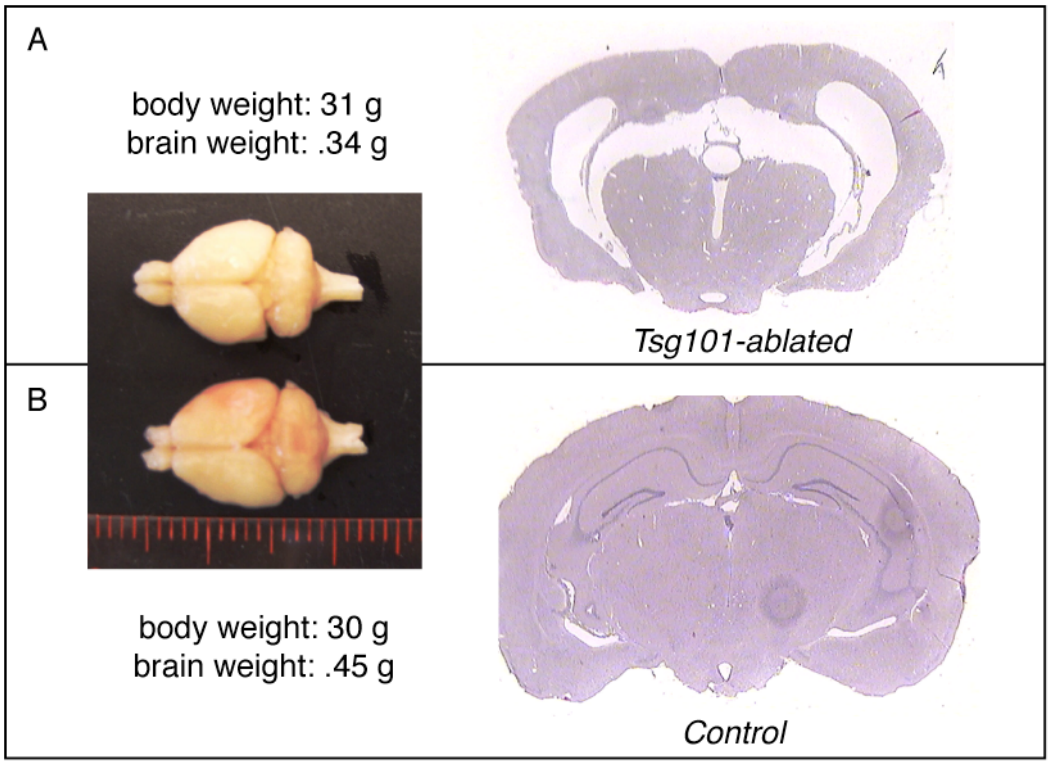

Figure 5.8. Cerebral and hippocampal atrophy with expanded lateral ventricles after deletion of *Tsg101* in forebrain neurons of adult mouse. (A) H&E-stained coronal section of brain from *Tsg101*$^{flox/flox}$*; CamKCreER(T2)+* mouse 8 weeks after injection with tamoxifen. (B) Control section from *Tsg101*$^{flox/flox}$*; CamKCreER(T2)-* mouse 8 weeks after injection with tamoxifen. Inset shows appearance of whole brains with atrophy of the cerebral hemispheres evident in the *Tsg101*-ablated brain (top).

Figure 5.9. Microscopic appearance of neurodegeneration in *Tsg101*-ablated forebrain. A: View of cerebral cortex and hippocampal region of control [*Tsg101*$^{cKO/cKO}$*; CamKCreERT2(-);* tamoxifen(+)] brain. B: Comparable region of *Tsg101*-ablated [*Tsg101*$^{cKO/cKO}$*; CamKCreERT2(+);* tamoxifen(+)] brain. Note expansion of lateral ventricle, atrophy of cerebral cortex. C,E,G: higher magnification images of control brain. D,F,H: higher magnification images of *Tsg101*-ablated brain. Note spongiform-change-like appearance of vacuoles in H.

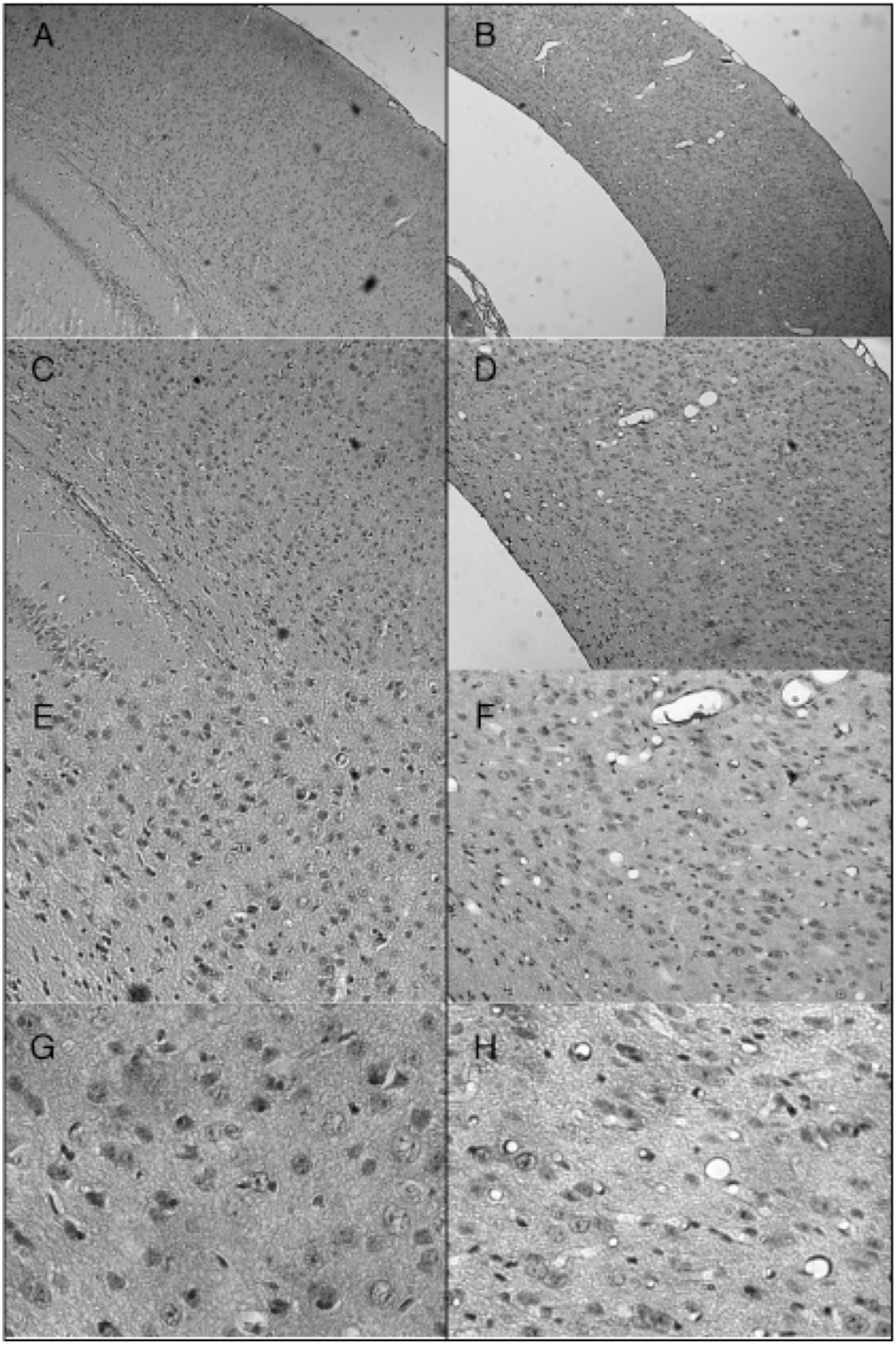
A
B
C
D
E
F
G
H

mice rarely sought food. This suggests that reduced caloric intake contributes to the weight loss of these mice, perhaps partly due to a reduction in foraging behavior, drive, or efficiency. Since widespread neurodegeneration was not observable at the time of weight loss, it would be interesting to know whether the apparent reduction in food intake is caused by a specific dysfunction in a neural pathway involved in feeding behavior, such as an impairment in agouti-related protein (AGRP) signaling in the hypothalamic orexigenic signaling pathway.

As discussed in chapter 1, AGRP is believed to promote feeding behavior by inhibiting signaling through the melanocortin-4 receptor (MC4R), in an analogous mechanism to the inhibition of MC1R signaling by ASP (Ollmann *et al.*, 1997). If ESCRT processing of MC4R is required for AGRP signaling by hypothalamic neurons (as I have proposed that ESCRT processing of MC1R is required for ASP signaling in melanocytes), then *Tsg101* deletion in hypothalamic neurons could impair this orexigenic signaling pathway and cause a reduction in feeding behavior. This speculative proposal is, of course, only one among many possible interpretations of the data presented here; there are many imaginable nonspecific pathways by which a general neuronal housekeeping gene impairment could lead to a disability affecting food intake. However, my data are consistent with the observed consequences of an acute impairment in central AGRP signaling: significantly, adult mice subjected to ablation of AGRP-expressing hypothalamic neurons stop feeding and starve (Gropp *et al.*, 2005; Luquet *et al*, 2005). The rate of weight loss in AGRP-neuron-ablated mice averages 20% of body weight (~4g) per week, similar in severity what I observed in this study. Mice in both of the AGRP neuron ablation studies cited above were euthanized when their weight loss reached 20% of starting body weight, so it is not known whether the anorexic effect of AGRP neuron ablation is transient; however, the orexigenic signaling network is capable of compensating for perturbation of AGRP

signaling, as partial depletion of AGRP neurons causes a moderate initial decrease in feeding that is corrected back to near-normal levels (Bewick *et al.,* 2005). Hypothalamic neurogenesis has been reported to promote a similar compensatory response to progressive AGRP neuron degeneration (Pierce and Xu, 2010), suggesting that regeneration of *Tsg101*$^{+/+}$ hypothalamic neurons from non-recombined precursors might contribute to the recovery of mice in my study.

The weight-loss phenotype, while potentially informative about the role of ESCRT in orexigenic signaling, presents an obstacle to the examination of neurodegeneration in *Tsg101*-depleted brains due to the high mortality of the informative mice in this study. As the heaviest mice seem to be the best equipped to survive the period of transient weight loss, future cohorts of mice injected for this study will be composed entirely of animals with body weights over 25 grams. The realization that mortality seen in this study is related to weight loss should allow effective targeting of palliative care to maintain the welfare of future cohorts of injected animals. If the weight loss is determined to be caused by a transient anorexia in treated mice, hand-feeding of the affected animals during the second week post-treatment should provide a means of maintaining their body weight at healthy levels until normal feeding activity returns after day 15.

Spongiform neurodegeneration as a consequence of ESCRT depletion: potential implications for other neurodegeneration models and human disease.

The preliminary data presented here (representing a single brain collected at the 8 week mark after *Tsg101* ablation) suggest that neuronal *Tsg101* depletion may cause a profound neurodegenerative response. While the detailed pathological characteristics of this neurodegeneration are obscured in some regions of the brain (*i.e.,* the hippocampus) by severe tissue atrophy, the appearance of other regions of the

affected brain is suggestive of spongiform neurodegeneration. While great caution must be taken in interpreting such a limited data set, this provides preliminary support for the hypothesis that ESCRT dysfunction is a cause of spongiform change.

If additional data confirm this preliminary result, it will be of great interest to determine to what extent ESCRT dysfunction explains spongiform neurodegeneration in other mouse models of spongiform change and in human disease. In the case of several mouse models of spongiform change, links to ESCRT biology are already known to exist. *Mgrn1* mutant animals provide a clear link to ESCRT dysfunction, as MGRN1 has been demonstrated to ubiquitinate TSG101 in a way that is important for lysosomal cargo sorting (Kim *et al*, 2007, Jiao *et al*, 2009a). Partial impairment of TSG101 function in *Mgrn1* mutant mice might be plausibly supposed to underlie the relatively slow development of spongiform change seen in these animals, in contrast to the severe pathology reported here in a case of TSG101 deletion. As ATRN and MGRN1 appear to be partners in at least a subset of their activities, the spongiform change seen in *Atrn* mutants could be explained as a similar consequence of loss of a subset of MGRN1-related ESCRT trafficking events. As shown in Figure 5.2, cultured neurons with defective function of the ESCRT-III proteins SNF7-2 and CHMP2B accumulate abnormal membrane, so it would be interesting to determine whether the histopathological consequence of similar impairments in brain tissue could be spongiform change. Finally, as the ESCRT protein CHMP3/VPS24 has been shown to have $PI(3,5)P_2$ dependent activity (Whitley *et al.*, 2003), the spongiform vacuolation in the $PI(3,5)P_2$ regulatory mutants *Fig4* and *Vac14* (see Figure 5.3) could be explained as a consequence of an inhibition of ESCRT activity by $PI(3,5)P_2$ depletion.

Of the human spongiform neuroencephalopathies, retrovirus-associated spongiform change (discussed in Chapter One) is an attractive subject for explanation

as an effect of ESCRT dysfunction. It is well understood that human immunodeficiency virus (HIV) "hijacks" ESCRT proteins through an interaction between TSG101 and the GAG protein of the viral capsids (Garrus *et al.,* 2001; Pornillos *et al.,* 2003; reviewed by Hurley and Emr 2009; Bieniasz 2010). This interaction subverts the ESCRT machinery by directing the ESCRT-mediated sorting of HIV not into the MVB, but out of the host cell. It can be imagined that the "hijacking" of TSG101 by HIV could cause a functional depletion of ESCRT at the MVB, resulting in ESCRT dysfunction as a consequence of HIV infection. Significantly, HIV infection in cells of the CNS causes spongiform change. Taken together, these observations suggest that HIV-associated spongiform neurodegeneration could be a consequence of ESCRT loss-of-function due sequestration of TSG101 by HIV GAG (Teresa Gunn, personal communication).

The canonical example of spongiform encephalopathy in humans is prion disease. As discussed in Chapter One, neither the physiological role of PrP^{C} nor the pathological mechanisms set in motion by PrP^{D} are well understood, making it difficult to confidently identify a likely point of intersection between prion biology and ESCRT function. Interestingly, however, there are parallels between prion biology and retroviral budding that provide food for thought. Both PrP^{D} and budding retroviruses have been proposed to escape the cell using exosomes, which are essentially ESCRT-derived MVB-like organelles which fuse with the plasma membrane (rather than with the lysosome) in order to eject their contents to the outside of the cell (Nguyen *et al.*, 2003; Gould, Booth, and Hildreth, 2003; Fevrier *et al.,* 2004; Fevrier *et al.,* 2005; Fang *et al.,* 2007). Notably, co-infection of PrP^{D} and a murine retrovirus strongly increased the release of scrapie infectivity in cell culture, suggesting that retroviruses may serve as cofactors in the spread of PrP^{D} (LeBlanc *et al*, 2006). While the dominant "protein only" hypothesis of prion pathogenesis

considers PrP pathology to occur strictly as a consequence of PrP protein misfolding, some voices have long emphasized evidence that viral cofactors could be important for the spread of PrP^D: with certain protocols, the majority of scrapie infectivity sediments at 120S and can be filtered out at 25nm, consistent with the size and density of a viral particle rather than an isolated PrP^D oligomer (Sklaviadis, Manuelidis, and Manuelidis, 1989; Manuelidis *et al.,* 1995). Furthermore, intracellular virus-like particles of approximately 25 nm in diameter are produced in cultured cells infected with scrapie and are a consistent finding in ultrastructural studies of prion-infected brains (Manuelidis *et al.,* 2007; Liberski *et al.,* 2008). Considering these observations, the hypothesis of a viral cofactor in prion disease is attractive. Defenders of the "protein only" hypothesis can rightly insist, however, that prion infection can occur in the absence of any viral cofactor, as scrapie infectivity can survive irradiation, heat treatment, and chemical denaturation that would destroy viral cofactors. If viruses subsequently come to serve as co-factors for prion spread, where do they come from?

One intriguing possibility is that prion infection could promote expression of some of the endogenous retroviruses (ERV) that reside in thousands of copies throughout mammalian genomes. Several groups have produced data consistent with this hypothesis. ERV RNA sequences have been shown to co-purify with scrapie infectivity (Akowitz, Manuelidis, and Manuelidis, 1993; Akowitz, Sklaviadis, and Manuelidis, 1994), prion infection up-regulates expression of some ERV in infected murine neuronal cells (Stengel *et al,* 2006), and cerebrospinal fluid from human Creutzfeldt-Jakob disease patients shows increased prevalence of some families of human ERV (Jeong *et al,* 2010). These data suggest that PrP^D may cause the irruption of endogenous retroviruses from the host genome. To the extent that these endogenous retroviruses behave like HIV and "hijack" ESCRT function, loss of

ESCRT function could ensue and cause spongiform neurodegeneration in prion-infected hosts.

Why PrP^D might cause irruption of endogenous retroviruses is an interesting question. ERV make up a major portion of mammalian genomes; in the case of the mouse genome, almost 10% of the total sequence is ERV-derived (Mouse Genome Sequencing Consortium, 2002). This heavy load of selfish DNA elements presents a challenge for the host genome, which must find ways to edit, suppress or co-opt ERV elements to maintain its own function within acceptable limits. One possibility is that PrP^C is a member of an ERV control mechanism, and that conversion of PrP^C to PrP^D ablates or subverts this activity. Remarkably, PrP^C has been reported to mimic several distinct properties of the HIV nucleocapsid protein NCP7. A succession of papers from the Darlix lab report that i*n vitro,* PrP^C facilitates the dimerization of retroviral RNA, inhibits self-primed reverse transcription of the viral genome, mediates initial tRNA annealing, and chaperones ssDNA strand transfers during reverse transcriptase activity (Gabus *et al.,* 2001a; Gabus *et al.,* 2001b; Derrington *et al.,* 2002; Moscardini *et al.,* 2002; Leblanc, Bass, and Darlix, 2004). One view to emerge from these observations is that PrP^C can be described as a host-encoded retrovirus nucleocapsid mimic that may be deployed by the host cell as a defense measure, mimicking retroviral protein structures to subvert replication of endogenous and/or exogenous retroviruses. While this is not a majority view within the field, a very interesting study by Lotsher *et al.* (2007) provides some independent support for this hypothesis. Immune stimulation was found to cause massive up-regulation of ERV transcription in mouse spleen, which in turn induced up-regulation of PrP^C, leading to suppression of ERV expression. Significantly, *Prnp* $^{-/-}$ mice failed to suppress ERV. These results suggest that PrP^D conversion may disable an innate mechanism for suppression of

endogenous retrovirus activity, leading to unrestrained irruption of viral capsids from host-encoded proviral sequence.

These considerations suggest a view of PrP^D and retroviruses, not as competing explanations for scrapie-like diseases, but as coevolved pathogens mutually reinforcing each other's replication efficiency. The abnormal PrP^D form promotes the production of retroviral (including ERV) gene products by disabling the host genome's PrP^C-dependent retrovirus defense pathway. In return, the budding of the resulting ERV viral capsids promotes the escape of converted PrP^D from the cell, and perhaps also promotes the uptake of PrP^D–containing viral capsids and/or exosomes by new host cells. This arrangement is mutually beneficial from the point of view of both the PrP^D conformer and the ERV viral genome, and the resulting mutualism would be favored and refined by natural selection. This proposed cooperative relationship between an exogenous protein-only pathogen and an endogenous selfish element could provide a unifying explanation for observations that have seemed difficult to synthesize; namely, the clear ability of mere PrP^D to initiate disease, and the several lines of evidence suggesting that additional cofactors are involved in the efficient propagation of pathology and infectivity. In addition, the hypothesis of linear causal relationship leading from prion conversion to ERV irruption and budding, ESCRT dysfunction, and spongiform neurodegeneration suggests the exciting possibility that antiretroviral therapeutic strategies could be effective in the prevention and treatment of spongiform neurodegeneration in prion diseases, for which at present no effective treatment exists. This possibility warrants further investigation of the relationships connecting prion propagation, ERV activation and budding, ESCRT dysfunction, and spongiform change.

Aside from the potential medical importance of understanding the connections between prions and ERV biology, the elucidation of their relationship is a matter of

considerable intrinsic and theoretical interest. If the proposed mutualism is found to be a real aspect of prion and ERV biology, it will provide yet another example of the immense resourcefulness and subversive creativity exhibited by selfish elements (nucleic acid or otherwise) over evolutionary time. This author finds it fascinating to consider that PrP^{C}, as a host-encoded mimic of viral nucleocapsid protein, may have been developed in the ancient intragenomic conflict against ERVs as a subversive countermeasure to viral function, only to be subverted in turn by an evolutionary partnership between budding ERVs and a rogue, self-perpetuating folding conformation of the PrP protein itself. As an example of the endless creativity of living systems, this story of evolutionary subversion and counter-subversion underscores the fact that life is a masterful improvisationalist, appropriating and reinventing existing molecular pathways in unpredictable but fascinating ways to accomplish novel and interesting functions. This work has followed a single thread of mechanistic and evolutionary connections along a winding path, starting at the point of MC1R downregulation in the hair follicle and arriving, eventually, at a potentially new vantage point from which to understand spongiform neurodegeneration. But living things, in the richness of their history, blaze many such paths. Where these paths lead is often unpredictable. Given the nature of life, perhaps the discovery of an unexpected view along the way should never come as a surprise.

REFERENCES

Aberdam, E., Bertolotto, C., Sviderskaya, E.V., de Thillot, V., Hemesath, T.J., Fisher, D.E., Bennett, D.C., Ortonne, J.P., and Ballotti, R. (1998). Involvement of microphthalmia in the inhibition of melanocyte lineage differentiation and of melanogenesis by agouti signal protein. J. Biol. Chem. *273*, 19560-19565.

Acconcia, F., Sigismund, S., and Polo, S. (2009). Ubiquitin in trafficking: the network at work. Exp. Cell Res. *315*, 1610-1618.

Aguzzi, A., Baumann, F., and Bremer, J. (2008). The prion's elusive reason for being. Annu. Rev. Neurosci. *31*:439-77.

Akowitz, A., Manuelidis, E.E., and Manuelidis, L. (1993). Protected endogenous retroviral sequences copurify with infectivity in experimental Creutzfeldt-Jakob disease. Archives of Virology *130:* 301-316

Akowitz, A., Sklaviadis, T., and Manuelidis, L. (1994). Endogenous viral complexes with long RNA cosediment with the agent of Creutzfeldt-Jakob disease. Nucleic Acids Research *22*: 1101-1107.

Ardley, H.C., and Robinson, P.A. (2005). E3 ubiquitin ligases. Essays Biochem. *41*, 15-30.

Artigas, J., Niedobitek, F., Grosse, G., Heise, W., and Gosztonyi, G. (1989). Spongiform encephalopathy in AIDS dementia complex: report of five cases. J. Acquir. Immune Defic. Syndr. *2*: 374-81.

Aune, C.N., Chatterjee, B., Zhao X.O., Francis, R., Bracero, L., Yu, Q., Rosenthal, L., Leatherbury, L., and Lo, C.W. (2008). Mouse model of heterotaxy with single ventricle spectrum of cardiac anomalies. Pediatr. Res. *63*:9-14

Babst, M., Odorizzi, G., Estepa, E. J., and Emr, S.D. (2000). Mammalian tumor susceptibility gene 101 (TSG101) and the yeast homologue, Vps23p, both function in late endosomal trafficking. Traffic *1:*248-258.

Bampton, E.T.,Goemans, C.G., Niranjan, D., Mizushima, N., and Tolkovsky, A.M. (2005). The dynamics of autophagy visualized in live cells: from autophagosome formation to fusion with endo/lysosomes. Autophagy *1*: 23-36.

Bennett, D.C., Cooper, P.J., and Hart, I.R. (1987). A line of non-tumorigenic mouse melanocytes, syngeneic with the B16 melanoma and requiring a tumor promoter for growth. Int. J. Cancer *39*:414-8.

Bennett, D.C., and Lamoreux, M.L. (2003). The color loci of mice--a genetic century. Pigment Cell Res. *16*, 333-344.

Bertolotto, C., Abbe, P., Hemesath, T.J., Bille, K., Fisher, D.E., Ortonne, J.P., and Ballotti, R. (1998). Microphthalmia gene product as a signal transducer in cAMP-induced differentiation of melanocytes. J. Cell Biol. *142*, 827-835.

Bewick, G.A., Gardiner, J.V., Dhillo, W.S., Kent, A.S., White, N.E., Webster, Z., Ghatei, M.A., and Bloom, S.R. (2005). Post-embryonic ablation of AgRP neurons in mice leads to a lean, hypophagic phenotype. FASEB J. *19*:1680-2.

Bieniasz, P.D. (2009) The cell biology of HIV-1 virion genesis. Cell Host Microbe. *18*:550-8.

Blanchard, S.G., Harris, C.O., Ittoop, O.R., Nichols, J.S., Parks, D.J., Truesdale, A.T., and Wilkison, W.O. (1995). Agouti antagonism of melanocortin binding and action in the B16F10 murine melanoma cell line. Biochemistry *34*, 10406-10411.

Bonangelino, C.J., Nau, J.J., Duex, J.E., Brinkman, M., Wurmser, A.E., Gary, J.D., Emr, S.D., Weisman, L.S. (2002). Osmotic stress-induced increase of phosphatidylinositol 3,5-bisphosphate requires Vac14p, an activator of the lipid kinase Fab1p. J Cell Biol 156: 1015–1028

Bonilla, C., Boxill, L.A., Donald, S.A., Williams, T., Sylvester, N., Parra, E.J., Dios, S., Norton, H.L., Shriver, M.D., and Kittles, R.A. (2005). The 8818G allele of the agouti signaling protein (ASIP) gene is ancestral and is associated with darker skin color in African Americans. Hum. Genet. *116*, 402-406.

Bork, P., and Beckman, G. (1993). The CUB domain. A widespread module in developmentally regulated proteins. J Mol Biol. *231*:539-45.

Box, N.F., Wyeth, J.R., O'Gorman, L.E., Martin, N.G., and Sturm, R.A. (1997). Characterization of melanocyte stimulating hormone receptor variant alleles in twins with red hair. Hum. Mol. Genet. *6*, 1891-1897.

Braulke, T. and Bonifacino, J.S. (2009) Sorting of lysosomal proteins. Biochim Biophys Acta. 1793:605-14.

Bronson, R.T., Donahue, L.R., Samples, R., Kim, J.H., and Naggert, J.K. (2001). Mice with mutations in the mahogany gene Atrn have cerebral spongiform changes. J. Neuropathol. Exp. Neurol. *60*, 724-730.

Brooks, B.R., Swarz, J.R., Narayan, O., and Johnson, R.T. (1979). Murine neuropathic retrovirus spongiform polioencephalomyelopathy: acceleration of disease by virus inoculum concentration. Infect. Immun. *23:* 540-4.

Brown, J., Ashworth, A., Gydesen, S., Sorensen, A., Rossor, M., Hardy, J., and Collinge, J. (1995). Familial non-specific dementia maps to chromosome 3. Hum. Mol. Genet. *4*: 1625–1628.

Brown, P., Cathala, F., Raubertas, R.F., Gajdusek, D.C., and Castaigned, P. (1987). The epidemiology of Creutzfeldt-Jakob disease: conclusion of a 15-year investigation in France and review of the world literature. Neurology *37*:895-904.

Bultman, S.J., Michaud, E.J., and Woychik, R.P. (1992). Molecular characterization of the mouse agouti locus. Cell *71*, 1195-1204.

Calebiro, D., Nikolaev, V.O., Gagliani, M.C., de Filippis, T., Dees, C., Tacchetti, C., Persani, L., and Lohse, M.J. (2009). Persistent cAMP-signals triggered by internalized G-protein-coupled receptors, PLoS Biol. *7:* e1000172.

Campana, V., Sarnataro, D., and Zurzolo, C. (2005). The highways and byways of prion protein trafficking. Trends Cell Bio. *15*: 102-111.

Campana, V., Caputo, A., Sarnataro, D., Paladino, S., Tivodar, S., and Zurzolo, C. (2007). Characteriztion of the properties and trafficking of an anchorless form of the prion protein. J. Biol. Chem. *282:* 22747-22756.

Candille, S.I., Kaelin, C.B., Cattanach, B.M., Yu, B., Thompson, D.A., Nix, M.A., Kerns, J.A., Schmutz, S.M., Millhauser, G.L., and Barsh, G.S. (2007). A β-defensin mutation causes black coat color in domestic dogs. Science *318*, 1418-1423.

Canuel, M., Korkidakis, A., Konnyu, K., and Morales, C.R. (2008). Sortilin mediates the lysosomal targeting of cathepsins D and H, Biochemical and Biophysical Research Communications *373:* 292-297.

Chai, B.X., Pogozheva, I.D., Lai, Y.M., Li, J.Y., Neubig, R.R., Mosberg, H.I., and Gantz, I. (2005). Receptor-antagonist interactions in the complexes of agouti and agouti-related protein with human melanocortin 1 and 4 receptors. Biochemistry *44*, 3418-3431.

Chakraborty, A., and Pawelek, J. (1993). MSH receptors in immortalized human epidermal keratinocytes: a potential mechanism for coordinate regulation of the epidermal–melanin unit. J. Cell Physiol. *157*:344–50.

Chakraborty, A., Funasaka, Y., Slominski, A., Ermak, G., Hwang, J., Pawelek, J.M., and Ichihashi, M. (1996). Production and release of proopiomelanocortin (POMC) derived peptides by human melanocytes and keratinocytes in culture: regulation by ultraviolet B. Biochim. Biophys. Acta *1313*, 130-138.

Chan, L.F., Webb, T.R., Chung, T-T., Meimaridou, E., Cooray, S.N., Guasti, L., Chapple, J.P., Egertova, M., Elphick, M.R., Cheetham, M.E., Metherell, L.A., and Clark, A.J.L. (2009). MRAP and MRAP2 are bidirectional regulators of the melanocortin receptor family. Proc. Nat. Acad. Sci. USA *106*:6146-51.

Chen, Z.J., and Sun, L.J. (2009). Nonproteolytic functions of ubiquitin in cell signaling. Mol. Cell *33*, 275-286.

Chen, S., Yadav, S.P., Surewicz, W.K. (2010). Interaction between human prion protein and Aβ oligomers: the role of N-terminal residues. J. Biol. Chem. Electronically published ahead of print Jun 24, 2010. doi: 10.1074/jbc.M110.145516.

Chladny, M.J., and Ehrhart, E.J. (2000). Brain vacuolization induced by 70% ethanol. Histologic May 2000.

Choe, W., Stoica, G., Lynn, W., Wong, P.K.Y. (1998). Neurodegeneration induced by MoMuLV-ts1 and increased expression of Fas and TNF-α in the central nervous system. Brain Res. *779:* 1-8.

Chow, C.Y., Zhang, Y., Dowling, J.J., Jin, N., Adamska, M., Shiga, K., Szigeti, K., Shy, M.E., Li, J., Zhang, X., Lupski, J.R., Weisman, L.S., and Meisler, M.H. (2007). Mutation of FIG4 causes neurodegeneration in the pale tremor mouse and patients with CMT4J. Nature. *448*:68-72.

Cone, R.D., Mountjoy, K.G., Robbins, L.S., Nadeau, J.H., Johnson, K.R., Roselli-Rehfuss, L., and Mortrud, M.T. (1993). Cloning and functional characterization of a family of receptors for the melanotropic peptides. In The Melanotropic Peptides, H. Vaudry, and A.N. Eberle, eds. (New York), pp. 342-363.

Costa, M.D., Paludo, K.S., Klassen, G., Lopes, M.H., Mercadante, A.F., Martins, V.R., Camargo, A.A., Nakao, L.S., and Zanata, S.M. (2009). Characterization of a specific interaction between ADAM23 and cellular prion protein. Neurosci Lett. *461*:16-20.

Cota, C.D., Bagher, P., Pelc, P., Smith, C.O., Bodner, C.R., and Gunn, T.M. (2006). Mice with mutations in Mahogunin ring finger-1 (Mgrn1) exhibit abnormal patterning of the left-right axis. Dev. Dyn. *235*, 3438-3447.

Creemers, J.W., Pritchard, L.E., Gyte, A. et al. (2006). Agouti-related protein is posttranslationally cleaved by proprotein convertase 1 to generate agouti-related protein (AGRP)83-132: interaction between AGRP83-132 and melanocortin receptors cannot be influenced by syndecan-3. Endocrinology *147*, 1621-1631.

Creutzfeldt, H.G. (1920). Über eine eigenartige herdförmige Erkrankung des Zentralnervensystems. Vorläufige Mitteilung. Zeitschrift für die gesamte Neurologie und Psychiatrie, *57*: 1-18.

Cropley, J.E., Suter, C.M., Beckman, K.B., and Martin, D.I. (2006). Germ-line epigenetic modification of the murine Avy allele by nutritional supplementation. Proc. Natl. Acad. Sci. U. S. A. *103*, 17308-17312.

DeArmond, A.J., Ironside, J.W., Bouzamondo-Bernstein, E., Peretz, D., and Frazer, J.R. (2004). Neuropathology of Prion Disease. In S.B. Prusiner (ed.) *Prion Biology and Diseases*, 2nd edition. Cold Spring Harbor USA, Cold Spring Harbor Laboratory Press. p. 777-856.

Deinhardt, K., Salinas, S., Verastegui, C., Watson, R., Worth, D., Hanrahan, S., Bucci, C., and Schiavo, G. (2006). Rab5 and Rab7 control endocytic sorting along the axonal retrograde transport pathway. Neuron. *52*: 293-305.

Derrington, E., Gabus, C., Leblanc, P., Chnaidermann, J., Grave, L., Dormont, D., Swietnicki, W., Morillas, M., Marck, D., Nandi, P., and Darlix, J.L. (2002). PrPC has nucleic acid chaperoning properties similar to the nucleocapsid protein of HIV-1. C. R. Biol. *325*:17-23.

Deshaies, R.J., and Joazeiro, C.A. (2009). RING domain E3 ubiquitin ligases. Annu. Rev. Biochem. *78*, 399-434.

Dove, S.K., Dong, K, Kobayashi, T., Williams, F.K., and Michell, R.H. (2009). Phosphatidylinositol 3,5-biphosphate and Fab1p/PIKfyve underpin endo-lysosome function. Biochem. J. *419*: 1-13.

Doyotte, A., Russell, M.R., Hopkins, C.R., and Woodman, P.G. (2005). Depletion of TSG101 forms a mammalian "Class E" compartment: a multicisternal early endosome with multiple sorting defects. J. Cell Sci. *118*:3003-17.

Duex, J.E., Nau, J.J., Kauffman, E.J., and Weisman, L.S. (2006). Phosphoinositide 5-phosphatase Fig 4p is required for both acute rise and subsequent fall in stress-induced phosphatidylinositol 3,5-bisphosphate levels. Eukaryot Cell *5*: 723–31.

Duhl, D.M., Vrieling, H., Miller, K.A., Wolff, G.L., and Barsh, G.S. (1994). Neomorphic agouti mutations in obese yellow mice. Nat. Genet. *8*, 59-65.

Duke-Cohan, J.S., Morimoto, C., Rocker, J.A., and Schlossman, S.F. (1995) A novel form of dipeptidylpeptidase found in human serum. J. Biol. Chem. *270:* 14107-14114.

Duke-Cohan, J.S., Gu, J., McLaughlin, D.F., Xu, Y., Freeman, G.J., and Schlossman, S.F. (1998). Attractin (DPPT-L), a member of the CUB family of cell adhesion and guidance proteins, is secreted by activated human T lymphocytes and modulates immune cell interactions. Proc. Natl. Acad. Sci. U. S. A. *95*, 11336-11341.

Dunn, R. and Hicke, L. (2001). Domains of the Rsp5 ubiquitin-protein ligase required for receptor-mediated and fluid-phase endocytosis. Mol. Biol. Cell. *12*:421-35.

Eberle, A. (1988). *The melanotropins: chemistry, physiology and mechanism of action*. New York, S Karger Publishing.

Erdmann, G., Schutz, G., and Berger, S. (2007). Inducible gene inactivation in neurons of the adult mouse forebrain. BMC Neurosci. *8*:63.

Erlich, P., Dumestre-Pérard, C., Ling, W.L., Lemaire-Vieille, C., Schoehn, G., Arlaud, G.J.,Thielens, N.M., Gagnon, J., and Cesbron, J.Y. (2010). Complement protein C1q forms a complex with cytotoxic prion protein oligomers. J Biol Chem. *285*:19267-76.

Eskelinen, E.L. (2005). Maturation of autophagic vacuoles in mammalian cells. Autophagy *1:*1-10.

Fang, Y., Wu, N., Gan, X., Yan, W., Morrell, J.C., Gould, S.J. (2007). Higher-order oligomerization targets plasma membrane proteins and HIV gag to exosomes. PLoS Biol. *5*:e158.

Feil, R., Wagenr, J., Metzger,D. and Chambon, P. (1997).Regulation of Cre recombinase activity by mutated estrogen receptor ligand-binding domains. Biochem. Biophys. Res. Commun. *237*: 752-7.

Ferguson, C.J., Lenk, G.M., and Meisler, M.H. (2009). Defective autophagy in neurons and astrocytes from mice deficient in PI(3,5)P2. Hum. Mol. Genet.*18*:4868-78.

Fevrier, B., Vilette, D., Archer, F., Loew, D., Faigle, W., Vidal, M., Laude, H., and Raposo, G. (2004). Cells release prions in association with exosomes. Proc. Natl. Acad. Sci. USA. *101*:9683-8.

Février, B., Vilette, D,, Laude, H., and Raposo, G. (2005). Exosomes: a bubble ride for prions? Traffic. *6:*10-17.

Fidler, I.J., (1975) Biological behavior of malignant melanoma cells correlated to their survival in vivo. Cancer Res. *35*:218-24.

Flechsig, J.C., Manson, R., Barron, A., Aguzzi, A., and Weismann, C. (2004). Knockouts, knockins, transgenics, and transplants in prion research. In S.B. Prusiner (ed.) *Prion Biology and Diseases*, 2nd edition. Cold Spring Harbor USA, Cold Spring Harbor Laboratory Press. p. 373-434.

Gabus, C., Derrington, E., Leblanc, P., Chnaiderman, J., Dormont, D., Swietnicki, W., Morillas, M., Surewicz, W.K., Marc, D., Nandi, P., Darlix, J.L. (2001a). The prion protein has RNA binding and chaperoning properties characteristic of nucleocapsid protein NCP7 of HIV-1. J. Biol. Chem. *276*:19301-9.

Gabus, C., Auxilien, S., Péchoux, C., Dormont, D., Swietnicki, W., Morillas, M., Surewicz, W., Nandi, P., and Darlix, J.L. (2001b). The prion protein has DNA strand transfer properties similar to retroviral nucleocapsid protein. J. Mol. Biol. *307*:1011-21.

Garcia-Borron, J.C., Sanchez-Laorden, B.L., and Jimenez-Cervantes, C. (2005). Melanocortin-1 receptor structure and functional regulation. Pigment Cell Res. *18*, 393-410.

Garrus, J.E., von Schwedler, U.K., Pornillos, O.W., Morham, S.G., Zavitz, K.H., Wang H.E., Wettstein, D.A., Stray, K.M., Cote, M., Rich, R.L., Myszka, D.G., and Sundquist, W.I. (2001). Tsg101 and the vacuolar protein sorting pathway are essential for HIV-1 budding. Cell *107*:55-65.

Ghosh, P., Dahms, N.M., and Kornfeld, S. (2003). Mannose 6-phosphate receptors: new twists in the tale, Nat. Rev. Mol. Cell Biol. *4*:202–212.

Goldfarb, L.G., Petersen, R.B., Tabaton, M., Brown, P., LeBlanc, A.C., Montagna, P., Cortelli, P., Julien, J., Vital, C., Pendelbury, W.W., *et al.* (1992). Fatal familial insomnia and familial Creutzfeldt-Jakob disease: disease phenotype determined by a DNA polymorphism. Science *258:*806-808.

Goldwater, P.N., and Paton, J.C. (1989) Apparent non-involvement of prions in the pathogenesis of spongiform change in HIV-infected brain. J. Neuropathol. Exp. Neurol. *48*:184-6.

Gomez-Lucia, E. (2005).The other transmissible spongiform encephalopathies. Rev Neurosci. *16*:159-79.

Gomi, H., Ikeda, T., Kunieda, T., Itohara, S., Prusiner, S.B., and Yamanouchi, K. (1994). Prion protein (PrP) is not involved in the pathogenesis of spongiform encephalopathy in zitter rats. Neurosci. Lett. *166:*171-4.

Gomi, H., Ueno, I., and Yamanouchi, K. (1994). Antioxidant enzymes in the brain of zitter rats: abnormal metabolism of oxygen species and its relevance to

pathogenic changes in the brain of zitter rats with genetic spongiform encephalopathy. Brain Res. *653*:66-72.

Gould, C.M., Diella, F., Via, A., Puntervoll, P., Gemund, C., Chabanis-Davidson, S., Michael, S., Sayadi, A., Bryne, J.C., Chica, C., Seiler, M., Davey, N.E., Haslam, N., Weatheritt, R.J., Budd, A., Hughes, T., Pas, J., Rychlewski, L., Travé, G., Aasland, R., Helmer-Citterich, M., Linding, R., and Gibson, T.J. (2010). ELM: the status of the 2010 eukaryotic linear motif resource Nucleic Acids Research *38:* (Database issue):D167-D180

Gould, S.J., Booth, A.M., and Hildreth, J.E. (2003).The Trojan exosome hypothesis. Proc. Natl. Acad. Sci. USA. *100*:10592-7.

Gravel, C., Kay, D.G., and Jolicoeur,P. (1993). Identification of the infected target cell type in spongiform myeloencephalopathy induced by the Cas-Br-E murine leukemia virus. J. Virol. *67:* 6648-6658.

Gropp, E., Shanabrough, M., Borok, E., Xu, A.W., Janoschek, R., Buch, T., Plum, L., Balthasar, N., Hampel, B., Waisman, A., Barsh, G.S., Horvath, T.L., and Brüning, J.C. (2005) Agouti-related peptide-expressing neurons are mandatory for feeding. Nature Neuroscience *8:*1289-91.

Guignot, J., Caron, E., Beuzón, C., Bucci, C., Kagan, J., Roy, C., and Holden, D.W. (2004). Microtubule motors control membrane dynamics of Salmonella-containing vacuoles. J. Cell Sci. *117*:1033-45.

Gunn, T.M., Inui, T., Kitada, K., Ito, S., Wakamatsu, K., He, L., Bouley, D.M., Serikawa, T., and Barsh, G.S. (2001). Molecular and phenotypic analysis of Attractin mutant mice. Genetics *158*, 1683-1695.

Gunn, T.M., Miller, K.A., He, L., Hyman, R.W., Davis, R.W., Azarani, A., Schlossman, S.F., Duke-Cohan, J.S., and Barsh, G.S. (1999). The mouse mahogany locus encodes a transmembrane form of human attractin. Nature *398*, 152-156.

Gurevich, V.V. and Gurevich, E.V. (2008). GPCR monomers and oligomers: it takes all kinds. Trends Neurosci. *31*:74-81.

Gydesen, S., Brown, J.M., Brun, A., *et al*. (2002). Chromosome 3 linked frontotemporal dementia (FTD-3). Neurology *59*:1585–94.

Haqq, A.M., Rene, P., Kishi, T., Khong, K., Lee, C.E., Liu, H., Friedman, J.M., Elmquist, J.K., and Cone, R.D. (2003). Characterization of a novel binding partner of the melanocortin-4 receptor: attractin-like protein. Biochem. J. *376*, 595-605.

Harikumar, K.G., Morfis, M.M., Sexton, P.M., and Miller, L.J. (2008). Pattern of intra-family hetero-oligomerization involving the G-protein-coupled secretin receptor. J. Mol. Neurosci. *36*: 279-85.

Harris, D.A., Peters, P.J.,Taraboulos, A., Lingappa, V., DeArmond, S.J., and Prusiner, S.B. (2004). Cell Biology of Prions. In S.B. Prusiner (ed.) *Prion Biology and Diseases,* 2nd edition. Cold Spring Harbor USA, Cold Spring Harbor Laboratory Press. p. 483-544.

He, L., Gunn, T.M., Bouley, D.M., Lu, X.Y., Watson, S.J., Schlossman, S.F., Duke-Cohan, J.S., and Barsh, G.S. (2001). A biochemical function for attractin in agouti-induced pigmentation and obesity. Nat. Genet. *27*, 40-47.

He, L., Lu, X.Y., Jolly, A.F., Eldridge, A.G., Watson, S.J., Jackson, P.K., Barsh, G.S., and Gunn, T.M. (2003). Spongiform degeneration in mahoganoid mutant mice. Science *299*, 710-712.

Hicke, L., and Riezman, H. (1996). Ubiquitination of a yeast plasma membrane receptor signals its ligand-stimulated endocytosis. Cell. *26*:277-87.

Hida, T., Wakamatsu, K., Sviderskaya, E.V. et al. (2009). Agouti protein, mahogunin, and attractin in pheomelanogenesis and melanoblast-like alteration of melanocytes: a cAMP-independent pathway. Pigment Cell. Melanoma Res. *22*, 623-634.

Hislop, J.N., Marley, A., and von Zastrow, M. (2004.) Role of mammalian vacuolar protein-sorting proteins in endocytic trafficking of a nonubiquitinated G protein-coupled receptor to lysosomes. J. Biol. Chem. *279*: 22522–31.

Hollander, W.F., and Gowen, J.W. (1956) An extreme non-agouti mutant in the mouse. J. Hered. *47*: 221-224.

Hsiao, K., Baker, H.F., Crow, T.J., Poulter, M., Owen, F., Terwilliger, J.D., Westaway, D., Ott, J., and Prusiner S.B. (1989) Linkage of a prion protein misense cariant to Gerstmann-Straussler syndrome. Nature *338*: 342-345.

Hu, W., Kieseier, B., Frohman, E., Eagar, T.N., Rosenberg, R.N., Hartung, H.P., and Stüve, O. (2008). Prion proteins: physiological functions and role in neurological disorders. J. Neurol. Sci. *264*:1-8.

Hu, W., Rosenberg, R.N., and Stüve, O. (2007). Prion proteins: a biological role beyond prion diseases. Acta Neurol. Scand. *116*:75-82.

Hunt, G., and Thody, A.J. (1995). Agouti protein can act independently of melanocyte-stimulating hormone to inhibit melanogenesis. J. Endocrinol. *147*, R1-4.

Hurley, J.H. and Emr, S.D. (2006). The ESCRT complexes: structure and mechanism of a membrane-trafficking network. Annu. Rev. Biophys. Biomol. Struct. *35*:277-98.

Ikonomov, O.C., Sbrissa, D., Shisheva, A. (2001). Mammalian cell morphology and endocytic membrane homeostasis require enzymatically active phosphoinositide 5-kinase PIKfyve. J. Biol. Chem. *276*:26141-7.

Indra, A.K., Warot, X., Brocard, J., Bornert, J.M., Xiao, J.H., Chambon, P., Metzger, D. (1999). Temporally controlled site-specific mutagenesis in the basal later of the epidermis: comparison of the recombinase activity of the tamoxifen-inducible Cre-ER(T) and Cre-ER(T2) recombinases. Nucleic Acids Res. *27*:4324-4327.

Jackson, I.J., Budd, P.S., Keighren, M., and McKie, L. (2007). Humanized MC1R transgenic mice reveal human specific receptor function. Hum. Mol. Genet. *16*, 2341-2348.

Jakob, A., (1921). Über eigenartige Erkrankungen des Zentralnervensystems mit bemerkenswertem anatomischen Befunde (spastische Pseudosklerose-Encephalomyelopathie mit disseminierten Degenerationsherden). Zeitschrift für die gesamte Neurologie und Psychiatrie, *64*: 147-228.

Jalink, K. and Moolenaar W.H. (2010). G protein-coupled receptors: the inside story. Bioessays. 32:13-6.

Jeong, B-H., Lee, Y-J., Carp, R.I., and Kim, Y-S. (2010). The prevalence of endogenous retroviruses in cerebrospinal fluids from patients with sporadic Creutzfeldt-Jakob disease. Journal of Clinical Virology *47:* 136-142.

Jiao, J., Sun, K., Walker, W.P., Bagher, P., Cota, C.D., and Gunn, T.M. (2009a). Abnormal regulation of TSG101 in mice with spongiform neurodegeneration. Biochim. Biophys. Acta *1792*, 1027-1035.

Jiao, J., Kim, H.Y., Liu, R.R., Hogan, C.A., Sun, K., Tam, L.M., and Gunn, T.M. (2009b). Transgenic analysis of the physiological functions of Mahogunin Ring Finger-1 isoforms. Genesis *47*, 524-534.

Jin, N., Chow, C.Y., Liu, L., Zolov, S.N., Bronson, R., Davisson, M., Petersen, J.L., Zhang, Y., Park, S., Duex, J.E., Goldowitz, D., Meisler, M.H., and Weisman, L.S. (2008). VAC14 nucleates a protein complex essential for the acute

interconversion of PI3P and PI(3,5)P(2) in yeast and mouse. EMBO J. *27*:3221-34.

Jolicoeur, P., Masse, G., and Kay, D.G. (1996). The prion protein gene is dispensable for the development of spongiform myeloencephalopathy induced by the neurovirulent Cas-Br-E murine leukemia virus. J. Virol. *70*: 9031-4.

Kanetsky, P.A., Swoyer, J., Panossian, S., Holmes, R., Guerry, D., and Rebbeck, T.R. (2002). A polymorphism in the agouti signaling protein gene is associated with human pigmentation. Am. J. Hum. Genet. *70*, 770-775.

Katzmann, D.J., Odorizzi, G., and Emr, S.D. (2002). Receptor downregulation and multivesicular-body sorting. Nat. Rev. Mol. Cell Biol. 3, 893–905.

Kerns, J.A., Newton, J., Berryere, T.G., Rubin, E.M., Cheng, J.F., Schmutz, S.M., and Barsh, G.S. (2004). Characterization of the dog Agouti gene and a nonagouti mutation in German Shepherd Dogs. Mamm. Genome *15*, 798-808.

Kim, B.Y., Olzmann, J.A., Barsh, G.S., Chin, L.S., and Li, L. (2007). Spongiform neurodegeneration-associated E3 ligase Mahogunin ubiquitylates TSG101 and regulates endosomal trafficking. Mol. Biol. Cell *18*, 1129-1142.

Kim, Y-O., Park, S-J., Balaban, R.S., Nirenberg, M., and Kim, Y. (2004). A functional genomic screen for cardiogenic genes using RNA interference in developing *Drosophila* embryos. PNAS *101*:159-164.

Kingsley, E.P., Manceau, M., Wiley, C.D., and Hoekstra, H.E. (2009). Melanism in *peromyscus* is caused by independent mutations in *agouti*. PLoS One *4*, e6435.

Kingston, R.E., Chen, C.A., and Rose, J.K. (2003). Calcium phosphate transfection. Curr. Protoc. Mol. Biol. 2003;Chapter 9:Unit 9.1.

Klungland, H., and Vage, D.I. (2003). Pigmentary switches in domestic animal species. Ann. N. Y. Acad. Sci. *994*, 331-338.

Kondo, A., Nagara, H., Akizawa, K., Tateishi, J., Serikawa, T. and Yamada, J. (1991). CNS pathology in the neurological mutant rats zitter, tremor and zitter-tremor double mutant (spontaneously epileptic rats, SER). Brain, *114*: 979-999.

Kondo, A., Sato, Y., and Nagara, H. (1991). An ultrastructural study of oligodendrocytes in zitter rat: a new animal model for hypomyelination in the CNS. J. Neurocytol. *20*, 929-939.

Kondo, A., Sendoh, S., Akazawa, K., Sato, Y., and Nagara, H. (1992). Early myelination in zitter rat: morphological, immunocytochemical and morphometric studies. Brain Res. Dev. Brain Res. *67*, 217-228.

Kondo, A., Sendoh, S., Miyata, K., and Takamatsu, J. (1995). Spongy degeneration in the zitter rat: ultrastructural and immunohistochemical studies. J. Neurocytol. *24*, 533-544.

Krempler, A., Henry, M.D., Triplett, A.A., and Wagner, K-U. (2002). Targeted deletion of the *Tsg101* gene results in cell cycle arrest and G_1/S and p53-independent cell death. J. Biol. Chem. *277*, 43216-43223.

Krude, H., Biebermann, H., Luck, W., Horn, R., Brabant, G., and Gruters, A. (1998). Severe early-onset obesity, adrenal insufficiency and red hair pigmentation caused by POMC mutations in humans. Nat. Genet. *19*, 155-157.

Kuramoto, T., Kitada, K., Inui, T., Sasaki, Y., Ito, K., Hase, T., Kawagachi, S., Ogawa, Y., Nakao, K., Barsh, G.S., Nagao, M., Ushijima, T., and Serikawa T. (2001). Attractin/mahogany/zitter plays a critical role in myelination of the central nervous system. Proc. Natl. Acad. Sci. U S A. (2001). *98*, 559-564.

Kuwamura, M., Maeda, M., Kuramoto, T. Kitada, K., Kanehara, T., Moriyama, M., Nakane, Y., Yamate, J., Ushijima, T., Kotani, T., and Serikawa, T. (2002). The myelin vacuolation (mv) rat with a null mutation in the attractin gene. Lab. Invest. *82*, 1279-1286.

Laemmli, U. K (1970) Cleavage of structural proteins during the assembly of the head of bacteriophage T4. Nature *227*:680-5.

Lane, P.W. (1960). New Mutants. Mouse News Letter *22*, 35.

Lane, P.W., and Green, M.C. (1960). Mahogany, a recessive color mutation in linkage group V of the mouse. J. Hered. *51*, 228-230.

Larkin, M.A., Blackshields, G., Brown, N.P., Chenna, R., McGettigan, P.A., McWilliam, H. ,Valentin, F., Wallace, I.M., Wilm, A., Lopez, R., Thompson, J.D., Gibson, T.J., Higgins, D.G.. (2007). Clustal W and Clustal X version 2.0. Bioinformatics. *23*:2947-8.

Le Pape, E., Passeron, T., Giubellino, A., Valencia, J.C., Wolber, R., and Hearing, V.J. (2009). Microarray analysis sheds light on the dedifferentiating role of agouti signal protein in murine melanocytes via the Mc1r. Proc. Natl. Acad. Sci. U. S. A. *106*, 1802-1807.

Le Pape, E., Wakamatsu, K., Ito, S., Wolber, R., and Hearing, V.J. (2008). Regulation of eumelanin/pheomelanin synthesis and visible pigmentation in melanocytes by ligands of the melanocortin 1 receptor. Pigment Cell. Melanoma Res. *21*, 477-486.

Leblanc, P., Baas, D., and Darlix, J.L. (2004). Analysis of the interactions between HIV-1 and the cellular prion protein in a human cell line. J. Mol. Biol. *337*:1035-51.

LeBlanc, P., Alais, S., Porto-Carreiro, I.P., Lehmann, S., Grassi, J., Raposo, G., and Darlix, J.L. (2006). Retrovirus infection strongly enhances scrapie infectivity release in cell culture. EMBO J. *25*:2674-85.

Lee, J-A., Beigneux, A., Ahmad, S.T., Young, S. G., and Gao, F-B. (2007) ESCRT-III dysfunction causes autophagosome accumulation and neurodegeneration. Current Biology *17:* 1561-67.

Lee, J-A. and Gao, F-B. (2008) Roles of ESCRT in autophagy-associated neurodegeneration. Autophagy *4:* 230-32.

Lee, J-A., Liu, L., and Gao, F-B. (2009) Autophagy defects contribute to neurodegeneration induced by dysfunctional ESCRT-III. Autophagy *5:* 1070-72.

Leighton, P.A., Mitchell, K.J., Goodrich, L.V., Lu, X., Pinson, K., Scherz, P., Skarnes, W.C., and Tessier-Lavigne, M.. (2001). Defining brain wiring patterns and mechanisms through gene trapping in mice. Nature.*410*:174-9.

Letunic, I., Doerks, T., and Bork, P. (2009) SMART 6: recent updates and new developments. Nucleic Acids Res. 37:D229-32.

Levy, C., Khaled, M., and Fisher, D.E. (2006). MITF: master regulator of melanocyte development and melanoma oncogene. Trends Mol. Med. *12*, 406-414.

Li, L., and Cohen, S.N. (1996). Tsg101: a novel tumor susceptibility gene isolated by controlled homozygous functional knockout of allelic loci in mammalian cells. Cell *85*: 319-329.

Li, W., and Ye, Y. (2008). Polyubiquitin chains: functions, structures, and mechanisms. Cell Mol. Life Sci. *65*, 2397-2406.

Liberski, P.P. (2004). Spongiform change – an electron microscopic view. Folia Neuropath. *42* Supplement B: 59-70.

Liberski P.P., and Brown, P. (2004). Kuru: a half-opened window onto the landscape of neurodegenerative diseases. Folia Neuropathol. *42* Supplement A:3-14.

Liberski, P.P., Sikorska, B., Hauw, J-J., Kopp, N., Streichenberger, N., Giraud, P., Budka, H., Boellaard, J.W., and Brown, P. (2008). Tubulovesicular structures are a consistent (and unexplained) finding in the brains of humans with prion diseases. Virus Research *132:* 226-8.

Lotscher, M., Recher, M., Lang, K.S.,Navarini, A., Hunziker, L., Santimaria, R., Glatzel, M., Schwarz, P., Boni, J., and Zinkernagel, R.M. (2007). Induced prion protein controls immune-ctivated retroviruses in the mouse spleen. PLoS One *2:*e1158.

Lu, D., Willard, D., Patel, I.R., Kadwell, S., Overton, L., Kost, T., Luther, M., Chen, W., Woychik, R.P., and Wilkison, W.O. (1994). Agouti protein is an antagonist of the melanocyte-stimulating-hormone receptor. Nature *371,* 799-802.

Lucocq, J. and Walker, D. (1997). Evidence for fusion between multilamellar endosomes and autophagosomes in HeLa cells. Eur. J. Cell Biol. *72*: 307-13.

Lupas, A., Van Dyke, M., and Stock, J. (1991). Predicting Coiled Coils from Protein Sequences. Science *252*:1162-1164.

Luquet, S., Perez, F.A., Hnasko, T.S., and Palmiter, R.D. (2005). NPY/AgRP neurons are essential for feeding in adult mice but can be ablated in neonates. Science *310:*683-5.

Manuelidis, L., Sklaviadis, T., Akowitz., A., and Fritch, W. (1995). Viral particles are required for infection in neurodegenerative Creutzfeldt-Jakob disease. Proc.Natl. Acad. Sci. USA, *92*: 5124-5128.

Manuelidis, L., Yi, Z.-X., Banquero, N., and Mullins, B. (2007). Cells infected with scrapie and Creutzfeldt-Jakob disease produce intracellular 25-nm virus-like particles. Proc. Natl. Acad. Sci. USA *104*: 1965–1970.

Masters, C.L. and Richardson, E.P. Jr. (1978). Subacute spongiform encephalopathy (Creutzfeldt-Jakob disease). The nature and progression of spongiform change. Brain. *101*:333-44.

Masters, C.L., Harris, J.O., Gajdusek D.C., Gibbs, C.J. Jr.,Bernoulli, C., and Asher, D.M. (1978). Creutzfeldt-Jakob disease: patters of worldwide occurrence and the significance of familial and sporadic clustering. Ann. Neurolo.*5*:177-88.

McKinley, M.P., Bolton, D.C., and Prusiner, S.B. (1983). A protease-resistant protein is a structural component of the scrapie prion. Cell *35:* 57-62.

Miaczynska, M. and Bar-Sagi, D. (2010). Signaling endosomes: seeing is believing. Curr Opin Cell Biol. Electronically published ahead of print, June 8 2010.

Millar, S.E., Miller, M.W., Stevens, M.E., and Barsh, G.S. (1995). Expression and transgenic studies of the mouse agouti gene provide insight into the mechanisms by which mammalian coat color patterns are generated. Development *121*, 3223-3232.

Miller, K.A., Gunn, T.M., Carrasquillo, M.M., Lamoreux, M.L., Galbraith, D.B., and Barsh, G.S. (1997). Genetic studies of the mouse mutations mahogany and mahoganoid. Genetics *146*, 1407-1415.

Miller, M.W., Duhl, D.M., Vrieling, H., Cordes, S.P., Ollmann, M.M., Winkes, B.M., and Barsh, G.S. (1993). Cloning of the mouse agouti gene predicts a secreted protein ubiquitously expressed in mice carrying the lethal yellow mutation. Genes Dev. *7*, 454-467.

Milligan, G. (2007). G protein-coupled receptor dimerisation: molecular basis and relevance to function. Biochim. Biophys. Acta. *1768*:825-35.

Moestrup, SK., Kozyraki, R., Kristiansen, M., Kaysen, J.H., Rasmussen, H.H., Brault, D., Pontillon , F., Goda, F.O., Christensen, E.I., Hammond, T.G., and Verroust, P.J. (1998). The intrinsic factor-vitamin B12 receptor and target of teratogenic antibodies is a megalin-binding peripheral membrane protein with homology to developmental proteins. J. Biol. Chem. *273*:5235-42.

Moore, C.A., Milano, S.K., and Benovic, J.L. (2007). Regulation of receptor trafficking by GRKs and arrestins. Annu Rev Physiol.*69*: 451-82.

Morgan, H.D., Sutherland, H.G., Martin, D.I., and Whitelaw, E. (1999). Epigenetic inheritance at the agouti locus in the mouse. Nat. Genet. *23*, 314-318.

Moscardini, M., Pistello, M., Bendinelli, M., Ficheux, D., Miller, J.T., Gabus, C., Le Grice, S.F., Surewicz, W.K., and Darlix, J.L. (2002). Functional interactions of nucleocapsid protein of feline immunodeficiency virus and cellular prion protein with the viral RNA. J. Mol. Biol. *318*:149-59.

Mouse Genome Sequencing Consortium. (2002). Initial sequencing and comparative analysis of the mouse genome. Nature *420:*520-62.

Moustafa, M., Szabo, M., Ghanem, G.E., Morandini, R., Kemp, E.H., MacNeil, S. et al. (2002) Inhibition of tumor necrosis factor-alpha stimulated NFkappaB/p65 in human keratinocytes by alpha-melanocyte stimulating hormone and adrenocorticotropic hormone peptides. J Invest Dermatol *119*:1244–53.

Muto, Y. and Sato, K. (2003) Pivotal role of attractin in cell survival under oxidative stress in the zitter rat brain with genetic spongiform encephalopathy. Brain Res. Mol. Brain Res. *111*:111-22.

Nagle, D.L., McGrail, S.H., Vitale, J. et al. (1999). The mahogany protein is a receptor involved in suppression of obesity. Nature *398*, 148-152.

Nakadate, K., Noda, T., Sakakibara, S., Kumamoto, K., Matsuura, T., Joyce, J.N., and Ueda, S. (2006). Progressive dopaminergic neurodegeneration of substantia nigra in the zitter mutant rat. Acta Neuropathol. *112*:64-73.

Nakadate, K., Sakakibara, S., and Ueda, S. (2008). Attractin/mahogany protein expression in the rodent central nervous system. J Comp Neurol. *508*:94-111

Nandi, D., Tahiliani, P., Kumar, A., and Chandu, D. (2006). The ubiquitin-proteasome system. J. Biosci. *31*, 137-155.

Nguyen, D.G., Booth, A., Gould, S.J., and Hildreth, J.E. (2003). Evidence that HIV budding in primary macrophages occurs through the exosome release pathway. J Biol Chem. *278*:52347-54.

Odorizzi, G., Babst, M., and Emr, S.D. (1998). Fab1p PtdIns(3)P 5-kinase function is essential for protein sorting in the multivesicular body. Cell. *95*:847-58.

Odorizzi, G., Babst, M., and Emr, S.D. (2000). Phosphoinositide signaling and the regulation of membrane trafficking in yeast. Trends Biochem Sci. *25*: 229-35.

Ollmann, M.M., and Barsh, G.S. (1999). Down-regulation of melanocortin receptor signaling mediated by the amino terminus of Agouti protein in Xenopus melanophores. J. Biol. Chem. *274*: 15837-15846.

Ollmann, M.M., Lamoreux, M.L., Wilson, B.D., and Barsh, G.S. (1998). Interaction of Agouti protein with the melanocortin 1 receptor in vitro and in vivo. Genes Dev. *12:* 316-330.

Ollmann, M.M., Wilson, B.D., Yang, Y.K., Kerns, J.A., Chen, Y., Gantz, I., and Barsh, G.S. (1997). Antagonism of central melanocortin receptors in vitro and in vivo by agouti-related protein. Science *278*, 135-138.

Ookohchi T, Ito H, Serikawa T, Sato K. Detection of apoptosis in the brain of the zitter rat with genetic spongiform encephalopathy. Biochem Mol Biol Int. 1997Feb;41(2):279-84.

Osiecka, K.M., Nieznanska, H., Skowronek, K.J., Karolczak, J., Schneider, G., and Nieznanski, K. (2009). Prion protein region 23-32 interacts with tubulin and inhibits microtubule assembly. Proteins *77*:279-96.

Parameswaran, N., and Spielman, W.S. (2006). RAMPs: the past, present and future. Trends Biochem. Sci. *31*:631-8.

Paz, J., Yao, H., Lim, H.S., Lu, X.Y., and Zhang, W. (2007). The neuroprotective role of attractin in neurodegeneration. Neurobiol. Aging. *28*:1446-56.

Peden, A.H., and Ironside, J.W. (2004) Review: pathology of variant Creutzfeldt-Jakob disease. Folia Neuropathologica Suppl. A, 85-91.

Pello, O.M., Martínez-Muñoz, L., Parrillas, V., Serrano, A., Rodríguez-Frade, J.M., Toro, M.J., Lucas, P., Monterrubio, M., Martínez, A.C., and Mellado, M. (2008). Ligand stabilization of CXCR4/delta-opioid receptor heterodimers reveals a mechanism for immune response regulation. Eur J Immunol. *38*:537-49.

Perez-Oliva, A.B., Olivares, C., Jiménez-Cervantes, C.,, García-Borrón, J.C., (2009). Mahogunin ring finger-1 (MGRN1) E3 ubiquitin ligase inhibits signaling from melanocortin receptor by competition with Galphas. J. Biol. Chem. *284*, 31714-31725.

Petrakis, S and Sklaviadis, T. (2006). Identification of proteins with hig affinity for refolded and native PrP^{C}. Proteomics *6:* 6476-84.

Phan, L.K., Lin, F., LeDuc, C.A., Chung, W.K., and Leibel, R.L. (2002). The mouse mahoganoid coat color mutation disrupts a novel C3HC4 RING domain protein. J. Clin. Invest. *110*, 1449-1459.

Phillips, R.J.S. (1963). New mutant: non-agouti curly. Mouse News Letter *29*, 38.

Pierce, A.A. and Xu, A.W. (2010). De novo neurogenesis in adult hypothalamus as a compensatory mechanism to regulate energy balance. J. Neurosci. *30*:723-30.

Pornillos O, Higginson DS, Stray KM, Fisher RD, Garrus JE, Payne M, He GP, Wang HE, Morham SG, and Sundquist WI. (2003) HIV Gag mimics the Tsg101-recruiting activity of the human Hrs protein. J Cell Biol. 162:425-34.

Prusiner, S.B., Scott, M.R., DeArmond, S.J. and Carlson, G. (2004a). Transmission and replication of prions. In S.B. Prusiner (ed.) *Prion Biology and Diseases*, 2nd edition. Cold Spring Harbor USA, Cold Spring Harbor Laboratory Press. p. 187-242.

Prusiner, S.B., Williams, E., Laplanche, J-L., and Shinagawa, M. (2004b). Scrapie, Chronic Wasting Disease, and Transmissable mink encephalopathy. In S.B. Prusiner (ed.) *Prion Biology and Diseases*, 2nd edition. Cold Spring Harbor USA, Cold Spring Harbor Laboratory Press. p. 545-594.

Puntervoll, P., Linding, R., Gemünd, C., Chabanis-Davidson, S., Mattingsdal, M., Cameron, S., Martin, D.M., Ausiello, G., Brannetti, B., Costantini, A., Ferrè, F., Maselli, V., Via, A., Cesareni, G., Diella, F., Superti-Furga, G., Wyrwicz, L.,

Ramu, C., McGuigan, C., Gudavalli, R., Letunic, I., Bork, P., Rychlewski, L., Küster, B., Helmer-Citterich, M., Hunter, W.N., Aasland, R., and Gibson, T.J. (2003). ELM server: A new resource for investigating short functional sites in modular eukaryotic proteins. Nucleic Acids Res. 31:3625–3630.

Raymond, C.K., Howald-Stevenson, I., Vater, C.A., and Stevens, T.H. (1992). Morphological classification of the yeast vacuolar protein sorting mutants: evidence for a prevacuolar compartment in class E *vps* mutants. Mol Biol Cell. *3*:1389-402.

Rehm, S., Mehraein, P., Anzil, A.P., and Deerberg, F. (1982). A new rat mutant with defective overhairs and spongy degeneration of the central nervous system: clinical and pathologic studies. Lab. Anim. Sci. *32*:70-3.

Rieder, S.E., Banta, L.M., Kohrer, K., McCaffery, J.M., and Emr, S.D. (1996). Multilamellar endosome-like compartment accumulates in the yeast *vps28* vacuolar protein sorting mutant. Mol. Biol. Cell. *7*: 985-999.

Robbins, L.S., Nadeau, J.H., Johnson, K.R., Kelly, M.A., Roselli-Rehfuss, L., Baack, E., Mountjoy, K.G., and Cone, R.D. (1993). Pigmentation phenotypes of variant extension locus alleles result from point mutations that alter MSH receptor function. Cell *72*, 827-834.

Roberts, D.W., Newton, R.A., and Sturm, R.A. (2007). MC1R expression in skin: is it confined to melanocytes? J. Invest. Dermatol. *127*:2472-3.

Romero, A., Romão, M.J., Varela, P.F., Kölln, I., Dias, J.M., Carvalho, A.L., Sanz, L., Töpfer-Petersen, E., and Calvete, J.J. (1997). The crystal structures of two spermadhesins reveal the CUB domain fold. Nat. Struct. Biol. *4*:783-8.

Rouzaud, F., Annereau, J.P., Valencia, J.C., Costin, G.E., andHearing, V.J. (2003). Regulation of melanocortin 1 receptor expression at the mRNA and protein levels by its natural agonist and antagonist. FASEB J. *17*, 2154-2156.

Rouzaud, F.,Costin G.E., Yamaguchi Y., Valencia, J. C., Chen, K., Bohm, M., Abdel-Malek A.A., and Hearing, V.J. (2004). Expression patterns of two MC1R Isoforms in human Melanocytes and skin of various Pigmentation/Ethnic origin upon stimulation by MSH/UVR. Pigment Cell Research *17:*431.

Rouzaud, F., Costin, G.E., Yamaguchi, Y., Valencia, J.C., Berens, W.F., Chen, K.G. et al. (2006). Regulation of constitutive and UVR-induced skin pigmentation by melanocortin 1 receptor isoforms. FASEB J. *20*:1927–9

Ruland, J., Sirard, C., Elia, A., MacPherson, D., Wakeham, A., Li, L., Luis, D.L.P., Cohen, S.N., and Mak, T.W. (2001). P53 accumulation, defective cell

proliferation, and early embryonic lethality in mice lacking TSG101. Proc. Nat. Acad. Sci. USA *98*: 1859-1864.

Rutherford, A.C., Traer, C., Wassmer, T., Pattni, K., Bujny, M.V., Carlton, J.G., Stenmark, H., and Cullen, P.J. (2006). The mammalian phosphatidylinositol 3-phosphate 5-kinase (PIKfyve) regulates endosome-to-TGN retrograde transport. J. Cell Sci. *119*:3944-57.

Sakai, C., Ollmann, M., Kobayashi, T., Abdel-Malek, Z., Muller, J., Vieira, W.D., Imokawa, G., Barsh, G.S., and Hearing, V.J. (1997). Modulation of murine melanocyte function in vitro by agouti signal protein. EMBO J. *16*, 3544-3552.

Saksena, S., Sun, J., Chu, T., and Emr, S.D. (2007). ESCRTing proteins in the endocytic pathway. Trends Biochem. Sci. *32*, 561-573.

Salazar-Onfray, F., Lopez, M., Lundqvist, A., Aguirre, A., Escobar, A., Serrano, A. et al. (2002). Tissue distribution and differential expression of melanocortin 1 receptor, a malignant melanoma marker. Br. J. Cancer *87*:414–22

Sanchez, M.J., Olivares, S.C., Ghanem, G., Haycock, J., Lozano Teruel, J.A., Garcia-Borron, J.C., and Jimenez-Cervantes, C. (2002). Loss of function variants of the human melanocortin-1-receptor gene in melanoma cells define structural determinants of receptor function. Eur. J. Biochem. *269*: 6133-41.

Sanchez-Mas, J., Hahmann, C., Gerritsen, I., Garcia-Borron, J.C., and Jimenez-Cervantes, C. (2004). Agonist-independent, high constitutive activity of the human melanocortin 1 receptor. Pigment Cell Res. *17*, 386-395.

Sanchez-Mas, J., Guillo, L.A., Zanna, P., Jimenez-Cervantes, C., and Garcia-Borron, J.C. (2005). Role of G Protein-coupled receptor kinases in the homologous desensitization of the human and mouse melanocortin 1 receptors. Mol. Endocrin. *19*: 1035-48.

Satoh, J., Obayashi, S., Misawa, T., Sumiyoshi, K., Oosumi, K., Tabunoki, H. (2009). Protein microarray analysis identifies human cellular prion protein interactors. Neuropathol Appl Neurobiol. *35*: 16-35.

Schiöth, H.B., Kuusinen, A., Muceniece, R., Szardenings, M., Keinänen, K., and Wikberg, J.E. (1996). Expression of functional melanocortin 1 receptors in insect cells. Biochem. Biophys. Res. Commun. *221*:807-14.

Schultz, J., Milpetz, F., Bork, P., and Ponting, C.P. (1998). SMART, a simple modular architecture research tool: Identification of signaling domains. Proc. Nat. Acad. Sci. (USA) 95: 5857-64.

Sharov, A.A., Fessing, M., Atoyan, R., Sharova, T.Y., Haskell-Luevano, C., Weiner, L., Funa, K., Brissette, J.L., Gilchrest, B.A., and Botchkarev, V.A. (2005). Bone morphogenetic protein (BMP) signaling controls hair pigmentation by means of cross-talk with the melanocortin receptor-1 pathway. Proc. Natl. Acad. Sci. U. S. A. *102*, 93-98.

Sheehan, D., and Hrapchak, B. Theory and practice of histotechnology, 2nd edition, 1980, pp262-4, Battelle Press, Ohio.

Sherer, N.M., Lehmann, M.J., Jimenez-Soto, L.F., Ingmundson, A., Horner, S.M., Cicchetti, G., Allen, P.G., Pypaert, M., Cunningham, J.M., and Mothes, W. (2003). Visualization of retroviral replication in living cells reveals budding into multivesicular bodies. Traffic. *4*:785-801.

Shiratori, H. and Hamada, H. (2006). The left–right axis in the mouse: From origin to morphology. Development 133:2095–2104.

Siegrist, W., Drozdz, R., Cotti, R., Willard, D.H., Wilkison, W.O., and Eberle, A.N. (1997). Interactions of alpha-melanotropin and agouti on B16 melanoma cells: evidence for inverse agonism of agouti. J. Recept. Signal Transduct. Res. *17*, 75-98.

Silva, J.L., Gomes, M.P., Vieira, T.C., and Cordeiro, Y. (2010). PrP interactions with nucleic acids and glycosaminoglycans in function and disease. Front. Biosci. *15*:132-50.

Silvers, W.K. (1979). *The Coat Colors of Mice.* New York, Springer Verlag.

Skibinski, G., Parkinson, N.J., Brown, J.M., Chakrabarti, L., Lloyd, S.L., Hummerich, H., Nielsen, J.E., Hodges, J.R., Spillantini, M.G., Thusgaard, T., Brandner, S., Brun, S., Rossor, M.N., Gade, A., Johannsen, P., Sorensen, S.A. Gydesen, S., Fisher, E.M., and Collinge, J. (2005). Mutations in the endosomal ESCRTIIIcomplex subunit CHMP2B in frontotemporal dementia, Nat. Genet. *37:* 806–808.

Sklaviadis, T.K., Manuelidis, L., and Manuelidis, E.E. (1989). Physical properties of the Creutzfeldt-Jakob disease agent. J. Virol. *63*:1212-22.

Slominski, A., Plonka, P.M., Pisarchik, A., Smart, J.L., Tolle, V., Wortsman, J., and Low, M.J. (2005). Preservation of eumelanin hair pigmentation in proopiomelanocortin-deficient mice on a nonagouti (a/a) genetic background. Endocrinology *146*, 1245-1253.

Slominski, A., Wortsman, J., Luger, T., Paus, R., and Solomon, S. (2000). Corticotropin releasing hormone and proopiomelanocortin involvement in the cutaneous response to stress. Physiol. Rev. *80,* 979-1020.

Soriano, P. (1999) Generalized lacZ expression with the ROSA26 Cre reporter strain. Nat. Genet. *21*:70-71.

Stengal, A., Bach, C., Vorberg, I., Frank, O., Gilch, S., Lutzny, G., Seifarth, W., Erfle, V., Maas, E., Schatzel, H., Leib-Mosch, C., and Greenwood, A.D. (2006). Prion infection influences murine endogenous retrovirus expression in neuronal cells. Biochem. Biophys. Res. Commun. *343:* 825-31.

Sturm, R.A., Duffy, D.L., Box, N.F., Newton, R.A., Shepherd, A.G., Chen, W., Marks, L.H., Leonard, J.H., and Martin, N.G. (2003). Genetic association and cellular function of MC1R variant alleles in human pigmentation. Ann N Y Acad Sci. *994*:348-58.

Sulem, P., Gudbjartsson, D.F., Stacey, S.N. et al. (2008). Two newly identified genetic determinants of pigmentation in Europeans. Nat. Genet. *40,* 835-837.

Sun, K., Johnson, B.S., and Gunn, T.M. (2007). Mitochondrial dysfunction precedes neurodegeneration in *mahogunin* (*Mgrn1*) mutant mice. Neurobiol. Aging *28*, 1840-1852.

Sviderskaya, E.V., Bennett, D.C., Ho., L., Bailin, T., Lee, S.T., and Spritz, R.A. (1997). Complementation of hypopigmentation in p-mutant (pink-eyed dilution) mouse melanocytes by normal human P cDNA, and defective complementation by OCA2 mutant sequences. J. Inv. Dermatol. *108*: 30-34

Sviderskaya, E.V., Kallenberg, D.M. & Bennett, D.C. (2010). Resource. The Wellcome Trust Functional Genomics Cell Bank: holdings. Pigment Cell Melanoma Res. *23,* 147-150.

Takase-Yoden, S., and Watanabe, R. (1997) Unique sequence and lesional tropism of a new variant of neuropathogenic Friend murine leukemia virus. Virology *223:* 411-22.

Tanowitz, M., and Von Zastrow, M. (2002). Ubiquitination-independent trafficking of G protein-coupled receptors to lysosomes. J. Biol. Chem. *277* :50219-22.

Thomas, Ruth (2005). *Studies on the function and mechanism of action of attractin.* Ph.D. dissertation. Oregon Health and Science University School of Medicine.

Ueda, S., Sakakibara, S., Nakadate, K., Noda, T., Shinoda, M., and Joyce, J.N. (2005). Degeneration of dopaminergic neurons in the substantia nigra of zitter mutant rat and protection by chronic intake of Vitamin E. Neurosci Lett. *380*:252-6.

Valverde, P., Healy, E., Jackson, I., Rees, J.L., and Thody, A.J. (1995). Variants of the melanocyte-stimulating hormone receptor gene are associated with red hair and fair skin in humans. Nat. Genet. 11, 328-330.

Vidi, P.A., Chemel, B.R., Hu, C.D., and Watts, V.J. (2008). Ligand-dependent oligomerization of dopamine D(2) and adenosine A(2A) receptors in living neuronal cells. Mol Pharmacol. *74* :544-51.

Voisey, J., Gomez-Cabrera Mdel, C., Smit, D.J., Leonard, J.H., Sturm, R.A., and van Daal, A. (2006). A polymorphism in the agouti signalling protein (ASIP) is associated with decreased levels of mRNA. Pigment Cell Res. *19*, 226-231.

Vrieling, H., Duhl, D.M., Millar, S.E., Miller, K.A., and Barsh, G.S. (1994). Differences in dorsal and ventral pigmentation result from regional expression of the mouse agouti gene. Proc. Natl. Acad. Sci. U. S. A. *91*, 5667-5671.

Wagner, K.U., Dierisseau, P., Rucker, E.B., Robinson, G.W., and Hennighausen, L. (1998). Genomic architecture and transcriptional activation of the mouse and human tumor susceptibility gene TSG101: common types of shorter transcripts are true alternative splice variants. Oncogene *17:* 2761-70.

Wagner, K.U., Krempler, A., Qi, Y., Park, K., Henry, M.D., Triplett, A.A., Riedlinger, G., Rucker III, E.B., and Hennighausen, L. (2003). Tsg101 is essential for cell growth, proliferation, and cell survival of embryonic and adult tissues. Mol. Cell. Biol. *23*, 150-162.

Walker, W.P., Aradhya, S., Hu, C.L., Shen, S., Zhang, W., Azarani, A., Lu, X., Barsh, G.S., and Gunn, T.M. (2007). Genetic analysis of attractin homologs. Genesis *45*, 744-756.

Walker, W.P., and Gunn, T.M. (2010a). Shades of meaning: the pigment-type switching system as a tool for discovery. Pigment Cell. Melanoma Res. *23*:485-95.

Walker, W.P., and Gunn, T.M. (2010b). Piecing together the pigment-type switching puzzle. Pigment Cell. Melanoma Res. *23*, 4-6.

Wells, G.A.H., and Wilesmith, J.W. (2004). Bovine spongiform encephalopathy and related diseases. In S.B. Prusiner (ed.) *Prion Biology and Diseases*, 2nd edition. Cold Spring Harbor USA, Cold Spring Harbor Laboratory Press. p. 595-628.

Westergard, L., Christensen, H.M., and Harris, D.A. (2007). The cellular prion protein (PrP(C)): its physiological function and role in disease. Biochim. Biophys. Acta *1772*:629-44.

Whitley, P., Reaves, B.J., Hashimoto, M., Riley, A.M., Potter, B.V., and Holman, G.D. (2003). Identification of mammalian Vps24p as an effector of Phosphatidylinositol 3,5-bisphosphate-dependent endosome compartmentalization. J. Biol. Chem. *278*:38786-95.

Wickliffe, K., Williamson, A., Jin, L., and Rape, M. (2009). The multiple layers of ubiquitin-dependent cell cycle control. Chem. Rev. *109*, 1537-1548.

Will, R.G. (1993) Epidemiology of Creutzfeldt-Jakob disease. Brit. Medical Bulletin *49:*960-970.

Willard, D.H., Bodnar, W., Harris, C., Kiefer, L., Nichols, J.S., Blanchard, S., Hoffman, C., Moyer, M., Burkhart, W., and Weiel, J. (1995). Agouti structure and function: characterization of a potent alpha-melanocyte stimulating hormone receptor antagonist. Biochemistry *34*, 12341-12346.

Wu, B.T.,, Su, Y.H., Tsai. M.T., Wasserman, S.M., Topper, J.N., and Yang, R.B. (2004). A novel secreted, cell-surface glycoprotein containing multiple epidermal growth factor-like repeats and one CUB domain is highly expressed in primary osteoblasts and bones. J. Biol. Chem. *279*:37485-90.

Yamada, T., Mori, M., Hamada, S., Serikawa ,T., and Yamada, J. (1989). Assignment of tremulous body mutant gene zitter (zi) to linkage group IV of the rat (Rattus norvegicus). J. Hered. *80:*:383-6.

Yancopoulou, D., Crwthier, R.A., Chakrabarti, L., Gydesen, S., Brown, J.M., and Spillantini, M.G. (2003). Tau protein in frontotemporal dementia linked to chromosome 3 (FTD-3). J. Neuropath. Exp. Neurol. *62*:878-882.

Yang, C.H., Shen, S.C., Lee, J.C., Wu, P.C., Hsueh, S.F., Lu, C.Y., Meng, C.T., Hong, H.S., and Yang, L.C. (2004). Seeing the gene therapy: application of gene gun technique to transfect and decolor pigmented rat skin with human agouti signaling protein cDNA. Gene Therapy *11*: 1033-1039.

Yang, H.Y., Cheng, C.F., Djoko, B., Lian, W.S., Tu, C.F., Tsai, M.T., Chen, Y.H., Chen, C.C., Cheng, C.J., and Yang, R.B. (2007) Transgenic overexpression of the secreted, extracellular EGF-CUB domain-containing protein SCUBE3 induces cardiac hypertrophy in mice. Cardiovasc. Res. *75*:139-47.

Yaswen, L., Diehl, N., Brennan, M.B., and Hochgeschwender, U. (1999). Obesity in the mouse model of pro-opiomelanocortin deficiency responds to peripheral melanocortin. Nat. Med. *5*, 1066-1070.

Zanna, P.T., Sánchez-Laorden, B.L., Pérez-Oliva, A.B., Turpín M.C., Herraiz, C., Jiménez-Cervantes, C., García-Borrón, J.C. (2008). Mechanism of dimerization of the human melanocortin 1 receptor. Biochem Biophys Res Commun. *368*:211-6.

Zhang, Y., Zolov, S.N., Chow, C.Y., Slutsky, S.G., Richardson, S.C., Piper, R.C., Yang, B., Nau, J.J., Westrick, R.J., Morrison, S.J., Meisler, M.H., and Weisman, L.S. (2007). Loss of Vac14, a regulator of the signaling lipid phosphatidylinositol 3,5-bisphosphate, results in neurodegeneration in mice. Proc Natl Acad Sci U S A. *104*:17518-23.

Zhang, X., Chow, C.Y., Sahenk, Z., Shy, M.E., Meisler, M.H., and Li, J. (2008). Mutation of FIG4 causes a rapidly progressive, asymmetric neuronal degeneration. Brain *131*:1990-2001.

Zhang, Z., Alpert, D., Francis, R., Chatterjee, B., Yu, Q., Tansey, T., Sabol, S.L., Cui, C., Bai, Y., Koriabine, M., Yoshinaga, Y., Cheng, J.F., Chen, F., Martin, J., Schackwitz, W., Gunn, T.M., Kramer, K.L., De Jong, P.J., Pennacchio, L.A., and Lo, C.W. (2009). Massively parallel sequencing identifies the gene Megf8 with ENU-induced mutation causing heterotaxy. Proc Natl Acad Sci U S A. 106(9):3219-24.